

AD-A249 874



ATION PAGE

Form Approved

OMB No. 0704-0188

average 1 hour per response, including the time for reviewing instructions, searching existing data sources, gathering the collection of information. Send comments regarding this burden estimate or any other aspect of this form to Washington Headquarters Services, Directorate for Information Operations and Reports, 1215 Jefferson Building, Management and Budget, Paperwork Reduction Project (0704-0188) Washington, DC 20503.

1. AGENCY USE ONLY (Leave blank)		2. REPORT DATE 1991	3. REPORT TYPE AND DATES COVERED THESIS/DISSERTATION	
4. TITLE AND SUBTITLE The Calculation of Mid-Latitude Meridional Neutral Winds from an Improved Servo Model Approximation Method			5. FUNDING NUMBERS	
6. AUTHOR(S) Theodore R. Ballard, Captain				
7. PERFORMING ORGANIZATION NAME(S) AND ADDRESS(ES) AFIT Student Attending: Utah State University			8. PERFORMING ORGANIZATION REPORT NUMBER AFIT/CI/CIA- 91-121	
9. SPONSORING/MONITORING AGENCY NAME(S) AND ADDRESS(ES) AFIT/CI Wright-Patterson AFB OH 45433-6583			10. SPONSORING/MONITORING AGENCY REPORT NUMBER	
11. SUPPLEMENTARY NOTES			DISTRIBUTION STATEMENT A Approved for public release; Distribution Unlimited	
12a. DISTRIBUTION/AVAILABILITY STATEMENT Approved for Public Release IAW 190-1 Distributed Unlimited ERNEST A. HAYGOOD, Captain, USAF Executive Officer			12b. DISTRIBUTION CODE	
13. ABSTRACT (Maximum 200 words)				
14. SUBJECT TERMS			15. NUMBER OF PAGES 107	
			16. PRICE CODE	
17. SECURITY CLASSIFICATION OF REPORT	18. SECURITY CLASSIFICATION OF THIS PAGE	19. SECURITY CLASSIFICATION OF ABSTRACT	20. LIMITATION OF ABSTRACT	

THE CALCULATION OF MID-LATITUDE MERIDIONAL
NEUTRAL WINDS FROM AN IMPROVED SERVO
MODEL APPROXIMATION METHOD

by

Theodore R. Ballard, Capt, USAF

A thesis submitted in partial fulfillment
of the requirements for the degree

of

MASTER OF SCIENCE

in

Physics
(Upper Atmospheric Option)

Center for Atmospheric and Space Sciences
Utah State University
Logan, Utah

1991

92-11940



02 5 01 024

Copyright: Theodore R. Ballard, 1991
All Rights Reserved

Accession For	
NTIS GRA&I	<input checked="checked" type="checkbox"/>
DTIC TAB	<input type="checkbox"/>
Unannounced	<input type="checkbox"/>
Justification	
By	
Distribution/	
Availability Codes	
Dist	Avail and/or Special
A-1	

THE CALCULATION OF MID-LATITUDE MERIDIONAL
NEUTRAL WINDS FROM AN IMPROVED SERVO
MODEL APPROXIMATION METHOD

by

Theodore Raymond Ballard

A thesis submitted in partial fulfillment
of the requirements for the degree

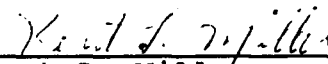
of

MASTER OF SCIENCE

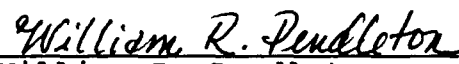
in

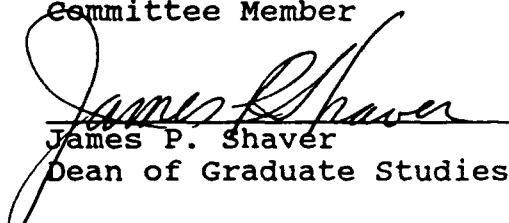
Physics
(Upper Atmospheric Option)

Approved:


Kent L. Miller
Major Professor


Vincent B. Wickwar
Committee Member


William R. Pendleton
Committee Member


James P. Shaver
Dean of Graduate Studies

UTAH STATE UNIVERSITY
Logan, Utah

1991

ACKNOWLEDGEMENTS

My education at Utah State University was sponsored by the Air Force Institute of Technology (AFIT).

This study was made under the direction of Dr. Kent L. Miller of the Center of Atmospheric and Space Sciences. I extend my sincere gratitude to Dr. Miller for his very fruitful questions and advice. I would also like to thank Dr. Vincent B. Wickwar and Dr. William R. Pendleton for their suggestions and critical review of my work, which enhanced the quality of this investigation. Additionally, I wish to thank Dr. Philip G. Richards for his expert advice on the Field Line Interhemispheric Plasma (FLIP) model, Dr. Michael J. Buonsanto for his time and graciousness in sending me Millstone Hill incoherent scatter radar data, Dr. Daniel J. Melendez-Alvira for sending me a copy of his enlightening doctoral thesis and Dr. Henry Rishbeth for beneficial discussions on the original servo model assumptions. I would also like to acknowledge Horng-Yu Wu for all his help and long discussions.

Finally, I would like to express my love to my wife, Sara Suzanne, for all her support and patience-she unselfishly held down the home fort and I could not have done this without her-and to my son, Jared, a bundle of happy energy who succeeds in bringing great joy to my life.

Theodore R. Ballard

TABLE OF CONTENTS

	Page
ACKNOWLEDGEMENTS	ii
LIST OF TABLES	v
LIST OF FIGURES	vi
ABSTRACT	ix
 CHAPTER	
I. INTRODUCTION	1
1.1 Overview	1
1.2 Problem Statement	2
1.3 Objectives of the Investigation	4
II. REVIEW OF LITERATURE	6
2.1 Meridional Neutral Winds	6
2.2 The F2 Peak as a Servo Mechanism	16
2.3 Chemical Loss in the F2-region	22
2.4 Plasma Diffusion	23
2.5 Supporting Ionospheric Models	29
III. METHOD	34
3.1 USU Servo Model Development	34
3.1.1 Model Equations	37
3.1.2 Daytime	40
3.1.3 Nighttime	43
3.1.4 Twilight Assumptions	45
3.1.5 Balance Height Adjustment	48
3.1.6 Topside Shape Factor	51
3.1.7 Daytime Steady Rate Assumption ...	54
3.1.8 Neutral Wind	56
3.2 Model Program Outline	57
3.3 Data Preparation	60
3.3.1 IRI hmF2 Data	61
3.3.2 Ionosonde hmF2 Data	61
3.3.3 Incoherent Scatter Radar Data	62
IV. RESULTS AND DISCUSSION	63
4.1 Winds from IRI hmF2	63

	iv
4.2 Winds from Ionosonde hmF2	67
4.3 Comparing Winds with Radar Data	80
V. CONCLUSIONS AND RECOMMENDATIONS	93
REFERENCES	97
APPENDICES	101
Appendix A. General Information on Station Locations	102
Appendix B. Geomagnetic and Solar Data	103
Appendix C. Copyright Permission Letters ..	104

LIST OF TABLES

Table	Page
1. Ion Chemistry and Reaction Rates, Adapted from Schunk [1983]	21
2. Collision Frequencies of O^+ Ions Through O , N_2 and O_2 Neutrals, Adapted from Banks and Kockarts [1973]	25
3. Geomagnetic A_p from 9-17 January, 1988	72
4. Ionosonde/Radar Station Parameters	102
5. Geomagnetic and Solar Data	103

LIST OF FIGURES

Figure	Page
1. Day/Night force balance relationship between the pressure gradient, ion drag and Coriolis forces in the northern hemisphere. U depicts the horizontal neutral wind. Adapted from Holton [1979].	15
2. Electron density profiles at Petropavlovsk generated with IRI data for low solar flux during winter solstice. Dashed lines indicate each profile's balance height computed by the USU servo model. A computed 40 m s^{-1} poleward wind lowers the daytime F2-peak, while a 135 m s^{-1} equatorward wind raises the nighttime F2-peak.	18
3. Plasma diffusion along an inclined geomagnetic field line. At steady state, the horizontal component of plasma motion induces a neutral wind which equals $W_d \cot I$. Adapted from Rishbeth and Garriott [1969].	28
4. Bradley-Dudeney model ionosphere. The ordinate and abscissa are linear in height and frequency. Reprinted by permission of Pergamon Press from Bradley and Dudeney [1973].	31
5. January mid-latitude variations of loss scale height factor k for low, medium, and high solar flux of 70, 130 and 190 s.f.u. ($10^{-22} \text{ W m}^{-2} \text{ Hz}^{-1}$).	36
6. USU servo and FLIP model comparisons of the diurnal coefficient c_x for a January, mid-latitude location. This figure shows agreement between the FLIP and USU servo models for F-region morning and evening transitions.	47
7. USU servo and FLIP model comparisons of diurnal coefficient c_x and corresponding balance heights h_o for a January, mid-latitude location. Figures 7a and 7b show differences in c_x and h_o comparisons during steady-state assumption (7a) and steady-rate assumption (7b).	55
8. Meridional neutral winds for two magnetically conjugate locations during low (January, 1985) and high solar activity (January, 1981) shown as solid and dashed lines respectively. Winds are calculated by the USU servo model using IRI F2-peak heights.	64

9. Neutral winds along a meridional string of ionosonde stations calculated by the USU servo model from IRI hmF2 data for January, 1988. Positive winds are poleward. Open and shaded circles mark local noon and midnight. 66
10. Prestorm neutral winds (positive poleward) for a meridional string of 20 ionosonde stations on January 12 and 13, 1988 (GISMOS-88). Winds calculated by USU servo model. 68
11. Neutral winds during GISMOS-88 storm on January 14 and 15, 1988 for a meridional string of 20 ionosonde stations. Winds calculated by USU servo model. 73
12. Post-storm neutral winds for a meridional string of 20 ionosonde stations on 16 January, 1988 (GISMOS-88). Winds are calculated by USU servo model. 78
13. Weather vs. Climatology: Neutral winds from the USU servo model for January 12 and 13, 1988 at Petropavlovsk, during GISMOS-88 prestorm period. Solid lines show IRI winds and dashed lines show ionosonde winds. 81
14. Neutral wind comparison above Millstone Hill during ETS period. All calculations include daily Ap history and 1.7 increase to $O^+ \rightarrow O$ collisions. Solid line is FLIP winds, short-dashed line is USU servo winds and long-dashed line is tuned servo model winds. 83
15. Neutral and ion temperatures at 300 km above Millstone Hill during ETS period. T_n is solid line from MSIS-86 and T_i is dashed line measured by IS radar. 87
16. Electron temperatures measured by IS radar at 300 km above Millstone Hill during ETS period. .. 88
17. USU servo neutral wind sensitivity to changes in ion temperature during Millstone Hill ETS period. Winds are calculated for different temperature ratios. Solid line is for $T_i/T_n = 1$, short-dashed line is for $T_i/T_n = 1.5$ and long-dashed line is for $T_i/T_n = 2.5$ 89

18. Neutral wind comparison at Millstone Hill during ETS (18-23 Sep 84). Dashed line with stars is USU servo wind. Error bars show statistical uncertainties of radar wind at 300 km. Both calculations include the 1.7 increase in $O^+ \rightarrow O$ collisions. Daily Ap history for USU servo and three hour ap history for radar was used in MSIS-86. 91

ABSTRACT

The Calculation of Mid-Latitude Meridional
Neutral Winds from an Improved Servo
Model Approximation Method

by

Theodore R. Ballard, Master of Science
Utah State University, 1991

Major Professor: Dr. Kent L. Miller
Department: Physics

The theoretical servo model of Rishbeth, Ganguly and Walker provided the impetus for a physically more practical version of a servo model, called the USU servo model. The USU servo model was developed to automatically calculate, with a personal computer, meridional neutral winds of the upper thermosphere for any mid-latitude location from F2-peak layer heights.

F2-peak layer heights were input into the USU servo model from three different sources for calculation of meridional neutral winds. The International Reference Ionosphere provided mid-latitude, geomagnetically quiet, monthly averages of F2-layer heights for different solar cycle conditions. The International Reference Ionosphere also provided a means of comparison with ionosonde F2-peak layer height deduced winds. F2-layer heights from different mid-latitude ionsondes were determined by using scaled

ionosonde critical frequencies from an empirical equation developed by Bradley and Dudeney. Millstone Hill incoherent scatter radar provided a means to compare the USU servo model with other neutral wind calculation techniques, including radar-derived winds.

Results of this investigation indicate that the USU servo model is a valuable tool in the calculation of mid-latitude meridional neutral winds and compares well with radar-deduced wind data during quiet to moderate geomagnetic activity. When combined with F2-layer heights produced by the International Reference Ionosphere, the USU servo model can become a meridional neutral wind prediction tool, computing solar cycle and latitudinal variations in neutral wind circulation patterns. (117 pages)

CHAPTER I

INTRODUCTION

1.1 Overview

This study involves mid-latitude meridional neutral winds derived from ionospheric F2-layer heights. Generally, the F2-layer peak (hmF2) occurs between 200 and 600 km [Hargreaves, 1979]. At these altitudes, neutral wind velocities are normally constant with height due to strong viscous drag effects [Richmond, 1983]. Therefore, winds derived at hmF2 are regarded as constant with height and approximate the neutral wind of the upper thermosphere.

Meridional neutral winds are calculated from an improved version of the F-region servo model, known in this study as the USU servo model. The servo model has been successfully used in previous studies and can reproduce the behavior of the mid-latitude F2-layer quite well [Ganguly et al., 1980]. The servo method provides a computational advantage by describing the F-region through physically simple processes at the F2-peak. The most serious assumption is that the model deals only with the F2-peak, so calculated values are assumed to apply throughout the upper thermosphere [Rishbeth et al., 1978]. Historically, the servo model has compared well with other methods to determine neutral winds [Buonsanto, 1986, 1990] and [Buonsanto et al., 1989, 1990]. Buonsanto et al. [1989, 1990] found that when the servo model is "tuned" from deduced-radar winds, servo model wind speeds are closer to radar wind

speeds throughout the period of study. Tuning allows for an empirical adjustment of a balance between chemical and diffusive loss of plasma at the F2-peak. The USU servo model is divorced from empirical tuning and is physically more realistic, while maintaining the servo advantages of speed and simplicity. This study explains improvements in the USU servo model and shows how the model may be applied to calculate the meridional neutral wind from a variety of sources explained in Section 1.3. Calculated neutral wind patterns are also qualitatively related to momentum sources during geomagnetically quiet and active conditions.

Global studies of neutral wind patterns that respond to changing momentum sources can improve our understanding of thermospheric dynamics. However, systematic observations of neutral winds are limited to a sparse network of Fabry-Perot interferometers (FPI) [Hernandez and Roble, 1976], incoherent scatter radars [Salah and Holt, 1974; Wickwar et al., 1984], and satellite measurements of the Doppler shift of the airglow spectra [Herraro et al., 1988]. It is logical that we can improve our understanding of thermospheric neutral wind circulation patterns by using a method which can expand our global coverage.

1.2 Problem Statement

Two methods of deriving the meridional component of the neutral wind from hmF2 values have been successfully used. One method [Miller et al., 1986, 1987, 1989] uses

the Field Line Interhemispheric-Plasma (FLIP) ionospheric model developed by Richards and Torr [1985]. The other method [Buonsanto, 1986, 1990] and [Buonsanto et al., 1989, 1990] uses the servo model of Rishbeth et al. [1978]. The servo model has a computational advantage, while the FLIP model is much more comprehensive. The servo model is more readily adaptable to parametric investigations, that is the variation of neutral winds due to gas composition and temperature changes.

The two models essentially use the same method to derive neutral winds and therefore should produce about the same results. A recent paper by Buonsanto et al. [1989] made a comparison of the two models using Millstone Hill incoherent scatter (IS) radar data. The servo model produced winds consistently more equatorward, especially during geomagnetically active periods, than the Miller et al. [1986] method. During this comparison the servo model was tuned to attain better agreement between radar and servo winds [Buonsanto et al., 1989]. This empirical tuning was done with the help of radar-deduced winds.

There are two objectives of the investigation reported here. The primary objective is to develop a USU servo model by finding the physical basis of servo model tuning and explain/reduce the differences found in the FLIP and servo model winds. A secondary objective is to show how the USU servo model is applied to different sources of hmF2 data and indicate the significance of this application.

1.3 Objectives of the Investigation

The main objective of this investigation is to develop the USU servo model on research originally published by Rishbeth [Rishbeth, 1967; Rishbeth et al., 1978] and [Buonsanto et al., 1989], which calculates mid-latitude meridional neutral winds from the height of the F2-peak. The USU servo model runs on a personal computer (PC) and requires no tuning. This enables greater flexibility in servo wind calculations: One can calculate USU servo winds at any mid-latitude location under different ionospheric conditions, without regard to tuning.

The USU servo model uses the Mass Spectrometer Incoherent Scatter (MSIS-86) model [Hedin, 1987], to represent the neutral atmosphere. The USU servo model uses typical mid-latitude estimates of ion temperatures but is easily adapted to use measured ion temperatures. The USU servo model does not need electron temperature, which is required to calculate the diffusion coefficient in previous servo models [Buonsanto, 1986, 1990; Buonsanto et al., 1989, 1990; Melendez-Alvira, 1990; Rishbeth and Edwards, 1989].

A second objective is to apply the USU servo model to three sources of hmF2 data and discuss or compare results. One source is the International Reference Ionosphere (IRI) [Bilitza et al., 1987], which models monthly averages of hmF2 data for magnetically quiet conditions in the non-auroral ionosphere. The main advantage in using IRI data is the ability to calculate global, climatological neutral

winds, for any mid-latitude location, under different solar cycle conditions.

A second source is scaled ionosonde critical frequencies, which are used to determine hmF2 values by an empirical equation developed by Bradley and Dudeney [1973]. In this study, USU servo model winds are calculated from ionosondes operating during January, 1988 (GISMOS-88 campaign). The ability to use ionosonde data greatly enhances global observational coverage. Approximately 126 ionosonde stations are operational and contribute to the World Data Center providing geographically dispersed observational data regardless of tropospheric weather conditions [Conkright and Brophy, 1982].

The third source of hmF2 data is IS radar measurements from Millstone Hill during the equinox transition study (ETS) of September, 1984. Two geomagnetic storms occurred during this period and prompted a comparative study of FLIP, servo and radar winds by Buonsanto et al. [1989]. By using this same ETS period, the USU servo model joins this comparison.

This investigation reveals the physical sources of the differences between the Miller et al. [1986] FLIP winds and the Buonsanto et al. [1989] servo winds. The sources stem from the theoretical assumption of diffusive equilibrium. This study also shows wind results from different hmF2 sources and indicates the value in using a servo model for global meridional neutral wind calculations.

CHAPTER II

REVIEW OF LITERATURE

2.1 Meridional Neutral Winds

In this thesis, meridional neutral wind is defined as the horizontal motion of neutral gas particles along a geomagnetic meridian. The distinction of neutral wind is used at high altitudes because neutral and ionized plasma gases have different constraints on their movements. In the F-region of the ionosphere, plasma is constrained to move along geomagnetic field lines. Plasma motions are driven by electromagnetic forces, neutral winds, plasma diffusion and thermal expansion and contraction [Rishbeth, 1972; Salah and Holt, 1974; Wickwar et al., 1984]. Meridional neutral winds cause neutral-air particles to collide with F-region ions, forcing them to move along inclined geomagnetic field lines. Nighttime equatorward winds raise the F-layer, which maintains ionization by decreasing chemical loss, while daytime poleward winds lower the F-layer and increase chemical loss [Hargreaves, 1979; Rishbeth, 1972; Schunk, 1983]. Normally, mid-latitude neutral-wind-induced plasma motions are greater in magnitude than electric field effects [Hargreaves, 1979; Rishbeth, 1972; Roble, 1983]. Methods that derive neutral winds from hmF2 values assume that electric field effects are negligible.

Neutral wind is mainly created by an uneven heating of the Earth's upper atmosphere, but neutral air may also be set into motion by ion collisions created from electric

fields, especially important at high latitudes [Killeen and Roble, 1984; Roble, 1983]. The driving energy is provided by heat created primarily from solar ultraviolet (UV) and extreme ultraviolet (EUV) radiation. But heat energy can be significantly enhanced by auroral processes, ion-neutral collisions and upward-propagating waves [Rishbeth, 1988; Richmond, 1983]. A daytime thermal expansion of the atmosphere creates a diurnal bulge, which gives rise to horizontal and vertical pressure gradients accounting for the solar driven neutral wind [Rishbeth, 1972]. Although the vertical component of the pressure gradient is the larger, it is almost completely balanced by gravity. This is the foundation of hydrostatic balance and is an excellent approximation, especially when considering large scale flows [Holton, 1979; Richmond, 1983]. As a consequence, the primary driver of the neutral wind is in the horizontal plane.

The acceleration of horizontal neutral winds is subject to four types of momentum [Rishbeth and Garriott, 1969; Rishbeth, 1972]. The four forces are caused by pressure gradients, the Earth's rotation, ion drag and viscous drag. To best describe these forces, we first introduce the equation of motion, represented as

$$\frac{d\mathbf{U}}{dt} = \nabla P - 2\boldsymbol{\Omega} \times \mathbf{U} - \nu_{ni}(\mathbf{U} - \mathbf{V}) + \frac{\mu}{\rho} \nabla^2 \mathbf{U} + \mathbf{g} \quad (1)$$

(a) (b) (c) (d) (e) (f)

where the terms are (a) acceleration, (b) pressure gradi-

ent, (c) Coriolis acceleration, (d) ion drag, (e) viscous drag and (f) gravity. For the parameters of Equation (1), U is the neutral wind velocity, P is pressure, Ω is the Earth's angular velocity, v_{ni} is the neutral-ion collision frequency, V is the ion drift velocity, μ is the dynamic viscosity, ρ is neutral mass density, g is gravity and the ratio μ/ρ is the kinematic viscosity.

As stated, gravity and the vertical pressure gradient act to cancel each other and neutral winds tend to move horizontally. As a result, vertical gradients of gas composition and temperature are much greater than horizontal gradients and horizontal wind speeds are usually several orders of magnitude greater than vertical wind speeds [Richmond, 1983; Rishbeth, 1972]. Given these conditions, the acceleration, pressure gradient, Coriolis force and ion drag tend to act in the horizontal, while viscous drag only appears under the presence of vertical wind shears.

As we are on the rotating Earth, we naturally prefer to use a reference frame which is fixed with respect to the Earth. The physical laws of motion require an inertial reference frame, such that an object set in uniform motion will remain in uniform motion in the absence of any forces (Newton's first law of motion). Since a rotating frame is a non-inertial reference frame, two "apparent" forces must be added to satisfy the equations of motion. These apparent forces are called Coriolis and centrifugal accelerations. Centrifugal acceleration is needed to offset cen-

tripetal acceleration, which acts toward the axis of rotation as viewed from a fixed reference frame in space. The centrifugal acceleration is an inertial reaction needed to balance the rotating coordinate acceleration as observed on a stationary point on the Earth. The centrifugal force partly balances the gravitational force, and it is thus convenient to combine the effects of gravitational and centrifugal accelerations into a term defined as gravity.

When the neutral wind appears as to move along a straight path from a fixed point in space (an inertial reference frame), it is observed from the rotating Earth to follow a curved path. The apparent force, which acts to deflect the neutral wind from its inertial straight-line path, is called the Coriolis force. The curved path is in a direction opposite to the direction of coordinate rotation. An object with a horizontal relative velocity is deflected to the right in the northern hemisphere and to the left in the southern hemisphere.

The driving mechanism behind the pressure gradient force is differential heating. Solar forcing is important throughout the atmosphere, but at high latitudes significant heat is also produced by auroral particle precipitation and ion-neutral collisions associated with the polar cap convective cells [Schunk, 1983]. At mid-latitudes, solar heating is normally the main mechanism in pressure gradient forcing. Temperature variations due to solar heating causes the atmosphere to expand or bulge on the

daylit side of the Earth. This creates a high-pressure region referred to as the daytime pressure bulge [Rishbeth, 1972]. The resulting mid-latitude daytime poleward and nighttime equatorward winds have a significant effect on the distribution of plasma at thermospheric heights.

The effect of colliding ions on neutral-air particles is called ion drag. The ion drag term in Equation (1) is usually negative at mid-latitudes, but ion drag is also capable of inducing motion to the neutrals from plasma drifts created by electric fields, especially important in the polar regions [Hargreaves, 1979]. At high latitudes, polar cap convective cells are connected to the magnetosphere and associated convective electric fields are enhanced during ionospheric and geomagnetic storms. These polar electric fields drive ions, which collide with neutral-air particles having a significant impact on the neutral winds [Schunk, 1983]. Collisions between electrons and ions and between electrons and neutrals have little effect on the ion drift velocity and overall neutral air motion [Kelley, 1989].

Physical constraints on charged ions are quite different than on neutral air movements and this leads to some interesting relations. Neutral air moves under the influence of horizontal forces, while at F-region heights, ions are constrained to move along the geomagnetic field lines and are influenced mainly by electric fields and neutral air collisions. As a simple analogy, consider ions as

beads "tied" to an inclined geomagnetic string acting as a brake against the neutral wind. If set into motion by electric fields, the ions move perpendicular to the field lines and take a more active role in inducing horizontal neutral wind movement.

The most significant cause of ion drag at mid and low-latitudes is due to F-region electric fields produced in the E-region [Hargreaves, 1979; Rishbeth, 1979]. E-region neutral winds can blow ions across the magnetic field lines at heights up to about 150 km, while neutral winds have little cross magnetic effect on electrons above about 70 km [Rishbeth, 1988]. Neutral wind effects on electron and ion motions perpendicular to the magnetic field lines depend on the ratio of collision frequency to gyrofrequency. Gyrofrequency is inversely proportional to particle mass, while collision frequency decreases exponentially with height. Therefore, neutral winds blow ions across geomagnetic field lines at greater heights than it does electrons, so that ions and electrons become separated. Bulk neutrality is maintained, but a potential difference is set up between ions and electrons, which is constantly changing as wind velocity and ion concentration change. Neutralizing currents are produced in the E-region. Geomagnetic field lines act as equipotential surfaces, due to the high longitudinal conductivity along the field lines as compared to the smaller transverse conductivities. Since the potential drop along a field line is small, the electric field pro-

duced in the E-region is reproduced in the F-region. The zonal electric field in the F-region then acts to raise or lower the F2-peak layer height, where the ion drift velocity becomes $\mathbf{V} = (\mathbf{E} \times \mathbf{B})/B^2$. An eastward electric field raises $h_m F2$ and a westward field lowers $h_m F2$. In this way, the E-region is considered an atmospheric dynamo and the F-region is analogous to a motor [Hargreaves, 1979; Kelley, 1989; Ratcliffe, 1972]. Normally, dynamo-induced ion drifts in the mid-latitude F-region are less than 30 m s^{-1} [Richmond, 1983; Rishbeth, 1972]. Miller et al. [1987] showed that for quiet or moderate geomagnetic conditions, electric field induced drifts are usually less than the overall statistical uncertainty in the calculation of neutral winds from $h_m F2$.

The viscosity of a fluid is a measure of its resistance to flow. The greater the resistance, the greater the viscosity. Viscous forces appear only under the presence of wind shears. Normally, only vertical wind shears are important: Vertical gradients dominate over horizontal gradients and horizontal winds are usually much greater than vertical winds. Dynamic viscosity depends on temperature. Since F2-region temperature gradients are small, we can treat the dynamic viscosity as a constant with respect to height [Rishbeth, 1972]. Kinematic viscosity is inversely proportional to neutral mass density, so that viscosity is large and important at great heights. The interchange of the horizontal momentum in the vertical

direction is manifested as viscosity, so that momentum tends to diffuse in such a way as to smooth out the vertical-height profile. At about 250 km, viscosity acts to smooth out velocity profiles in less than an hour, while at 130 km, viscous forces take about a day to smooth the velocity profiles [Richmond, 1983]. For this reason we can assume that the neutral wind calculated at the F2-peak is constant within the F-region.

The relative importance of the forcing terms in the F2-region is variable and depends on diurnal, geographical, seasonal, solar cycle and active solar/geomagnetic conditions. Solar activity causes the greatest variability, creating geomagnetic and ionospheric disturbances, that affect the entire thermosphere, especially at high latitudes. At solar cycle maximum, increased UV and EUV heating raises thermospheric temperatures by hundreds of degrees and changes the entire dynamic and chemical structure of the thermosphere [Roble, 1983; Rishbeth, 1986]. Although the momentum forcing terms do vary, we can make some general observations about their relative significance.

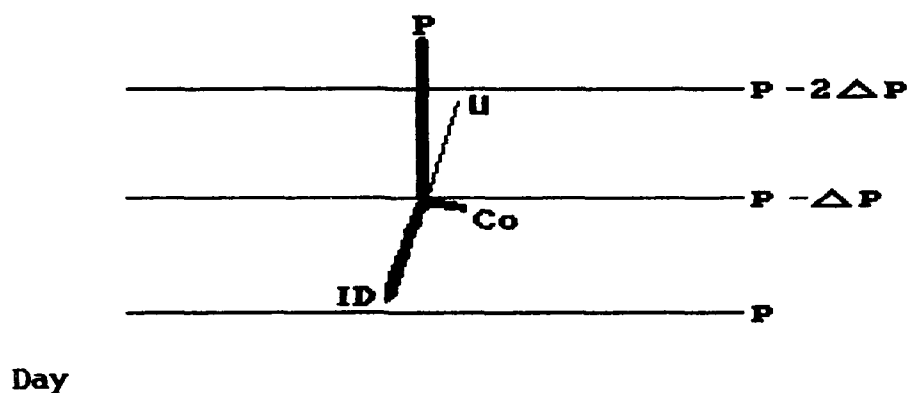
During geomagnetically active periods neutral wind circulation patterns are severely disturbed [Burnside et al., 1991]. Rapidly changing conditions give rise to differential horizontal momentums, so that viscous forces maximize to smooth out resulting vertical wind shears [Richmond, 1983]. Viscosity then acts as a governing force on the thermosphere, continually trying to restore the

neutral wind back to quiet, steady-state conditions.

At steady state, we may neglect acceleration and viscosity and a force balance relationship occurs between the pressure gradient, ion drag and Coriolis forces. In the daytime F2-region, ion drag is large compared to Coriolis force, so that the neutral wind blows almost parallel to the pressure gradient [Rishbeth, 1988]. At night, ionization is near zero and ion drag is smaller. Nighttime neutral wind speeds are greater, making the Coriolis force more important. The force balance relationship at night, then tends to cause neutral air to flow at greater angles to the pressure gradient.

Figure 1 shows how the relationship between forces works in the northern hemisphere. Ion drag acts in the opposite direction of the neutral wind velocity and Coriolis acts to the right of the wind. The pressure gradient force acts from high to low pressure.

The force balance is affected when pressure gradients or ion drag change. One major effect comes from solar cycle variations, which significantly change pressure gradients and ion drag. Increases in the pressure gradient and ion drag momentums are directly related to increases in solar activity [Rishbeth, 1972]. The study of changes in neutral wind force-balance relationships resulting from changes in the solar cycle can lead to an understanding of thermospheric circulation patterns.



Night

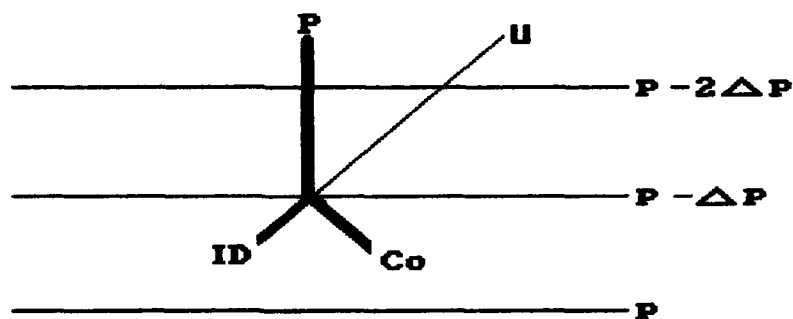


Fig. 1. Day/Night force balance relationship between the pressure gradient, ion drag and Coriolis forces in the northern hemisphere. U depicts the horizontal neutral wind. Adapted from Holton [1979].

2.2 The F2-Peak as a Servo Mechanism

The F2-peak marks the level of peak electron density concentration and occurs at the height where photochemical processes give way to gravitational or diffusive control [Rishbeth, 1988]. Below the peak, the electron density increases with height because the loss rate decreases more quickly than the production rate and neutral densities are large enough to make plasma diffusion of little importance as a loss mechanism [Hargreaves, 1979]. Above the peak, the atmospheric density is so low that chemical loss gives way to loss by diffusive vertical transport. Electron density behavior at the peak is governed by a balance of production, loss and a downward diffusion of plasma, where both chemical loss and diffusion are about equally important [Rishbeth and Garriott, 1969; Schunk, 1983].

Ions and electrons are held together by electrostatic forces, which maintain a total bulk neutrality [Richmond, 1983]. In the F-region, plasma is constrained to flow along the geomagnetic field lines, where meridional neutral winds or zonal electric fields can induce plasma motions [Schunk, 1983].

If the F2-layer is not disturbed by a neutral wind or electric field, then the F2-peak lies at a balance height, which we will call h_o . If the peak is shifted in altitude, there is a response to the change in chemical and diffusive equilibrium and the layer seeks to find a new equilibrium. In this way, the F2-peak acts as a servo mechanism, where

equilibrium is disturbed by a vertical drift treated as a time-varying perturbation [Rishbeth, 1967; Rishbeth et al., 1978].

To derive the meridional neutral wind, the USU servo model first calculates h_o from a balance of chemical and diffusive loss of plasma at the F2-peak with no applied drift. Measured or empirically modeled F2-peak layer heights defined as h_{mF2} or h_m , are input into the USU servo model and applied plasma drifts are calculated from a difference between h_m and h_o . Meridional neutral winds are then calculated from the plasma drift values.

Figure 2 shows how the F2-layer may be shifted in altitude by an applied force. In Figure 2, electron density profiles are generated by the International Reference Ionosphere (IRI-86), for a geomagnetically quiet period, with low solar activity. The profiles are calculated at Petropavlovsk on the Kamchatka Peninsula in January, at 1500 and 2200 local time. Solid lines show IRI h_m and dashed lines show h_o calculated by the USU servo model for each profile. Since h_o occurs where there is no applied force to disturb the F2-peak, then any height difference must be attributed to either a meridional neutral wind, zonal electric field or a combination of the two. If we assume the electric field is negligibly small, then the USU servo model takes advantage of equilibrium changes by calculating the required meridional component of the neutral wind. For the example of Figure 2, calculated values

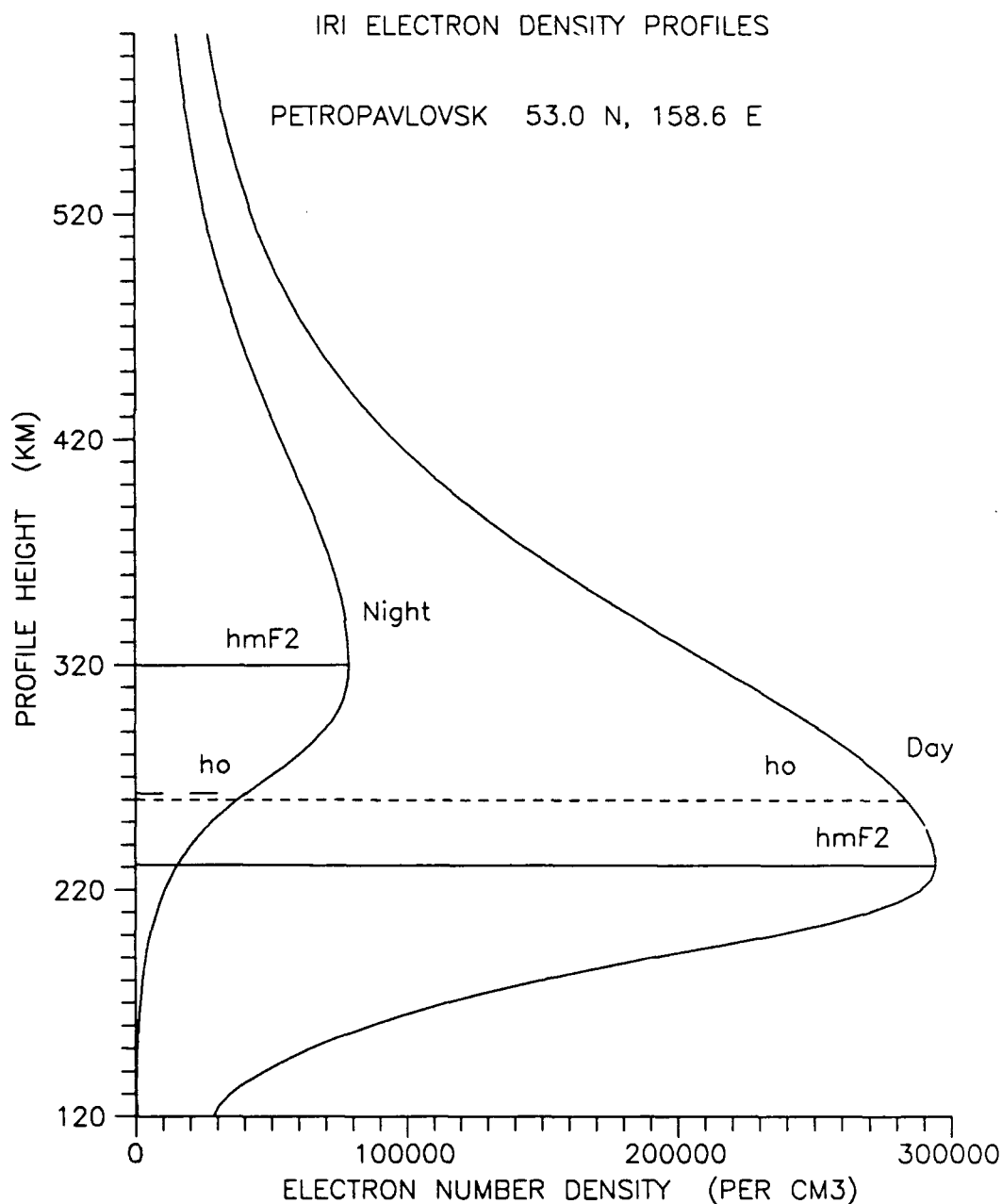


Fig. 2. Electron density profiles at Petropavlovsk generated with IRI data for low solar flux during winter solstice. Dashed lines indicate each profile's balance height computed by the USU servo model. A computed 40 m s^{-1} poleward wind lowers the daytime F2-peak, while a 135 m s^{-1} equatorward wind raises the nighttime F2-peak.

of a daytime poleward wind of 40 m s^{-1} and a nighttime equatorward wind of 135 m s^{-1} are needed to shift the F2-peak layer.

Since we assume the total plasma drift causing the F2-layer to move from h_o to h_m is from the neutral wind, it is important to know how much error is introduced by neglecting electric field effects. This same major assumption is used by any method deriving neutral winds from the height of the F2-peak. Miller et al. [1987] made a comparison study on the errors introduced when the effect of electric fields are neglected. By using the FLIP model, neutral winds were derived from F2-peak heights for quiet and moderate geomagnetic conditions over Millstone Hill and Ottawa. Coordinated measurements using an IS radar at Millstone Hill and an ionosonde over Ottawa, showed reasonable agreement in both wind speed and direction, as well as time of occurrence. Electric field effects produced errors less than the statistical uncertainties in the model and measurements. Buonsanto et al. [1989] made a similar study using Millstone Hill radar data and came up with the same conclusions, but added that for active geomagnetic periods electric fields should not be neglected.

Understanding F2-layer behavior resulting from ionospheric processes requires a mathematical basis beginning with mass continuity [Rishbeth, 1986]. The Rishbeth, Ganguly and Walker derivation of the servo model [Rishbeth et al., 1978], herein called the RGW servo model, begins

with the F-layer continuity equation. A review of this equation explains the reason for the F2-peak and leads to an understanding and derivation of servo relationships. The F-layer continuity equation for electron/ion density N is

$$\frac{\partial N}{\partial t} = q - \beta N - \frac{1}{H} \frac{\partial (NV_z)}{\partial z} \quad (2)$$

At the F2-peak, where gas densities are low, chemical loss is linear with N and is controlled by charge exchange reactions of the major ion O^+ with N_2 and O_2 [Rishbeth, 1986]. The linear loss coefficient β is inversely proportional to the N_2 (or O_2) concentration [Hargreaves, 1979]. Normally $[N_2]/[O_2] \approx 10$ in the F2-region, but loss reactions with O_2 are ≈ 10 times faster than with N_2 and both reactions are considered equally important [Rishbeth, 1986]. The F2-layer linear loss coefficient then takes the form $\beta = k_1[O_2] + k_2[N_2]$, where k_1 and k_2 are chemical rate reactions given in Table 1. General values of β are on the order of $1 \times 10^{-3} \text{ s}^{-1}$ by day and $1 \times 10^{-4} \text{ s}^{-1}$ at night [Rishbeth, 1986].

Horizontal motion contributes little to Equation (2), so the transport term includes only the vertical plasma velocity V_z [Rishbeth, 1986]. The value of V_z includes both plasma diffusion and vertical drift from an applied wind or electric field. In ionospheric theory, it is sometimes preferable to define a reduced height in terms of the major ionizable gas, atomic oxygen [Rishbeth, 1986].

TABLE 1. Ion Chemistry and Reaction Rates,
Adapted from Schunk [1983]

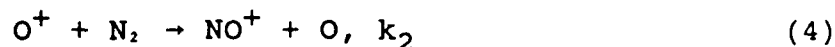
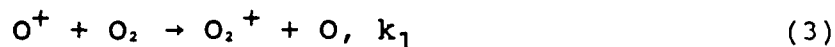
Chemical Equation	Rate Coefficient, $\text{cm}^3 \text{s}^{-1}$
$\text{O}^+ + \text{O}_2 \rightarrow \text{O}_2^+ + \text{O}$	$k_1 = 2.82 \times 10^{-11} - 7.74 \times 10^{-12}(\text{T}_r/300) + 1.073 \times 10^{-12}(\text{T}_r/300)^2 - 5.17 \times 10^{-14}(\text{T}_r/300)^3 + 9.65 \times 10^{-16}(\text{T}_r/300)^4; \quad 300 \leq \text{T}_r \leq 6000^\circ\text{K}$
$\text{O}^+ + \text{N}_2 \rightarrow \text{NO}^+ + \text{O}$	$k_2 = 1.533 \times 10^{-12} - 5.92 \times 10^{-13}(\text{T}_r/300) + 8.60 \times 10^{-14}(\text{T}_r/300)^2; \quad 300 \leq \text{T}_r \leq 1700^\circ\text{K}$
	$k_2 = 2.73 \times 10^{-12} - 1.155 \times 10^{-12}(\text{T}_r/300) + 1.483 \times 10^{-13}(\text{T}_r/300)^2; \quad 1700 < \text{T}_r < 6000^\circ\text{K}$

$\text{T}_r = (\text{T}_n + \text{T}_i)/2$ -- Effective temperature, where T_n and T_i are the neutral and ion temperatures in K.

We then assume the scale height H is of atomic oxygen, which is constant with height, since the F2-layer is nearly isothermal. H is equal to $k_b \text{T}_n / mg = RT_n / Mg$, where k_b is Boltzmann's constant, R is the universal gas constant, m is particle mass, M is molar mass, T_n is the neutral air temperature and g is gravity [Hess, 1979; Hargreaves, 1979]. Reduced height in the F-region is $z = (h - h_r)/H$ and is measured in units of H , where h is the altitude of interest and h_r is a reference height at a fixed boundary within the F2-layer. Equilibrium between sources and sinks of ionospheric plasma are normally in balance, except at sunrise and sunset [Ratcliffe, 1972]. The servo model uses equilibrium conditions to describe F2-peak behavior through a balance of terms in the F-layer continuity equation.

2.3 Chemical Loss in the F2-region

The F2-layer is well above the level of peak solar ionization [Hargreaves, 1979; Rishbeth et al., 1978]. This means the ion production rate q depends on the photochemistry of atomic oxygen and is proportional to $[O]$ and thus proportional to $\exp(-z)$. As stated, β depends on charge exchange reactions of O^+ ions with N_2 and O_2 and is proportional to $[N_2]$ and $[O_2]$ and thus proportional to $\exp(-kz)$, where k is the loss scale height factor. The use of the factor k allows for a scale height ratio adjustment to z , which is measured in units of atomic oxygen scale height H . Since z is measured in terms of H , β can be evaluated at any height in relation to $\exp(-kz)$, rather than use differently based scale heights in N_2 or O_2 . To evaluate k , consider Equation (2) at equilibrium, so that the electron density $N_m \approx q_m/\beta_m$, where m denotes the value at the F2-peak. The loss scale height factor k inversely corresponds to the ratio of N_2 or O_2 scale height to O scale height. This becomes a mass ratio relationship where 1.75 (28/16) corresponds to N_2 loss and 2 (32/16) corresponds to O_2 loss. The value of k varies, depending on loss reactions of O^+ with N_2 and O_2 . The chemical loss process is in two steps, where the first step dominates in the F2-region and the second step involves dissociative recombination reactions of molecular ions with electrons [Hargreaves, 1979; Schunk, 1983; Rees, 1989]. The controlling first step reactions are



where k_1 and k_2 are chemical rate reactions (see Table 1). The reaction rate k_2 given in Table 1 does not take into account the strong dependence on the degree of vibrational excitation of N_2 . Richards and Torr [1986] have shown that this effect is important at solar maximum in the summer and could be important during magnetically active conditions. When both N_2 and O_2 are considered equally important, an average constant for k may be taken as 1.875 [Buonsanto et al., 1989]. A better assumption of the loss scale height factor is to evaluate k as a linear interpolation between loss by N_2 and O_2 . This improves the value of k since molecular concentrations of nitrogen and oxygen vary as well as reaction rates, which both depend on temperature and density [Schunk, 1983]. This improved version of k is used in the USU servo model and is presented in Chapter III, Section 3.1.

2.4 Plasma Diffusion

The concentration of molecular nitrogen and oxygen decreases with height more quickly than atomic oxygen, so that atomic oxygen dominates the F2-region. Plasma in the F2-region is mainly of O^+ ions and electrons. Since the production of O^+ ions depends on $[O]$ and chemical loss depends on $[N_2]$ and $[O_2]$, then the production of electrons would increase indefinitely with height if there is only

loss by chemistry. The F2-peak exists because vertical transport by diffusion becomes important as gas concentrations decrease.

Diffusion of plasma depends mainly on the frequency of collisions between the ions and the neutrals. We neglect electron collisions because of their very small mass. Plasma diffusion is inversely proportional to the collision frequencies of O^+ moving through O, N_2 and O_2 (see Table 2 for collision frequencies). Neutral density decreases exponentially with height, since the F2-region is nearly isothermal [Richmond, 1983]. This means an exponential decrease of collisions, which indicates diffusion is proportional to $\exp(z)$ and becomes the main loss mechanism above the peak. At the peak, time scales for diffusion and chemical loss are approximately equal. For an inclined geomagnetic field at mid-latitudes, these time scales are [Schunk, 1983]

$$\tau_d = \frac{H_p^2}{D_{po} \sin^2 I} \approx \frac{1}{\beta_o} = \tau_c \quad (5)$$

where H_p is the plasma scale height, I is the dip angle between the magnetic field and the horizontal plane and the subscript o denotes any quantity at the balance height. D_p is the plasma diffusion coefficient (also called the ambipolar diffusion coefficient).

A plasma diffuses along magnetic field lines in an ambipolar state called ambipolar diffusion, which may be explained in terms of gravity and an electric field

TABLE 2. Collision Frequencies of O^+ Ions Through O, N_2 and O_2 Neutrals, Adapted from Banks and Kockarts [1973]

Species	$[n], \text{cm}^{-3}; \quad v_{in}, \text{s}^{-1}$
$O^+ \rightarrow O:$	$3.67 \times 10^{-11} [O] T_R^{\frac{1}{2}} \left[1 - 0.0278 \ln(T_R) \right]^2$
$O^+ \rightarrow N_2:$	$6.82 \times 10^{-10} [N_2]$
$O^+ \rightarrow O_2:$	$6.64 \times 10^{-10} [O_2]$
$v_{in} = (O^+ \rightarrow O) + (O^+ \rightarrow N_2) + (O^+ \rightarrow O_2)$	

$T_R = (T_n + T_i)/2$ -- Effective temperature, where T_n and T_i are the neutral and ion temperatures in K.

response. In a plasma, gravity acts to pull the heavier ions away from the electrons. A restoring electric field sets up to lift the ions and depress the electrons. This causes the plasma to behave as though each particle has a mass of $m_p = (m_i + m_e)/2 \approx m_i/2$. The resulting scale height of the plasma is $H_p \approx 2k_b T_p / (m_i g)$, where the plasma temperature $T_p = (T_i + T_e)/2$. The ambipolar diffusion coefficient is $D_p = k_b T_p / (m_i v_{in}) = g H_p / v_{in}$. At diffusive equilibrium, $T_i = T_e = T_n$ and the plasma scale height and ambipolar diffusion coefficient can be replaced with $2H$ and $2D$ [Hargreaves, 1979]. The theoretical RGW servo model makes this assumption for computational convenience. Buonsanto et al. [1989, 1990] established a computational contradiction by using this same assumption for the plasma scale height, while using radar measured ion and electron temperatures to calculate the diffusion coefficient.

Diffusion of plasma along a magnetic field line depends on density and temperature gradients as well as gravity, all acting in the vertical direction [Schunk, 1983]. Plasma is constrained to move along inclined magnetic fields at F-region heights. Equation (6) shows this plasma diffusion dependence for the vertical plasma velocity V_z , introduced in Equation (2) and given as

$$V_z = w - D_p \sin^2 I \left[\frac{1}{N} \frac{dN}{dh} + \frac{1}{T_p} \frac{dT_p}{dh} + \frac{1}{H_p} \right] \quad (6)$$

where w is an applied vertical drift resulting from the meridional neutral wind (neglecting electric field effects). At the F2-peak $dN/dh = 0$. If we assume thermal equilibrium between plasma and neutral temperatures in an isothermal atmosphere, we then have

$$V_{zm} = w - W_{dm} \sin^2 I = w - \frac{g \sin^2 I}{v_m} \quad (7)$$

where the subscript m refers to the current F2-peak height and W_{dm} is the plasma diffusion velocity at h_m . Here, D_{pm} is replaced by gH_p/v_m . Equation (7) does not assume diffusive equilibrium and there is no need for electron temperature. The RGW servo solution uses D_{pm} in its V_{zm} equation and replaces H_p with $2H$. Equation (7) is a more practical form of the peak vertical plasma velocity and is used in the USU servo model.

The ion-neutral collision frequency used in Equation

(7) is taken from Banks and Kockarts [1973] and is given in Table 2. It has recently been shown that the uncertainty in the collision cross-section of $O^+ \rightarrow O$ warrants an increase of 1.7 [Burnside et al., 1987]. This 1.7 increase is used in the USU servo model for applications in this study.

As plasma diffuses along an inclined geomagnetic field line, the horizontal component of the plasma motion will induce a horizontal neutral wind. The time it takes for the plasma to induce a neutral wind depends on the relative densities of the ions and neutrals. The steady-state effectiveness of plasma to induce motion in the neutrals is defined as plasma diffusion efficiency and depends mainly on the magnetic dip angle. Daytime neutral densities are about a 1000 times greater than ion densities in the mid-latitude F2-region [Rishbeth, 1972]. Therefore, downward diffusing ions take about 1000 seconds to induce neutral air motion. The time delay is regarded as a time constant τ_d for ion-neutral momentum transfer. Equation (5) gives this time constant relationship between diffusion and chemical loss.

Figure 3 shows that after steady-state conditions occur, the horizontal component of the plasma diffusion velocity equals the horizontal neutral wind, which is $W_d \cot I$ [Rishbeth and Garriott, 1969]. Before ion-neutral momentum transfer takes place, the vertical component of the plasma diffusion velocity is $W_d \sin I$. As conditions approach steady state, the induced horizontal neutral wind

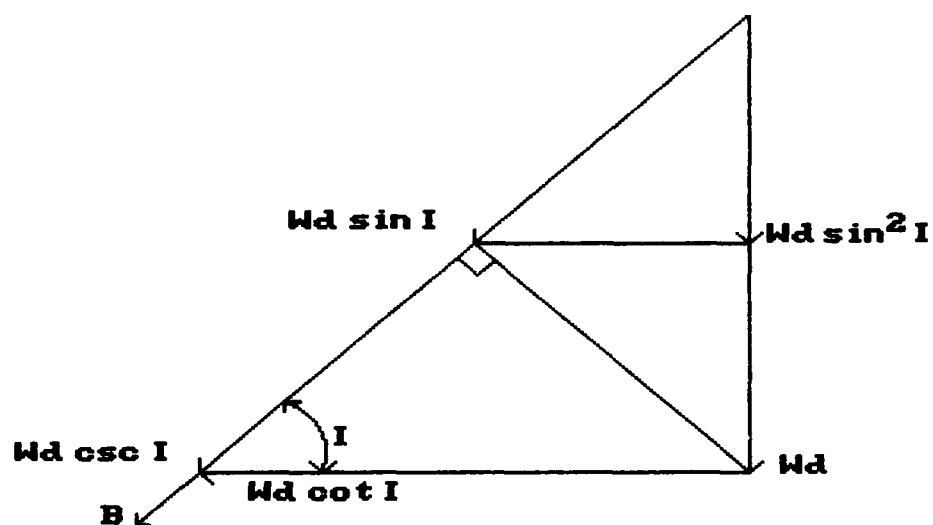


Fig. 3. Plasma diffusion along an inclined geomagnetic field line. At steady state, the horizontal component of plasma motion induces a neutral wind which equals $W_d \cot I$. Adapted from Rishbeth and Garriott [1969].

accelerates the plasma down the field line and the vertical component of the diffusion velocity becomes W_d . W_d is equal to the vertical velocity as would occur if there were no magnetic field.

The balance height in the servo model marks the level of the ionization peak if no ion-neutral momentum transfer has taken place and the neutral atmosphere is at rest. The balance height must take into account plasma diffusion efficiency, which depends mainly on dip angle as shown in Figure 3. A difference in plasma diffusion efficiency changes the balance of O^+ ion loss between diffusion and chemistry. The USU servo model calculates balance height by taking into account plasma diffusion efficiency through a physical process, not an empirical one. Buonsanto et al. [1989] made the comment that "tuning" the servo model physically alters the relative importance of loss by chemical recombination and diffusion. Buonsanto et al. [1989] empirically tuned the servo model from a comparison with radar winds and increased the chemical loss importance in the servo balance height relationship. This tuning was actually found necessary because of the relatively high dip angle at Millstone Hill (71.5°). Tuning the servo model at Millstone Hill compensates for the decreased efficiency of the downward diffusing plasma and produces better agreement between radar and servo model winds.

2.5 Supporting Ionospheric Models

The USU servo model depends on two key inputs to

calculate the meridional neutral wind: hmF2 as a function of time and the state of the neutral atmosphere. The Mass Spectrometer Incoherent Scatter (MSIS-86) neutral atmosphere model [Hedin, 1987] empirically describes neutral temperatures and densities and is used in the USU servo model. The height of the F2-peak is either measured or empirically modeled. The International Reference Ionosphere (IRI) [Bilitza et al., 1987] provides geomagnetically quiet, monthly averages of hmF2 data for the non-auroral ionosphere. IRI hmF2 values are modeled from Comité Consultatif International des Radiocommunications (CCIR) peak density maps. CCIR peak densities are determined from a large worldwide data base of ionosonde critical frequencies and IS radar data using the Bradley and Dudeney [1973] and Bilitza et al. [1979] empirical methods. In using IRI, the USU servo model calculates magnetically quiet, climatological neutral winds for any mid-latitude location, under different solar flux conditions. Both MSIS and IRI can run on IBM compatible personal computers and therefore complement the USU servo model quite well.

The Bradley-Dudeney model is used to determine hmF2 from ionosonde measurements of the ionosphere [Bradley and Dudeney, 1973]. Figure 4 shows the Bradley and Dudeney model ionosphere consisting of parabolic E and F layers with a linear region of electron concentration between them. Three input parameters are required by the Bradley and Dudeney model, which include the critical frequencies

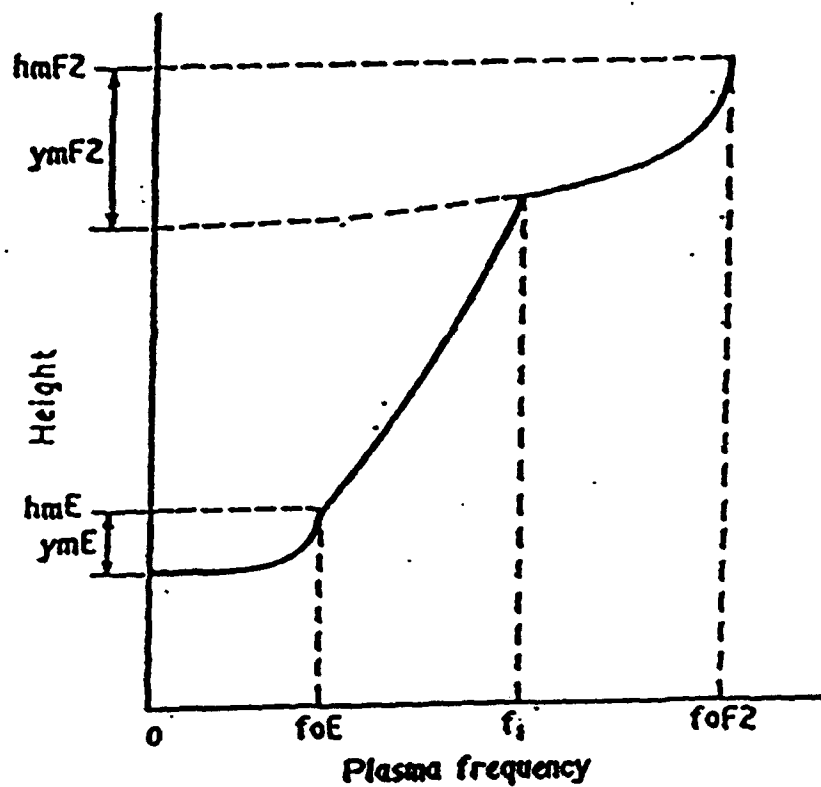


Fig. 4. Bradley-Dudeney model ionosphere. The ordinate and abscissa are linear in height and frequency. Reprinted by permission of Pergamon Press from Bradley and Dudeney [1973].

foE and foF2 and the ionospheric transmission factor $M(3000)F2 = MUF/foF2$. MUF is the maximum usable frequency refracted in the ionosphere, which is received at a distance of 3000 km. These three parameters are routinely measured on a 24-hour basis by more than 126 geographically distributed ionosonde stations. The ionosonde data is stored in the World Data Center at Boulder, Colorado, where it is made available to the scientific community.

The calculation of hmF2 from the Bradley and Dudeney model is restricted to the ratio of foF2 to foE greater than 1.7. At night, when the E-region has decayed away or during periods of sporadic E, the values of foE in this investigation are approximated from the IRI model densities, so that $foE = 9 \times 10^{-3} (NmE)^{\frac{1}{2}}$, where NmE is the electron number density at the E-peak layer height [Chen, 1984].

Estimated errors of hmF2 from the Bradley and Dudeney model are on the order of ± 10 km [Bradley and Dudeney, 1973; Dudeney, 1983] for the quiet daytime, mid-latitude ionosphere. Nighttime estimated errors are expected to be larger, due to the estimated values of foE. A recent study by Berkey and Stonehocker [1989] found errors of less than ± 5 km using the Bradley and Dudeney method in 27 hours of quiet data. Another recent investigation by Sica et al. [1990] concluded that for quiet periods, estimates of hmF2 from ionosonde data may have uncertainties of ± 20 km. Errors as great as ± 20 km could have a significant effect

on neutral wind calculations. More work is needed to accurately determine and reduce uncertainties in hmF2, which makes neutral wind calculations more viable.

The Field Line Interhemispheric-Plasma (FLIP) ionospheric model [Richards and Torr, 1985, 1988] is used to study the servo model balance relationship. The FLIP is a one-dimensional model, which uses a centered dipole approximation for the geomagnetic field and calculates plasma densities and temperatures along an entire geomagnetic flux tube from 80 km in the northern hemisphere through the plasmasphere to 80 km in the southern hemisphere. The continuity and momentum equations are solved for O^+ , H^+ and He^+ ions and includes ion-neutral collisions for momentum transfer in the E and F-regions. Since the FLIP is a one-dimensional model, it treats neutral density as a known quantity and assumes hydrostatic balance, adopting MSIS as its neutral atmosphere. The FLIP model requires an input of the meridional neutral wind, which it normally calculates by the Miller et al. [1986] method. For this study, a zero wind is input into FLIP so that balance heights (h_o) are calculated. Known diurnal patterns of FLIP model h_o values are used to study servo h_o values, to make the USU servo model physically more realistic.

CHAPTER III

METHOD

3.1 USU Servo Model Development

The servo model was originally presented by Rishbeth [1967] and explicitly derived again by Rishbeth, Ganguly and Walker [Rishbeth et al., 1978]. The development here uses the original RGW equations and concepts to develop a physically improved model to calculate the meridional neutral winds. The RGW servo model was originally developed for a theoretical investigation of F2-peak response to applied forces. Since the investigation was theoretical, Rishbeth et al. [1978] assumed diffusive equilibrium and constant values for several of the parameters for computational convenience. In order to use the servo model in a practical way, i.e. to use measured or empirical data to describe the dynamic behavior of the "real" neutral atmosphere, I have modified some of the RGW equations presented in this study.

The USU servo model is developed from an outline of the following principles, which describes the F2-layer as it responds to height changes in its peak electron density:

1. With no applied vertical drift, the F2-peak lies at a balance height h_0 , where the plasma diffusion time scale equals the chemical loss time scale of O^+ ions.
2. An applied meridional neutral wind (electric field effects are neglected) shifts h_0 to a new level.

3. At any instant, the actual F2-peak tries to maintain a balance of diffusion and chemical loss, with an exponential time constant.

4. The loss scale height factor is a function of time, since reaction rates and neutral densities are a function of time, i.e. $k = k(t)$.

5. The O^+ scale height is a function of time and, to a much lesser extent, location. Temperature varies with time and gravity varies with latitude (gravity is computed at an F2-layer reference height), i.e. $H = H(t, g)$.

The USU servo model interpolates the loss scale height factor k from the loss of O^+ with N_2 and O_2 between chemical reaction Equations (3) and (4). This linear interpolation equation is given as (see Table 1)

$$k = \left[\frac{k_1/k_2}{k_1/k_2 + [N_2]/[O_2]} \right] \times 0.25 + 1.75 \quad (8)$$

Figure 5 shows mid-latitude variations of calculated k values using Equation (8) for low, medium and high 10.7 cm solar flux. Neutral densities and reactions are based on MSIS-86 [Hedin, 1987]. The value of k changes mainly on a diurnal cycle, but Figure 5 shows that k also depends on changes in the neutral atmosphere during a solar cycle. Variations in k would approximate the same changes as shown in Figure 5, which would reflect changes in neutral densities and rate reactions as other ionospheric parameters are allowed to vary. The variation of k of about 1.3%, shown

k/Solar Flux Comparison

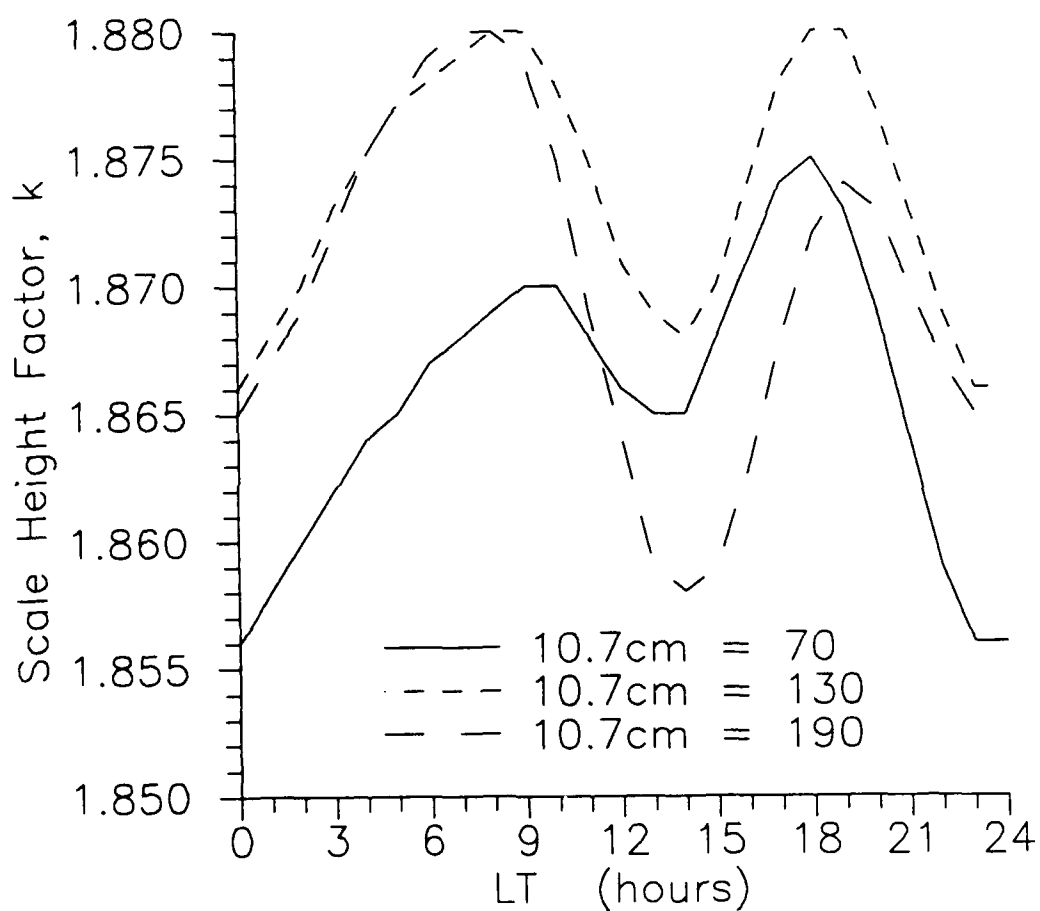


Fig. 5. January mid-latitude variations of loss scale height factor k for low, medium, and high solar flux of 70, 130 and 190 s.f.u. ($10^{-22} \text{ W m}^{-2} \text{ Hz}^{-1}$).

in Figure 5, would result in a variation of about 5 to 10% in the derived neutral winds. Values of k approximate 1.875 [Buonsanto et al., 1989], but Figure 5 indicates that k is variable and should be adjusted for different diurnal and ionospheric conditions.

3.1.1 Model Equations. The USU servo model equations are based on the RGW servo model [Rishbeth et al., 1978]. Some of the RGW servo concepts and solutions are reproduced here for clarity and for further development and discussion. A complete derivation of the servo equations are presented by Rishbeth et al. [1978] and compliment the USU servo model development presented here.

We begin the derivation by multiplying the F-layer continuity Equation (2) by H and integrating from the F2-peak to the top of the ionosphere. For this evaluation, let the reduced height be $z = (h - h_0)/H$, where h_0 is the balance height. At the F2-peak, $z = z_m$. This implies that $z_m = (h_m - h_0)/H$, so if $z_m = 0$ then the F2-peak lies at the balance height: Thus we do not apply a drift. The resulting equation is then

$$H \frac{\partial}{\partial t} \int_{z_m}^{\infty} N dz = H \int_{z_m}^{\infty} (q - \beta N) dz - \Phi_{\infty} + N_m (V_{zm} - H dz_m/dt) \quad (9)$$

where $N_m (V_{zm} - H dz_m/dt)$ is the relative vertical plasma flux at the F2-peak and Φ_{∞} is the vertically upward plasma flux at the top of the ionosphere and equal to the limiting value of NV_z . Consider the following RGW assumptions to

evaluate Equation (9):

1. The electron density profile above the F2-peak decays at the same rate as the peak electron density $N_m F2$, i.e. the height-integrated ion content is $\alpha H N_m$. The topside shape factor α is defined as [Melendez-Alvira, 1990]

$$\alpha \equiv \frac{1}{N_m} \int_{z_m}^{\infty} N(z) dz \quad (10)$$

The topside layer remains at a constant shape given by the Chapman alpha layer as $\alpha = 2.82$ and is used in the USU servo model.

2. The F2-peak is well above the level of peak production, so $q(z) = q_m \exp(-z)$.

3. The linear loss coefficient, β is proportional to $\exp(-kz)$, where k is the loss scale height factor depended on the dominant ion O^+ chemical reactions with N_2 and O_2 , given by Equation (8). The chemical loss rate of the electron density profile above the peak is $\beta N(z) \approx \beta_m N_m \exp(-kz)$.

We now integrate Equation (9) and get

$$\alpha H \frac{dN_m}{dt} = q_m H - \frac{\beta_m N_m H}{k} - \Phi_{\infty} + N_m (V_{zm} - H dz_m/dt) \quad (11)$$

The peak vertical plasma velocity, V_{zm} in Equation (11) is replaced by $w - (g/v_m) \sin^2 I$ from Equation (7). By replacing V_{zm} with Equation (7) there is no need for electron temperature (see Table 2 for collision frequency). Equation (7) does not assume diffusive equilibrium and is more practical to use than the original RGW servo solution,

which is $V_{zm} = w - (D_{pm}/2H)\sin^2 I$. We therefore substitute Equation (7) into (11), divide through by $N_m H$ and then rearrange to get

$$\frac{dz_m}{dt} = \frac{q_m - \Phi_\infty/H}{N_m} - \frac{\alpha}{N_m} \frac{dN_m}{dt} - \frac{\beta_m}{k} - \frac{g \sin^2 I}{v_m H} + \frac{w}{H} \quad (12)$$

An approximate F-layer continuity equation for the peak electron density, introduced by Rishbeth et al. [1978], is quite useful in getting a reasonable solution to Equation (12). We assume that any flux contributions from the top of the ionosphere is evenly distributed over the equivalent thickness αH of the topside layer. This continuity approximation is

$$\frac{dN_m}{dt} = q_m - c\beta_m N_m - \frac{\Phi_\infty}{\alpha H} \quad (13)$$

The coefficient c in Equation (13) is empirical of order unity and is introduced to take account of transport processes at the peak [Rishbeth et al., 1978]. This coefficient was first presented and used in Rishbeth's servo model equations in 1967. It is also part of the proportionality constant used to make the diffusion and chemical loss time scales equal at the balance height.

To continue the model development, we substitute Equation (13) for dN_m/dt in Equation (12) giving

$$\frac{dz_m}{dt} = (1 - \alpha) \frac{q_m}{N_m} + \frac{kac - 1}{k} \beta_m - \frac{g \sin^2 I}{v_m H} + \frac{w}{H} \quad (14)$$

Equation (14) is actually a generalized form of the final servo equation. To be useful, we need to make a diurnal evaluation of Equation (14).

3.1.2 Daytime. The daytime balance relationship between diffusion and chemistry is found from Equation (14), where $w = 0$ and $dz_m/dt = 0$. Assuming the change in peak electron density is slow during the day ($dN_m/dt = 0$ at equilibrium), an equilibrium approximation for the peak production from Equation (13) is

$$q_m = c_d \beta_m N_m + \frac{\phi_\infty}{\alpha H} \quad (15)$$

The subscript d is meant to indicate that c_d is a daytime derivative of the diurnal coefficient c . Now, assume ion production and chemistry dominate the daytime vertical plasma flux, so a balance relationship between β_0 and v_0 from Equation (14) gives

$$\beta_0 = \frac{k}{kc_d - 1} \frac{g \sin^2 I}{v_0 H} \quad (16)$$

When using measured hmF2 data from ionosondes, the resolution is too poor to determine an adequate layer height response with respect to time. This implies a steady state plasma drift assumption, where $dz_m/dt = 0$. This assumption does not greatly affect the overall calculation of the plasma drift [Buonsanto et al., 1989]. In fact, studies show w as mainly linear with respect to changes in layer height, especially if the drifts are small

[Rishbeth et al., 1978; Miller et al., 1986; Buonsanto et al., 1989]. If we do not neglect Φ_∞ in Equation (14), we can substitute Equation (15) for q_m in Equation (14) and solve for w to get the daytime plasma drift as

$$w = \frac{g \sin^2 I}{v_m} + H \left[\frac{\beta_m(1 - c_d k)}{k} + \frac{\Phi_\infty(\alpha - 1)}{\alpha H N_m} \right] \quad (17)$$

We find values for β_m and v_m by assuming $\beta_m = \beta_r \exp(-kz_{mr})$ and $v_m = v_r \exp(-z_{mr})$, where $z_{mr} = (h_m - h_r)/H$ and h_r is a convenient reference height within the F2-region. To use Equation (17), we can neglect the flux term, but we need to know c_d from the balance relationship in Equation (16).

Consider the plasma exchange boundary flux through the top of the ionosphere and recall that $\Phi_\infty/\alpha H$ assumes the flux is equally distributed throughout a layer thickness of αH . This indicates that there is no localized flux differences in the ionosphere/plasmasphere boundary allowed in this model. This means w should be insensitive to Φ_∞ unless the ratio of the exchange flux to N_m is very large. This argument is understood by examining the flux term in Equation (17). Compare a typical flux value used by Rishbeth et al. [1978] of $\Phi_\infty \approx 1.4 \times 10^{11} \text{ m}^{-2} \text{ s}^{-1}$ to a typical daytime value of $N_m \approx 1 \times 10^{12} \text{ m}^{-3}$ [Hargreaves, 1979]. In this case, less than a meter per second is contributed to w from flux effects, leading to the conclusion that daytime Φ_∞ can be neglected.

One final note is the use of a servo analysis in

finding a value for Φ_{∞} from a neutral wind. Due to the uncertainties in the servo equation parameters and the large daytime insensitivity of w to a change in Φ_{∞} , it seems doubtful that any accurate value of the topside flux can be ascertained. Yet an upward/downward flux sense may be found. This type of study was successfully done using a similar servo equation by Buonsanto [1986], relating daytime boundary flux comparisons to seasonal change.

If we solve Equation (16) for c_d and substitute the result into Equation (17) with $\Phi_{\infty} = 0$, our result becomes Equation (18). Since we used Equation (7) for the replacement of V_{zm} in Equation (11), Equation (18) does not assume diffusive equilibrium and does not need electron temperature for the calculation of w . Equation (18) is a similar form of the RGW servo equation used by Buonsanto et al. [1989]. Equation (19) is a linear form of Equation (18), which gives results that are approximately the same as the results from the nonlinear Equation (18) [Rishbeth et al., 1978; Buonsanto et al., 1989]. These equations are

$$w = \frac{g \sin^2 I}{v_o} [\exp(z_m) - \exp(-kz_m)] \quad (18)$$

$$w \approx = \frac{g \sin^2 I}{v_o} z_m(k + 1) \quad (19)$$

where again $z_m = (h_m - h_o)/H$. To calculate w from Equation (18) or (19), we must find the balance height instead of c_d , as in Equation (17). From the balance height, we can

calculate v_o and z_m to compute the plasma drift.

Equation (16) provides the means to derive the USU servo balance height. It is convenient to use an F2-region reference height, where $\beta_o = \beta_r \exp(-kz_{or})$ and $v_o = v_r \exp(-z_{or})$ and where $z_{or} = (h_o - h_r)/H$. Using Equation (16) to relate v_o to β_o gives the servo balance height

$$h_o = h_r + \frac{H}{(k + 1)} \ln \left[\frac{H\beta_r v_r (kc_x - 1)}{kg \sin^2(I)} \right] \quad (20)$$

where c_x is used instead of c_d to indicate that this coefficient is variable. The variation of c_x is mainly diurnal, but it also changes with location or ionospheric conditions. To calculate c_x , we can use either of the two following equivalent equations

$$c_x = \frac{g \sin^2 I}{H\beta_r v_r} \exp \left[\frac{(h_o - h_r)(k + 1)}{H} \right] + 1/k \quad (21)$$

$$c_x = \frac{g \sin^2 I}{H\beta_o v_o} + 1/k \quad (22)$$

We can use FLIP model balance heights to study the variation of c_x and calculate balance heights for different ionospheric conditions and locations. Adjusting the value of c_x is what Buonsanto et al. [1989, 1990] describes as tuning the servo model.

3.1.3 Nighttime. The nighttime balance relationship between β_o and v_o is different from daytime, since $q_m = 0$

in Equation (14). The same procedures used to find the daytime balance Equation (16) are used for a nighttime balance relationship, with the result that

$$\beta_o = \frac{k}{k\alpha c_n - 1} \frac{g \sin^2 I}{v_o H} \quad (23)$$

The added feature of the topside shape factor α appears at night and causes the night balance heights to rise about half a scale height above the day balance heights. Here, the subscript n in c_n denotes night, where c_n is slightly larger than c_d . The value of c_x in Equation (20) contains α when night occurs, so that $c_x = c_d$ during the day and $c_x = \alpha c_n$ at night. Over a 24 hour period a typical range for c_x is about 1.3 for day to about 5.0 for night.

To derive a nighttime plasma drift, we use the same procedures as with the daytime Equation (17). We use nighttime values in Equation (14), namely $q_m = 0$, to get

$$w = \frac{g \sin^2 I}{v_m} + \frac{H\beta_m(1 - k\alpha c_n)}{k} \quad (24)$$

If we solve Equation (23) for αc_n and substitute the result into Equation (24), our result becomes Equation (18). This makes Equations (18) or (19) the more convenient forms, since we can use them for day or night plasma drift calculations. The servo equations so far developed are specifically for either day or night and therefore a method is required to determine the diurnal behavior of c_x . We can then calculate the plasma drift for day and night as well

as the morning and evening transitions.

3.1.4 Twilight Assumptions. To find values of c_x for the morning and evening, one must define when the morning and evening periods begin and end in terms of solar zenith angle X . Rishbeth [1967] arbitrarily chose limits of the transitions to be 96° and 82° for morning and evening. When calculating c_x from FLIP model balance heights, it is found that the boundary limits for X are closer to 102° and 82° . Another method in finding the approximate F-region transition limits is to use the aid of the IRI model. By noting the time of decay and building of the E-layer, it is found that the limits are also closer to 102° and 82° . One other method will get an approximate value for X , in relation to when the F2-region may "turn on and off." Assume the Sun's rays are straight and parallel, so a relationship involving the Earth's radius, height above the Earth's surface and X is $R/(h_r + R) = \sin(180^\circ - X)$, where R is the Earth's radius and h_r is a reference height. From a typical F2-layer height of 300 km and $R = 6370$ km, the Sun's rays first affect the F2-region when $X \approx 107^\circ$. This simple analysis does not take into account ionizing efficiency, absorption cross-sections, solar intensity or any other feature which may affect when morning begins or evening ends. This analysis does give an indication of what the upper boundary should be and tends to support an upper limit of 102° versus 96° .

Given the above arguments a diurnal pattern is broken into four periods:

1. Morning $102^\circ > X > 82^\circ$, X decreasing;
2. Day $X < 82^\circ$;
3. Evening $82^\circ < X < 102^\circ$, X increasing;
4. Night $X > 102^\circ$ and $q_m = 0$.

Mornings and evenings tend to last about 2 hours at mid-latitudes. These twilight period limits make it possible to describe day and night balance height relationships.

The next problem is to determine a discontinuity function for c_x based on the defined solar zenith angle transition limits. Rather than use a Chapman function for the transitions [Buonsanto et al., 1990], the FLIP model is used to analyze a twilight discontinuity pattern for different ionospheric conditions and locations. Figure 6 shows a calculated diurnal pattern of c_x values from FLIP and USU servo model balance heights. Transition assumptions, as given above, are used in the servo calculation and show agreement with the FLIP model.

Figure 6 also indicates that morning and evening transitions are approximately linear with time between day and night. The c_x diurnal pattern for morning transitions are more abrupt than evening transitions. A sharp drop in c_x occurs during the first hour of the morning, nearly reaching a daytime value. This seems physically plausible considering the nighttime decay of ionization. With the advent of morning, production dominates and the ionosphere

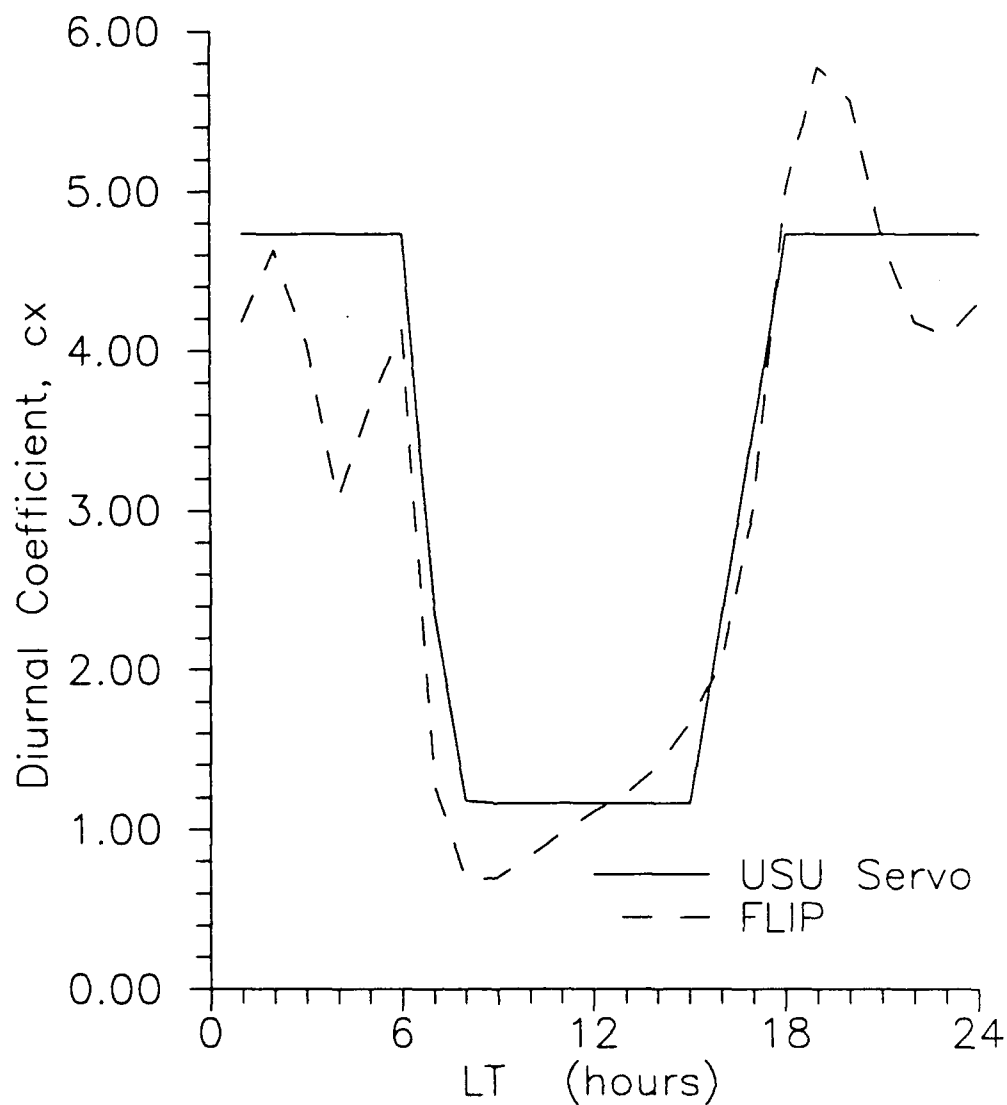
USU Servo/FLIP c_x Comparison

Fig. 6. USU servo and FLIP model comparisons of the diurnal coefficient c_x for a January, mid-latitude location. This figure shows agreement between the FLIP and USU servo models for F-region morning and evening transitions.

is literally "turned on." At evening there is a more gradual decay of the ionosphere, which continues at night in a shape preserving manner [Rishbeth and Garriott, 1969].

A final note about the transition periods is that equilibrium no longer applies, which is a major assumption in the derivation of the servo model. Uncertainties are largest during twilight periods due to rapidly changing conditions. A 20% uncertainty in c_x , which is similar to differences shown in Figure 6, results in about a 12% uncertainty in the derived neutral wind speeds.

3.1.5 Balance Height Adjustment. The empirical value for the diurnal coefficient c in Equation (13) was adjusted by Buonsanto et al. [1989; 1990] to "tune" the servo model winds to Millstone IS radar winds. For equal loss of O^+ with O_2 and N_2 , c is usually taken from Rishbeth as $c_d = 1.33$ and $c_n = 1.73$ [Rishbeth, 1967; Buonsanto et al., 1989, 1990]. Rishbeth [1967] used empirically derived values of c for a dip angle of 45° , which were found to be appropriate for Arecibo ($I = 48.5^\circ$) [Rishbeth, 1967; Rishbeth et al., 1978; Ganguly et al., 1980; Melendez-Alvira, 1990].

Tuning the servo model by adjusting c physically alters the balance height, where O^+ loss by diffusion and chemistry is equally important. Buonsanto et al. [1989, 1990] found it necessary to decrease c , which decreases the balance height, making diffusive loss of O^+ less important at Millstone Hill ($I = 71.5^\circ$). The reason for servo model

tuning stems from a difference in plasma diffusion efficiency, which is mainly dependent on dip angle (see Figure 3). Horizontal neutral wind motion induced by ion-neutral collisions is depended on plasma diffusion efficiency. Adjusting the value of c alters the diffusion transport effects in Equation (13), which leads to a change in balance height. Tuning is therefore a way to correct or adjust the balance height for differences in plasma diffusion efficiency.

Instead of tuning the value of c , the USU servo model adjusts h_0 based on the boundary conditions that during the day $c = c_d = 1$ and at night $c = c_n = 1.3$, at a dip angle of 90° . These boundary conditions are determined by using the continuity Equation (13) for equilibrium conditions. At $I = 90^\circ$, where diffusive ion-momentum transfer to the neutrals is zero, $q_m = \beta_m N_m$ during the day and therefore $c = c_d = 1$. We assume a nighttime boundary by a comparative linear regression using the Rishbeth [1967] values, where $1.33(.75) = 1$ and $1.73(.75) = 1.3$. The value of h_0 is then found by the following equation [Rishbeth et al., 1978]

$$h_0 = h_{obc} - \frac{H \ln(\sin^2 I)}{k + 1} \quad (25)$$

where h_{obc} is the boundary condition balance height calculated from Equation (20). In Equation (20), the boundary conditions for day/night are thus: $c_x = c_d = 1$ and $c_x = \alpha c_n = (2.82)(1.3)$.

Equation (25) is developed from Equation (18). In Equation (18), w corresponds to a steady-state difference of plasma diffusion velocity, where $W_d \sin^2 I$ occurs before ion-neutral momentum transfer takes place and W_d occurs after steady-state conditions apply, with an induced horizontal neutral wind of $W_d \cot I$ (see Figure 3). At the boundary condition of $I = 90^\circ$, $h_o = h_{obc}$. The term $(H) \ln(\sin^2 I) / k + 1$ is negative and allows for an increase in balance height to compensate for increased plasma diffusion efficiency at smaller dip angles. When we adjust h_o from Equation (25) for a decrease in dip angle and input the resulting h_o back into Equation (21) or (22) to calculate c_x , we find that c_x becomes larger than the value used to calculate h_{obc} . Larger c_x values produce higher h_o altitudes because diffusion becomes more important.

The calculation of new c_x values are not implemented in the USU servo model unless further adjustment is required to c_x , as will be discussed in Section 3.1.7. If c_x values are adjusted, then we calculate the final h_o values with Equation (20).

It is useful to compare calculated c_x values with radar-tuned values or FLIP c_x values for the same location and ionospheric conditions. Figure 6 is one example, which illustrates a comparison between adjusted servo c_x values and calculated FLIP c_x values.

The benefit of tuning or adjusting the servo model becomes significant with changes in dip angle or large

changes in ionospheric conditions. Buonsanto et al. [1989] showed that tuning the servo model at Millstone Hill resulted in a change in neutral wind by as much as 29 m s^{-1} , which was about a 35% change in the derived wind. By using Equation (25), the USU servo model is self adjusting and can be used for any mid-latitude location, under different ionospheric conditions, without the burden of tuning.

3.1.6 Topside Shape Factor. The topside ionosphere extends from the F2-peak to the ionosphere/plasmasphere boundary (800 - 1000 km) [Schunk, 1983; Moyer, 1976]. We assume the nighttime decay of the topside electron density profile occurs at the same rate of decay as NmF2, where a "shape preserving" solution of the diffusion equation is given as [Rishbeth and Garriott, 1969]

$$N(z,t) = N_r(z) \exp(-\beta' t) \quad (26)$$

We evaluate the effective chemical decay time coefficient β' by using Equation (13) with $q_m = 0$ and assuming that chemical loss at the peak dominates vertical plasma flux effects, so that

$$\frac{dN_m}{dt} = -c_n \beta_m N_m \rightarrow N_m(t) = N_m(0) \exp(-c_n \beta_m t) \quad (27)$$

For an equivalent rate of decay for the topside ionosphere and NmF2, it is apparent from Equations (26) and (27) that $\beta' = c_n \beta_m$.

Transport effects from c in Equation (13) are related

to the topside decay rate. We can compare the numerical values of c_n to c_d by qualitatively comparing nighttime and daytime decay rates, used to adjust β_m to acquire an effective decay coefficient β' . The effective decay decreases during the day, approaching β_m , because the ion production is most rapid below the F2-peak and ceases at night. The value of β' is increased at night to compensate for the decrease of β_m at a higher nighttime balance height, with $q_m = 0$: Hence c_d is numerically less than c_n .

The USU servo model assumes a topside shape factor α of 2.82, from the Chapman alpha layer solution [Rishbeth et al., 1978]. Comparisons of c_x values from the FLIP model shows that an assumption of $\alpha = 2.82$ is reasonable. The combination of αc_n is included in the c_x calculations from the FLIP model. Keeping α apart from c_n is useful, since any variability of c_x from FLIP calculations is attributed to either α or c_n for future study.

The assumption that vertical plasma flux effects are negligible in the nighttime decay of the topside ionosphere may warrant further scrutiny. A recent paper by Sica and Schunk [1990] shows that the ionosphere/plasmasphere vertical boundary flux Φ_∞ is important in finding the nighttime height of the F2-peak. If Φ_∞ can appreciably change the topside shape, then a relationship may exist between Φ_∞ and α . As an example, after a geomagnetic storm, upward plasma flux tends to refill the depleted plasmasphere from the topside ionosphere [Hargreaves, 1979; Sica and Schunk,

1990]. Slab thickness, which is a ratio measurement of ion content to NmF2, significantly increases for a few days after a storm and is an indication of upward plasma flow [Hargreaves, 1979]. Slab thickness is related to the topside shape factor, as indicated in Equation (10). An expected increase should then occur in α after a storm event. If α is allowed to increase, then h_o from Equation (20) will increase, implying hmF2 should also increase at night. This is the result shown by Sica and Schunk [1990], where a constant upward plasma flux raises the nighttime F2-peak by as much as 30 km, if holding NmF2 constant.

The implication is that perhaps there is a relationship between the topside shape, which can be measured by IS radar and vertical plasma flux, which is usually measured by satellite or calculated by a comprehensive plasma model. Still, h_o is not very sensitive to an increase in topside shape factor, where a factor of 3 increase in α is needed to increase h_o by about 30 km. The reason for this relatively large increase in α is probably from the assumption that NmF2 decays at the same rate as the topside electron density profile, which is physically more realistic than holding NmF2 constant. Future studies with c_x may show how nighttime plasma flux changes the decay rate of the F2-peak. This may then lead to a way to approximate vertical plasma exchange flux from calculations of $c_x = \alpha c_n$ using ground based measurements.

3.1.7 Daytime Steady Rate Assumption. During the day, the flux term in Equation (13) is normally neglected, since production and chemistry dominate. Under steady-state conditions, $q_m = c_d \beta_m N_m$. As shown in Figure 6 and again in Figure 7, the FLIP model c_x value has a fairly linear daytime slope. Earlier servo models assume daytime steady-state conditions of $c_x = c_d = \text{constant}$. Actually, the condition $q_m = c_d \beta_m N_m$ occurs close to solar noon, where $dN_m/dt = 0$. Before solar noon, ion production is greater than loss and $dN_m/dt > 0$. After solar noon $dN_m/dt < 0$. Thus $q_m > c_d \beta_m N_m$ before noon and $q_m < c_d \beta_m N_m$ after noon.

To correct for the steady-state assumption, the USU servo model has an option of assuming a daytime steady-rate, where $c_d = c_d(t)$. The FLIP model calculation of c_x indicates that $c_d(t)$ changes linearly with time, so we may assume a steady rate. This means that $q_m = c_d(t) \beta_m N_m$, where $dN_m/dt = 0$ for the entire day. Figure 7a shows how a steady-state assumption compares with the FLIP results during January at a mid-latitude location. Compare the daytime and nighttime deviations between FLIP and USU servo c_x values and note the larger deviation in day and night balance heights. This is because daytime c_x values are close to unity and therefore the percent change in c_x during the day are relatively large compared with the percent differences of the nighttime c_x values, where $c_x = \alpha c_n$. This justifies the need to model the daytime c_x pattern and assume a steady rate of change instead of a

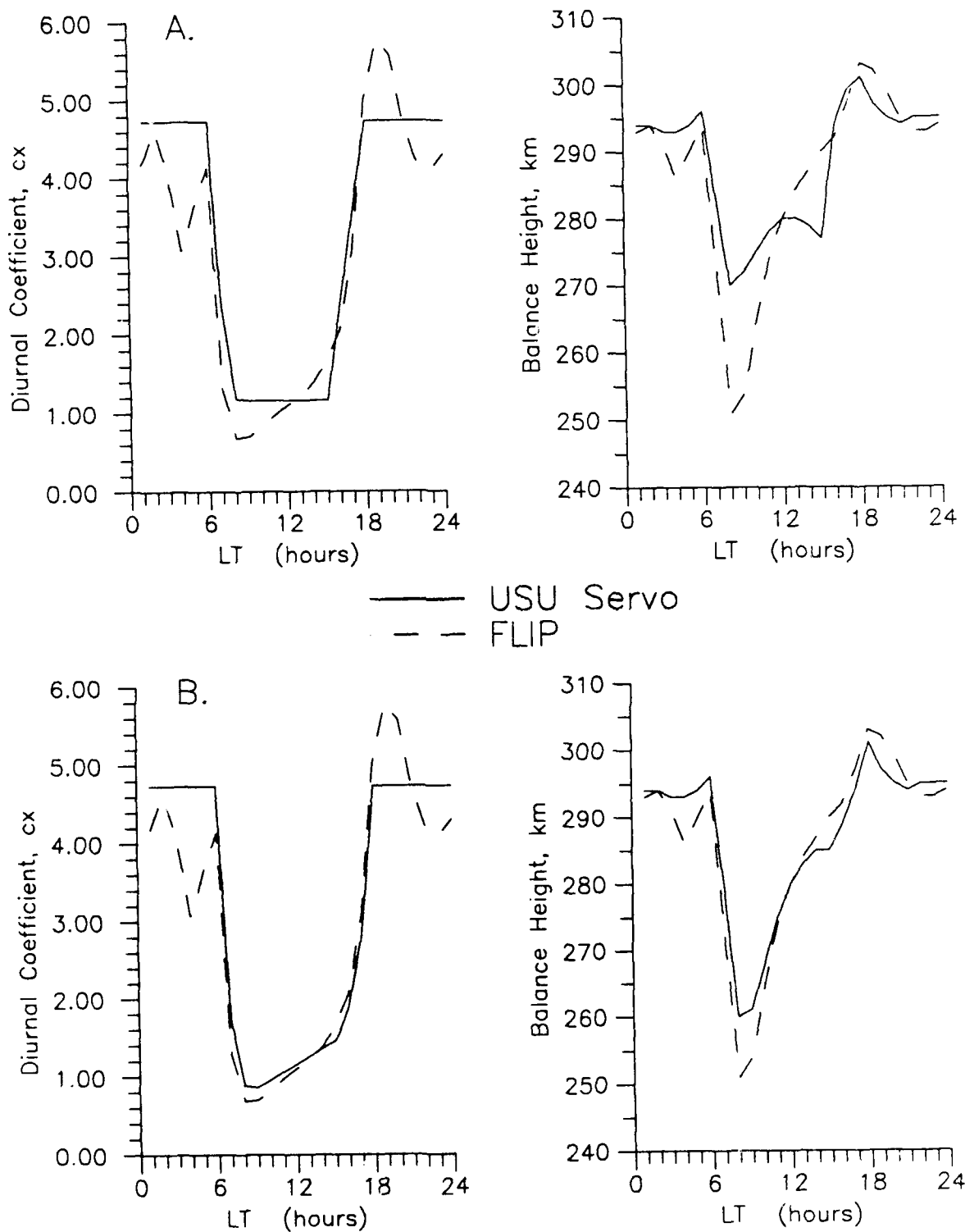


Fig. 7. USU servo and FLIP model comparisons of diurnal coefficient c_x and corresponding balance heights h_0 for a January, mid-latitude location. Figure 7a and 7b shows differences in c_x and h_0 comparisons during steady-state assumption (7a) and steady-rate assumption (7b).

constant value as in a steady-state assumption. Figure 7 indicates that a 30% difference between FLIP and USU servo daytime c_x values will result in about a 15 km difference in balance height, which translates to about a 14 m s^{-1} difference in neutral wind. To decrease the FLIP/USU servo difference in c_x , Figure 7b assumes a daytime steady-rate increase of 0.1 per hour in $c_d(t)$, with the boundary condition that $c_d = c_{ds}$ at solar noon, where c_{ds} is the steady-state value of c_d , as shown in Figure 7a. The result is a better match of servo daytime h_o with FLIP h_o .

The assumption of a daytime steady rate for c_d is a type of servo "fine tuning." The USU servo model makes this tuning optional. Daytime steady-rate slope values should range from zero (high solar radiation) to just over 0.1/hr (low solar radiation). FLIP model runs indicate that the daytime slope depends on the amount of solar radiation available for ionization production. The slope is close to zero for low geographic latitudes during high solar flux conditions. This indicates that steady-state assumptions are valid provided there is sufficient plasma production, e.g. in the summer hemisphere.

3.1.8 Neutral Wind. Once the vertically applied plasma drift w is found from Equation (18) or (19), the USU servo model calculates the meridional neutral wind from

$$U_p = \frac{-w}{\cos I \sin I} \quad (28)$$

where U_p is the poleward meridional neutral wind. Equation (28) assumes the total plasma drift w is due to the neutral wind. In general, w is produced by both the neutral wind and electric field. If the electric field is not neglected, then a more general equation for the upward plasma drift is

$$w = V_{\perp p} \cos I - U_p \cos I \sin I \quad (29)$$

where $V_{\perp p}$ is the ion drift velocity component, perpendicular to the geomagnetic field, in the poleward direction, and is caused by an eastward electric field (Electric field effects are explained in Section 2.1). For quiet to moderate geomagnetic conditions, the first term in Equation (29) can generally be neglected, leading to Equation (28).

Equation (28) is actually preferred for many ionospheric modeling applications. This is because the parameter of interest is the vertical ion drift, regardless of how that ion drift is produced. [Richards, P. G., An Improved Algorithm for Determining Neutral Winds from the Height of the F2-peak Electron Density, Submitted to J. Geophys. Res., January, 1991].

3.2 Model Program Outline

This section summarizes the equations, parameters and procedures used in the USU servo model program. The following steps are presented and explained in sequence and meant as a guide for programming:

1. Enter the location parameters; name, geographic latitude, longitude and dip angle (USU servo model calculates an optional centered dipole dip angle).

2. Enter the date. Solar zenith angles (X) are calculated from the date, and geographic coordinates, which are based on local or universal time [Blackadar, 1989].

3. Enter the optional value for the daytime steady-rate, which is the change in c_d per hour, or else a zero slope is used for steady-state approximation (c_d remains constant).

4. Input MSIS neutral atmospheric data at an F2-region reference height h_r (normally 300 km). This may be entered as an input data file or MSIS may be called as a subprogram.

5. Input hmF2 data file. Here the IRI may be used as an hmF2 data source from a file or subprogram.

6. Input optional ion temperature data or make a ratio assumption. The USU servo model assumes $T_i = 1.1T_n$ during the day, $T_i = 1.05T_n$ for morning or evening and $T_i = T_n$ at night.

7. Input a program routine to find when the day begins and ends based on X . This step is only needed if a daytime steady-rate was entered other than zero to change c_d , so that c_d is not constant (step 3).

8. The program determines diurnal periods of day, night, morning and evening based on X , where limits are 102° and 82° .

9. At h_r , calculate chemical reaction rates k_1 and k_2 , given in Table 1.
10. At h_r , calculate loss scale height factor k from Equation (8).
11. At h_r , and geographic latitude calculate gravity.
12. At h_r , calculate O^+ scale height H .
13. At h_r , calculate linear loss coefficient, introduced in Section 2.2 as $\beta_r = k_1[O_2] + k_2[N_2]$.
14. At h_r , calculate ion-neutral collision frequency ν_r , given in Table 2.
15. Use Equation (20) to calculate the boundary condition balance height h_{obc} . Use $c_x = c_d = 1$ and $c_x = \alpha c_n = (2.82)(1.3)$. For twilight periods, linear interpolate c_x between c_d and αc_n with time.
16. Use Equation (25) to calculate h_o .
17. Use Equation (21) to calculate the servo diurnal coefficients c_x , which are now "tuned" with an h_o input.
18. If the daytime slope from step 3 is not equal to zero, then recalculate $c_d = c_d(t)$. From step 17, $c_x = c_d = c_{ds}$, where c_{ds} is a constant steady-state value. Assume the boundary condition that $c_d(t) = c_{ds}$ at solar noon, which is the lowest x value. Begin to recalculate $c_d(t)$ when the day period first begins and add the slope value per hour so as to pass through c_{ds} at solar noon and end when the day period ends. This is a linear change in the daytime diurnal coefficient with time.
19. If the daytime slope is not equal to zero, then

use Equation (20) to recalculate h_o with tuned c_x values calculated from steps 17 and 18.

20. With final h_o values, calculate the ion-neutral collision frequency at h_o , where $\nu_o = \nu_r \exp(-z_{or})$ and $z_{or} = (h_o - h_r)/H$.

21. Use Equation (18) or (19) to calculate the vertical plasma drift w .

22. Use Equation (28) to calculate the meridional neutral wind U .

23. At this point, generate an output file.

Steps 1-23 are generalized and presented as a program guide to indicate which equations, parameters and procedures are necessary for servo calculations.

3.3 Data Preparation

As stated in Section 2.5, the USU servo model requires MSIS for neutral atmospheric parameters and a source of hmF2 data. MSIS depends on location, altitude, day of year, solar F10.7 cm flux and geomagnetic A_p , all given in Appendices A and B. This study uses three sources of hmF2 data to calculate the meridional neutral wind. The first source is from the IRI, which generates monthly averages of hmF2 data for magnetically quiet conditions in the non-auroral ionosphere. The second source is provided by 20 ionosonde stations, which were operating during a world day campaign from 12-16 January 1988 (GISMOS-88). The third source of hmF2 data comes from incoherent scatter radar

measurements, from the Millstone Hill Haystack Observatory, Massachusetts, during the ETS period of study, from 17-24 September 1984.

3.3.1 IRI hmF2 Data. The IRI is used to calculate two sets of data to show two types of application. Appendices A and B have the input parameters for location, 12-month-mean sunspot number and month. The first example shows a neutral wind comparison between low and high solar activity during geomagnetically quiet periods, for two magnetically conjugate locations. The two locations used in the solar cycle application are Petropavlovsk, USSR and Canberra, Australia. The second example from the IRI is used to calculate neutral winds along a meridional chain of ionosonde stations in the northern and southern hemispheres. This second IRI data set was picked to correlate with data from 20 ionosonde stations that made measurements during the GISMOS-88 world-day campaign.

3.3.2 Ionosonde hmF2 Data. F2-peak heights are determined using ionosonde data from an empirical relationship developed by Bradley and Dudeney [1973], as discussed in Section 2.5. The three necessary elements of data, namely foE, foF2 and M(3000)F2 are from the scientific archives in the World Data Center at Boulder, Colorado. As stated, there are problems in measuring foE at night, so that the E-layer critical frequency is calculated from the IRI model E layer density NmE, where $foE = 9 \times 10^{-3} (NmE)^{\frac{1}{2}}$. Values of

foE are used in a ratio of foF2 to foE, to compare the relative importance of the F and E-layer ionization in the calculation of hmF2. The variance between the IRI and measured values of foE is normally less than 10% and does not significantly impact the neutral wind calculation. Appendix A lists the 20 ionosonde locations and Appendix B shows the GISMOS-88 ionospheric parameters.

3.3.3 Incoherent Scatter Radar Data. For this study, Millstone Hill incoherent scatter radar data was graciously provided by Dr. Michael J. Buonsanto of the Millstone Hill Haystack Observatory. The radar data covers the ETS period of September 17-24, 1984. The radar was operated in a mode that used steerable north-south elevation scans and a fixed elevation measurement. The method of radar data collection and neutral wind derivation is fully discussed by Buonsanto et al. [1989]. Included in the radar data is hmF2, Ti, Te, radar-derived neutral winds and statistical uncertainties in the radar winds. Buonsanto et al. [1989] used this same ETS period to make neutral wind comparisons of radar-derived winds with Buonsanto et al. [1989] servo model winds and Miller et al. [1986] FLIP model winds. The ionospheric input parameters for the ETS period are presented in Appendix B.

CHAPTER IV

RESULTS AND DISCUSSION

4.1 Winds from IRI hmF2

Changes in mid-latitude neutral wind speeds depend on changes in momentum forcing terms in Equation (1). The pressure gradient force is the main driver of the neutral winds and is caused by temperature gradients created by UV and EUV radiation heating. An increase in solar activity directly increases radiation levels and intensity, thereby increasing horizontal pressure gradients. Increases in solar activity also leads to an increase in charged particle population, which leads to an increase in ion drag. The increase in pressure gradient force and increase in ion drag are counterproductive in the movement of neutral air. In general, as solar activity increases, neutral winds are expected to decrease because ion drag increases more rapidly than the pressure gradient force [Babcock and Evans, 1979; Rishbeth, 1972].

Figure 8 shows meridional neutral winds calculated for two magnetically conjugate locations during January, 1981 and 1985. Solar activity was high in 1981 and low in 1985. Values of hmF2 were modeled using the IRI. The dashed lines represent neutral winds for high solar activity, while the solid lines depict low solar activity. Ionospheric parameters for both periods are given in Appendix B. Figure 8 shows that nighttime neutral wind speeds are significantly smaller during high solar activity. When a

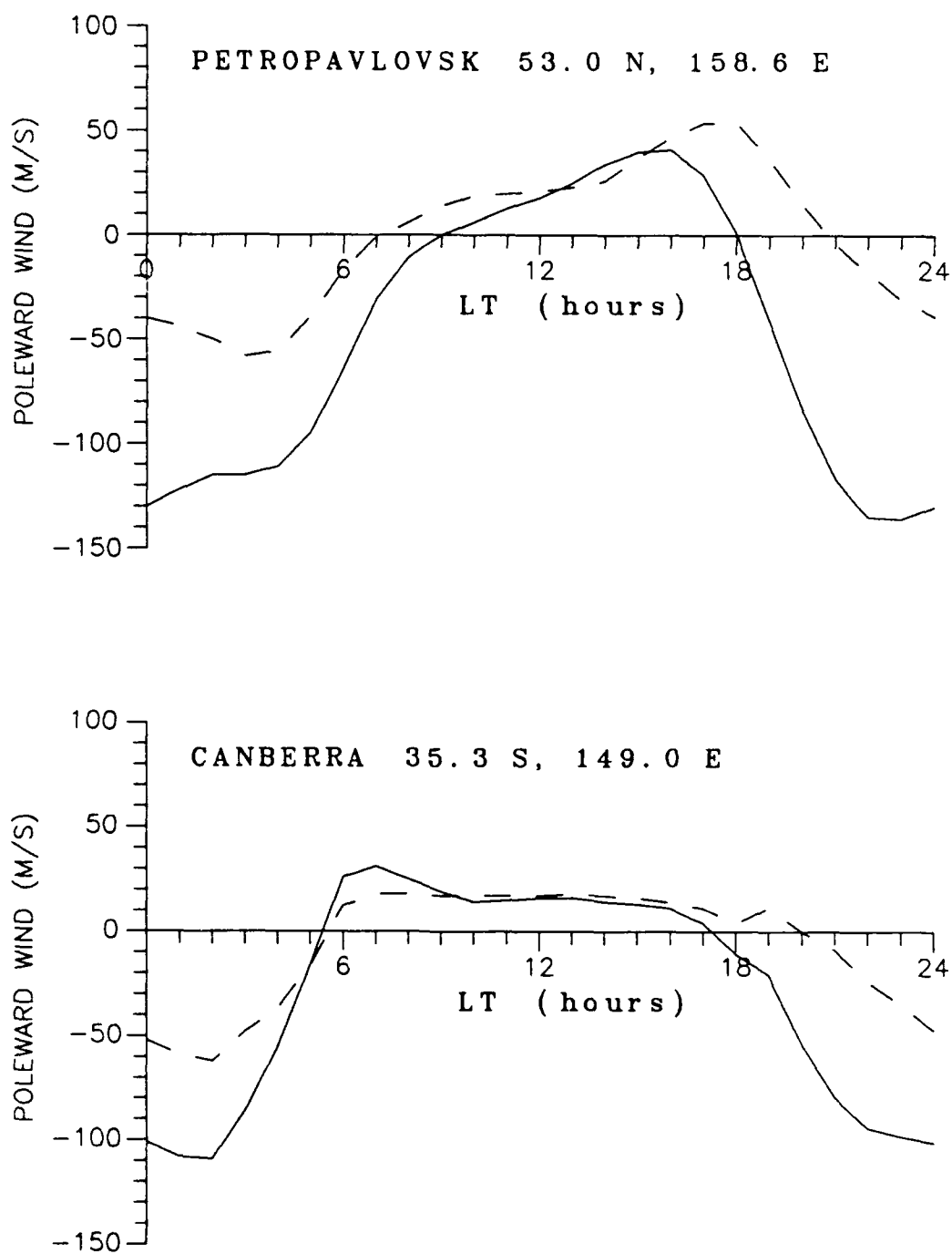


Fig. 8. Meridional neutral winds for two magnetically conjugate locations during low (January, 1985) and high solar activity (January, 1981) shown as solid and dashed lines respectively. Winds are calculated by the USU servo model using IRI F2-peak heights.

neutral particle strikes an ion moving at a different velocity, some of the neutral's momentum is transferred to the ion and the ion velocity is changed. The momentum lost to the neutral particle is an ion-drag force on the neutral. Ion drag increases with increasing ionized particle population. Figure 8 shows that increased solar activity decreases nighttime equatorward winds by as much as 50 m s^{-1} at Canberra and more than 75 m s^{-1} at Petropavlovsk. This decrease is attributed to a larger nighttime ion drag at high solar activity. Figure 8 also shows a marked increase in the poleward duration of the neutral winds during high solar activity, but little decrease in wind speed from low to high solar activity.

Figure 8 shows little change in daytime wind speeds when comparing wind patterns at low and high solar activity. Although ion production increases daytime ion drag, pressure gradients also increase during the day and at high solar activity. In this case, Figure 8 indicates that an increase in daytime pressure gradients at high solar activity tends to counterbalance the increased ion drag and therefore little change is observed in the daytime wind speeds.

Figure 9 shows another example of IRI produced winds. In this example, a meridional chain of 10 ionosonde stations show latitudinal changes in neutral wind patterns. These wind patterns are calculated for the GISMOS-88 period to allow future comparison with ionosonde produced winds.

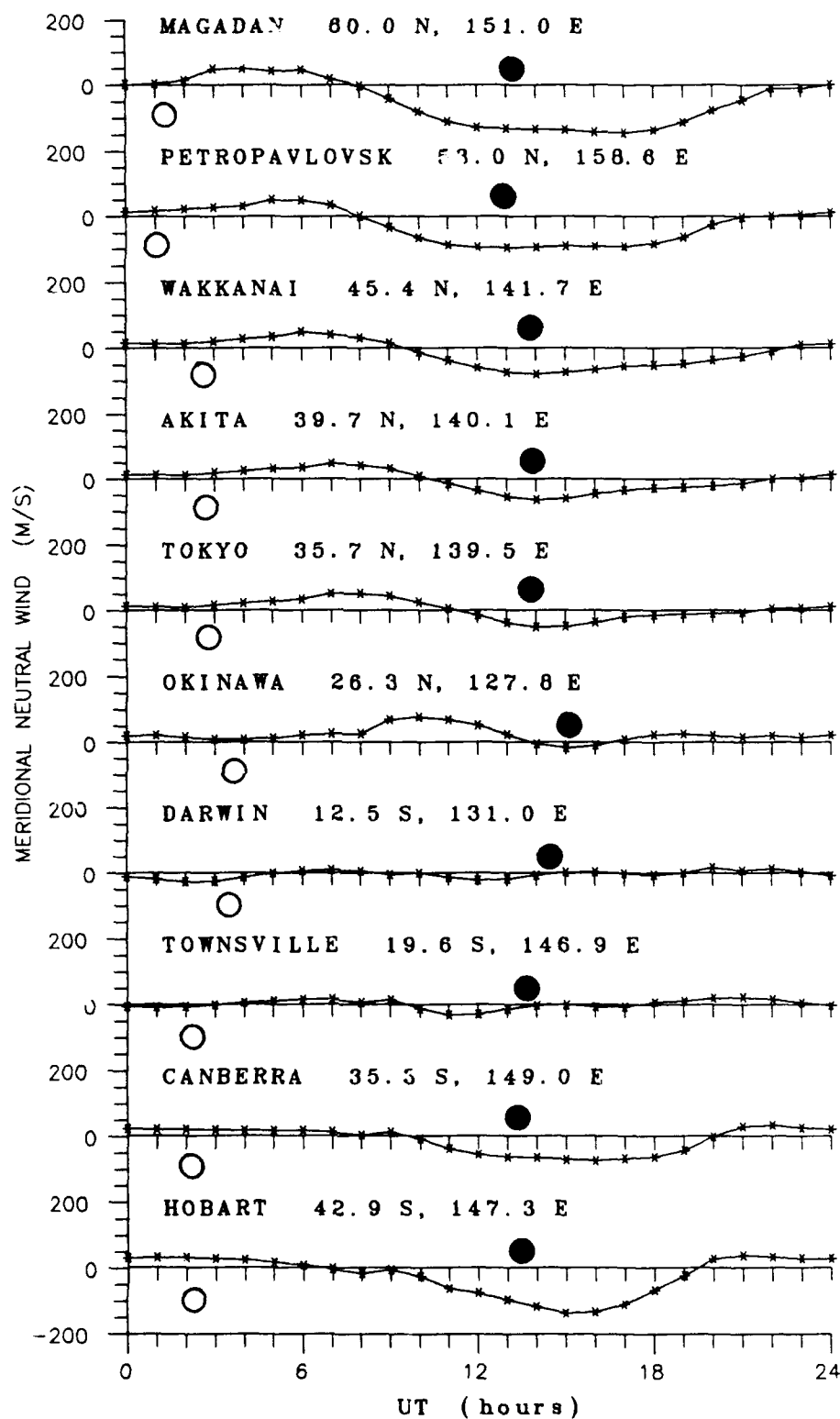


Fig. 9. Neutral winds along a meridional string of ionosonde stations calculated by the USU servo model from IRI hmF2 data for January, 1988. Positive winds are poleward. Open and shaded circles mark local noon and midnight.

As before, the diurnal patterns of daytime poleward winds and nighttime equatorward winds are quite plain. Of note is the evidence of a much stronger diurnal tide and greater magnitude of meridional neutral wind speeds at the higher latitudes. This is probably due to the much larger diurnal variation of atmospheric heating at higher latitudes.

Miller et al. [1989] made a similar comparison of IRI and ionosonde winds. Comparative results from the Miller et al. [1989] study shows that IRI winds are nearly the same as ionosonde winds derived from median ionosonde hmF2 values over a 15-day period.

4.2 Winds from Ionosonde ...

The World Day campaign from 12-16 January, 1988, also called the GISMOS-88 campaign, is used for a basis of study. For this application, 20 ionosonde stations along an approximate meridional longitude of 135° E geographic are used to show a latitudinal variation in the neutral winds. A moderately strong geomagnetic storm occurred about half way through the GISMOS-88 campaign. For comparison, the neutral wind plots are broken into prestorm, storm and post-storm periods of 12-13, 14-15 and 16 January respectively. Table 3 shows the change in daily Ap from 9-17 January. The changes in Ap are used to explain changes in neutral wind circulation patterns.

Figure 10 shows the meridional neutral wind patterns for two days prior to the storm event. Dashed lines are

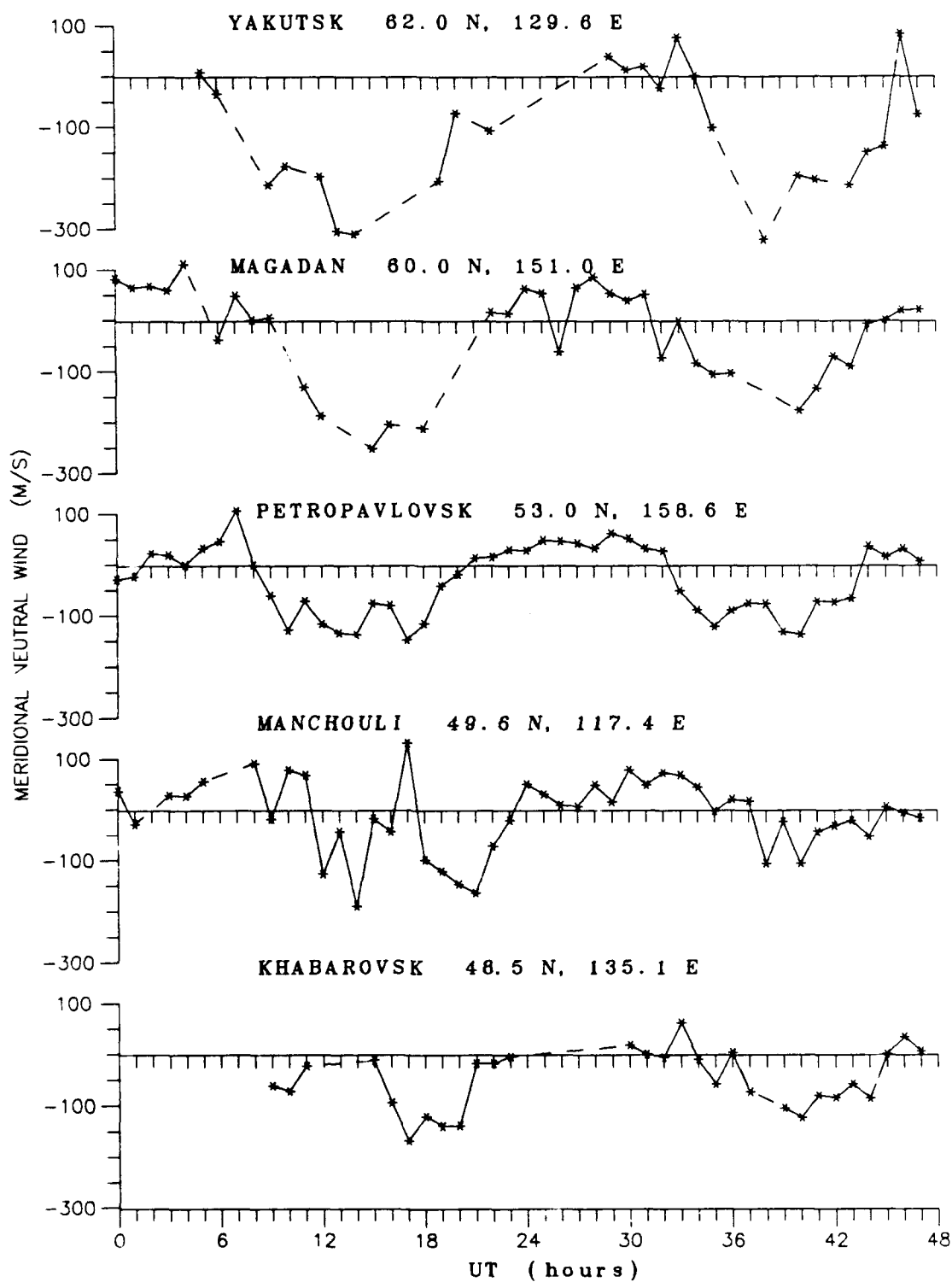


Fig. 10. Prestorm neutral winds (positive poleward) for a meridional string of 20 ionosonde stations on January 12 and 13, 1988 (GISMOS-88). Winds are calculated by the USU servo model.

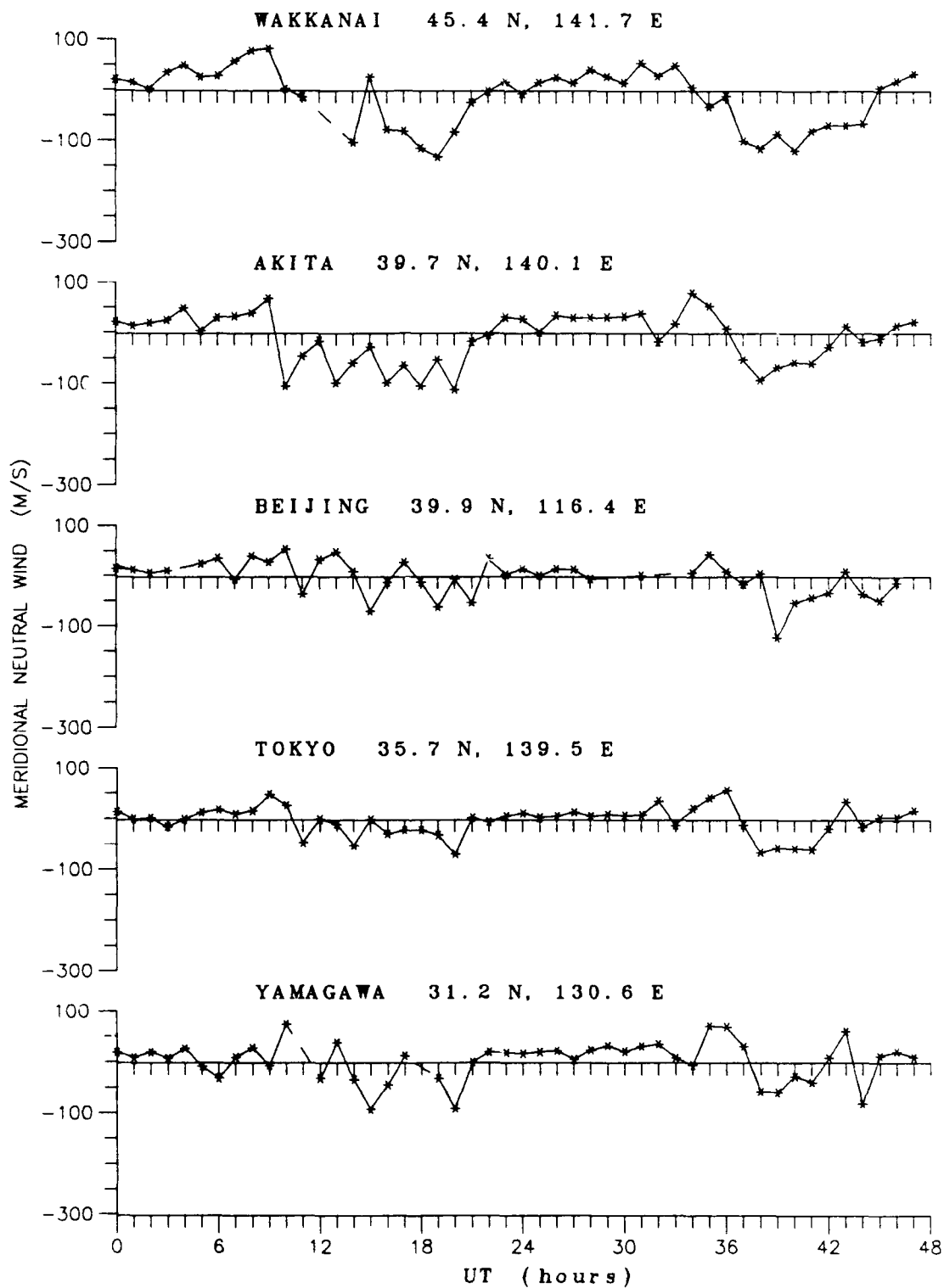


Fig. 10. (continued)

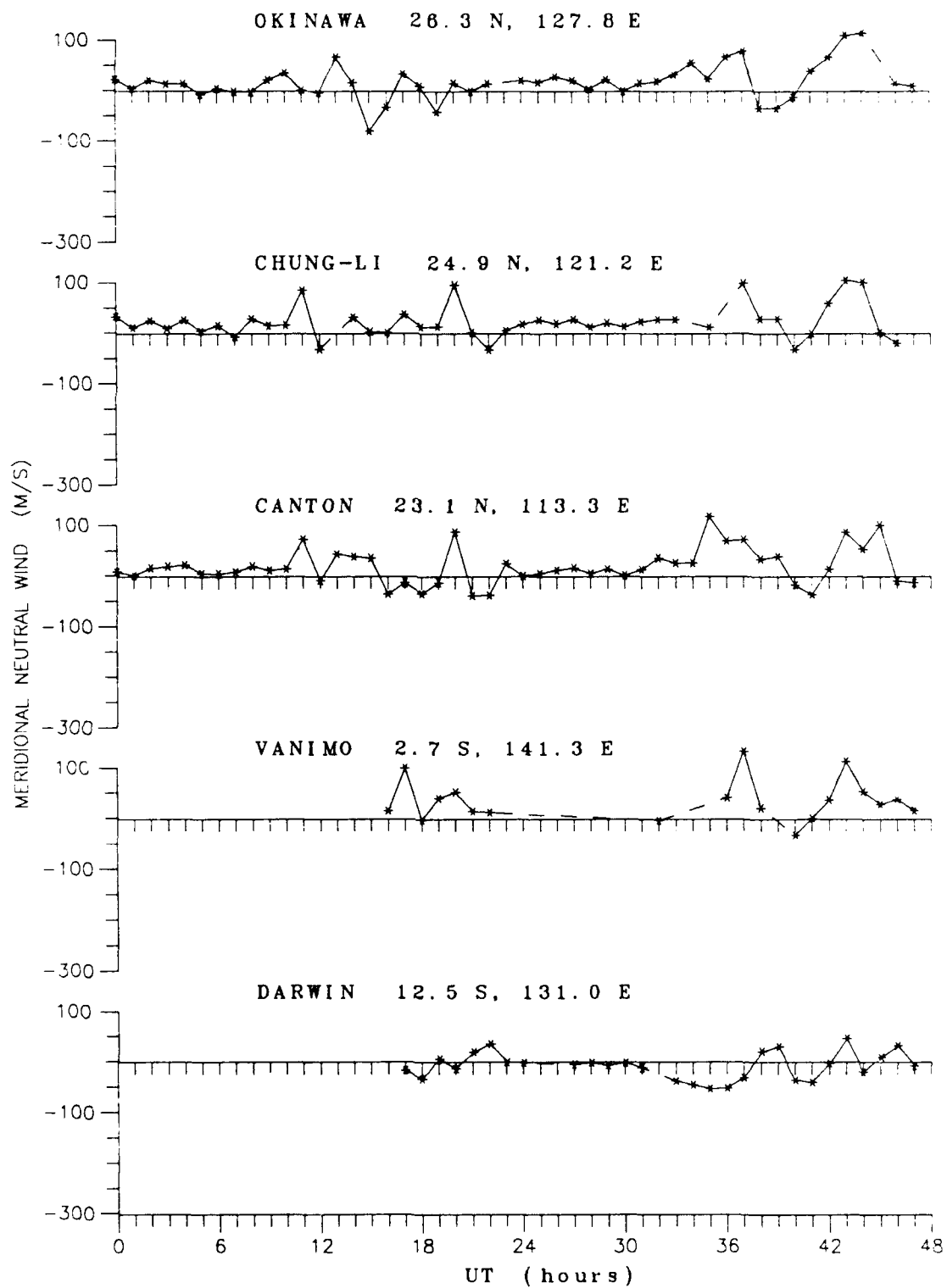


Fig. 10. (continued)

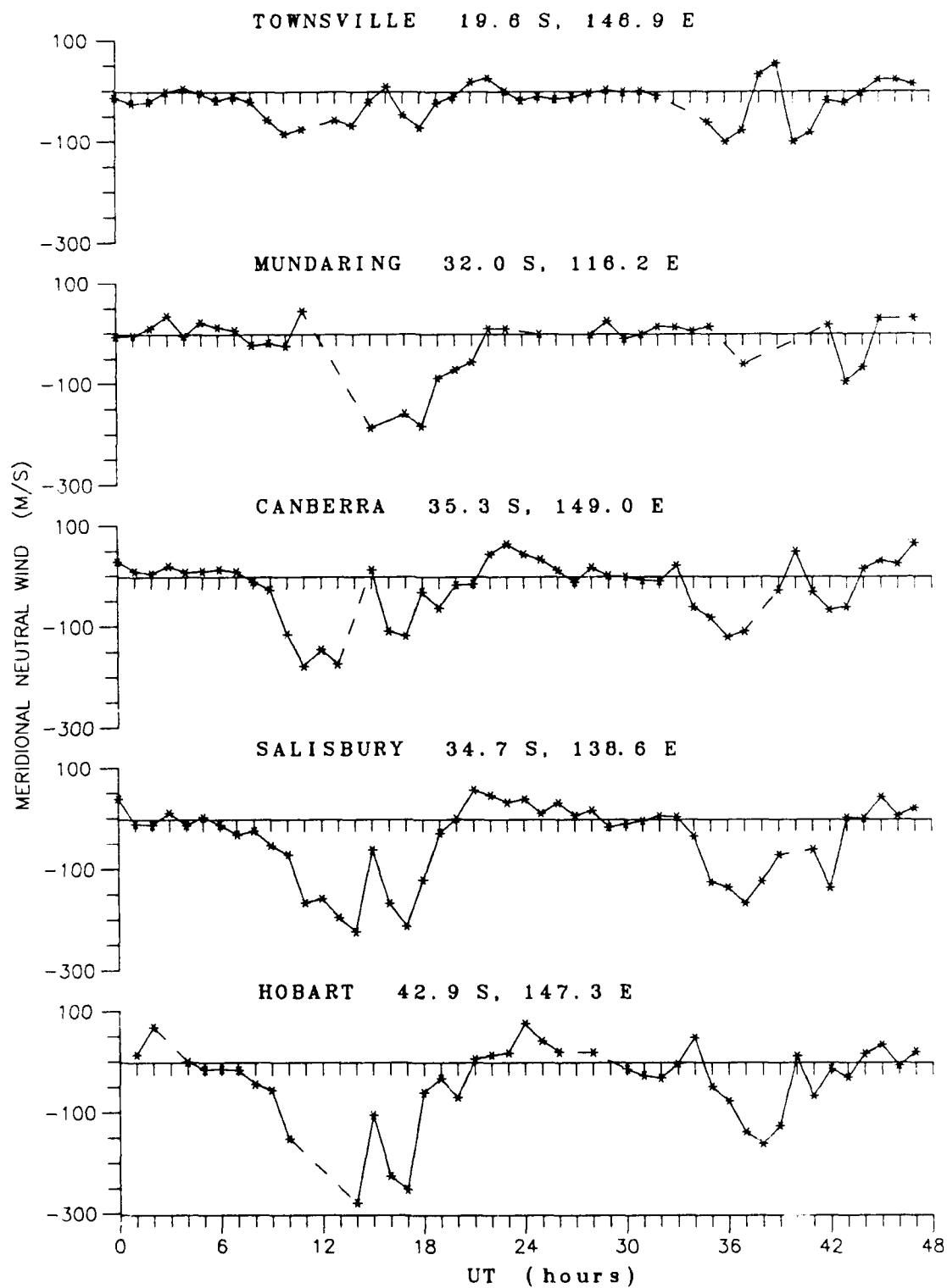


Fig. 10. (continued)

TABLE 3. Geomagnetic Ap from 9-17 January, 1988

Date:	9	10	11	12	13	14	15	16	17
Ap:	7	4	11	21	7	48	63	5	7

used to join the wind pattern at points where hourly observations are missing. Although the 12th and 13th are relatively quiet compared to the storm days, there are still distinguishable differences between the two days. The differences are probably attributable to differences in geomagnetic conditions. On the 12th, the wind pattern is more erratic and nighttime equatorward winds are greater at most locations in the northern and southern hemispheres. The stronger equatorward winds are most prevalent above 35° - 40° , suggesting that increases in auroral heating processes may have enhanced equatorward pressure gradients. There may also have been enhanced equatorward winds at the higher latitudes due to increased ion-neutral momentum transfer from the polar cap convective cells.

In Figure 11, much of the hourly observations are unfortunately not available. This is probably due to ionospheric short wave fadeout from the storm event [Hargreaves, 1979; Ratcliffe, 1972]. Most of the fadeout is probably caused by enhanced D-layer ionization. This condition normally affects higher latitudes, but missing data is evident throughout almost the entire ionosonde network. Again dashed lines are used to close the gap between known observations.

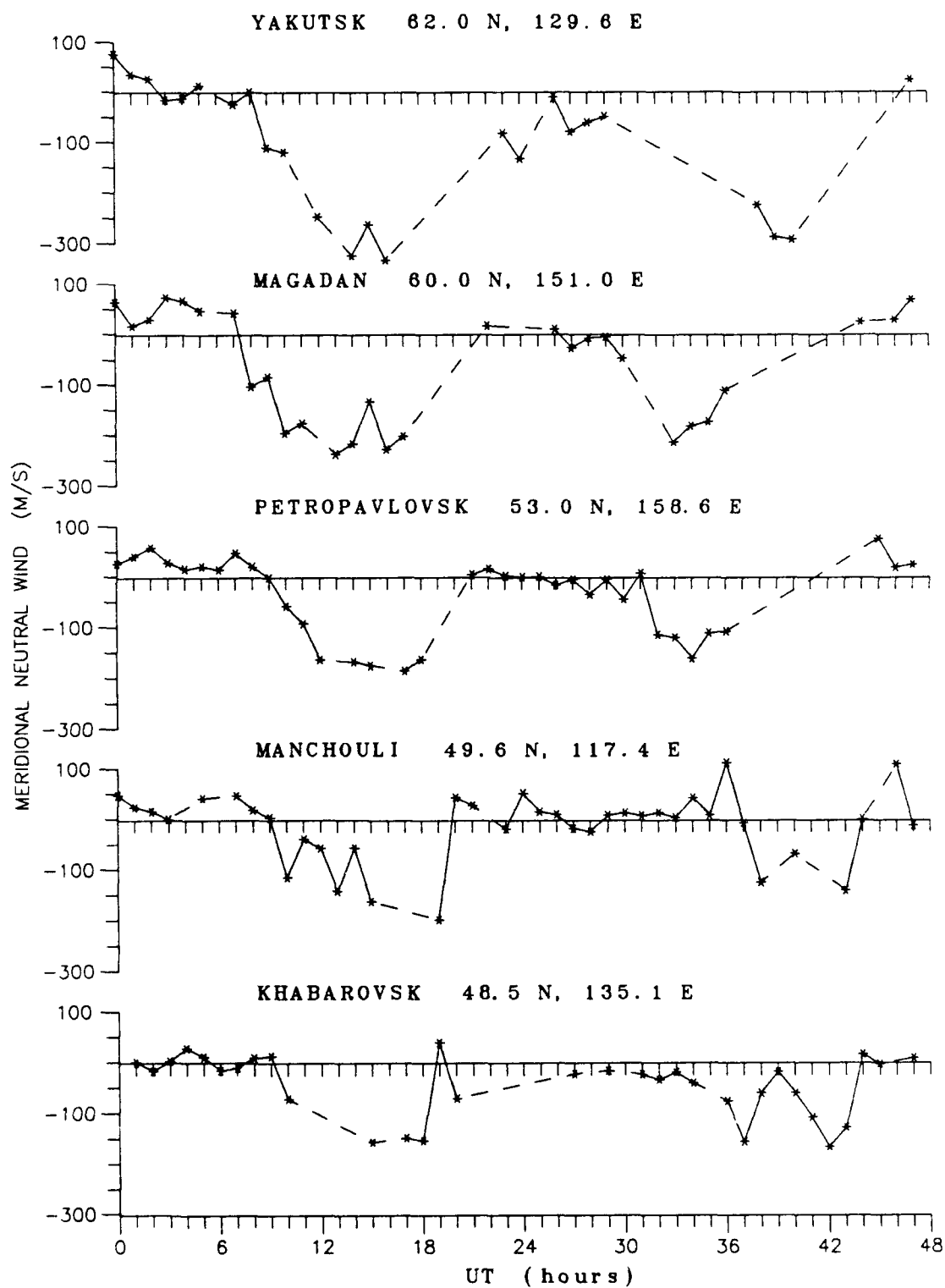


Fig. 11. Neutral winds during GISMOS-88 storm on January 14 and 15, 1988 for a meridional string of 20 ionosonde stations. Winds calculated by USU servo model.

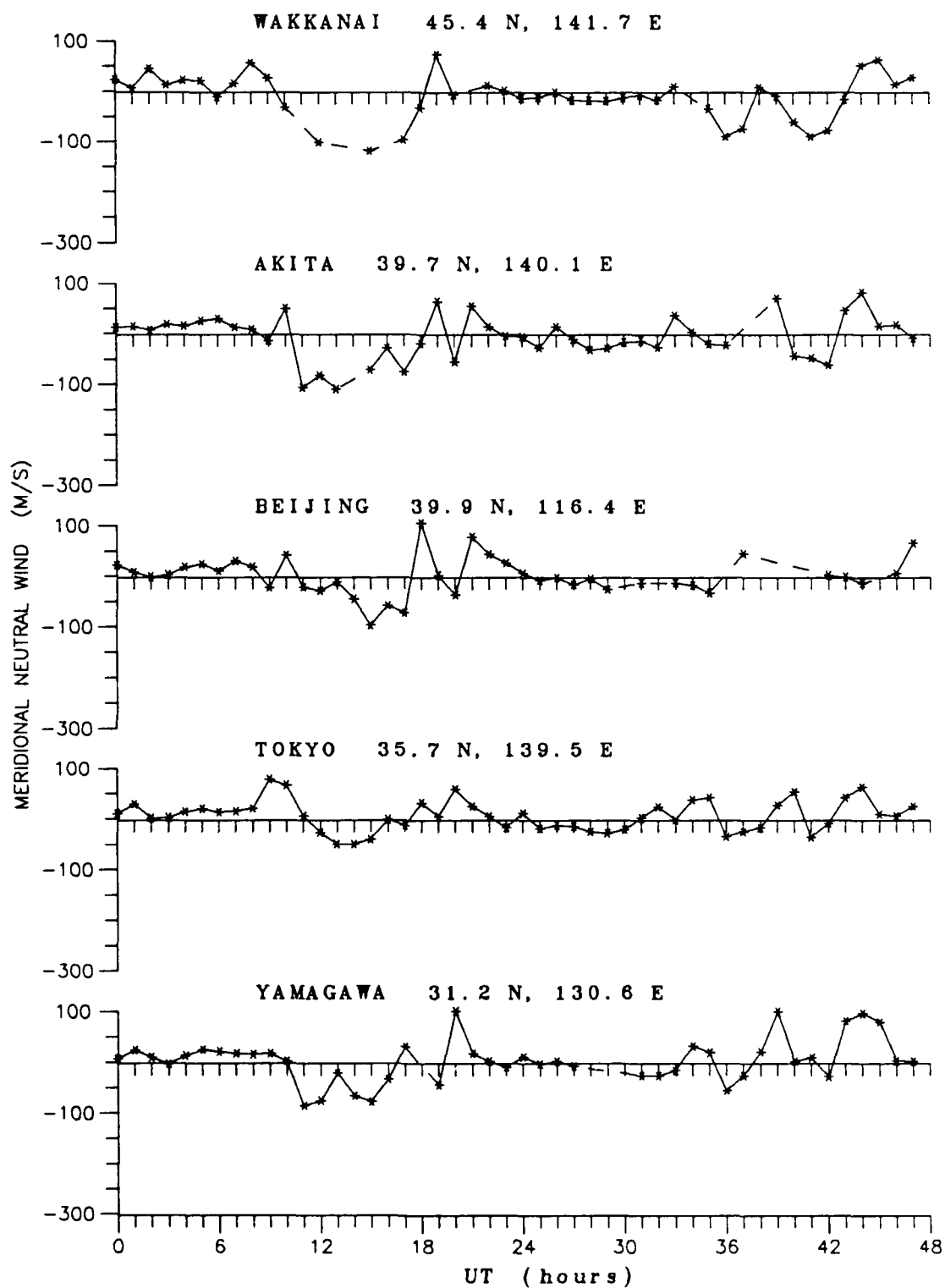


Fig. 11. (continued)

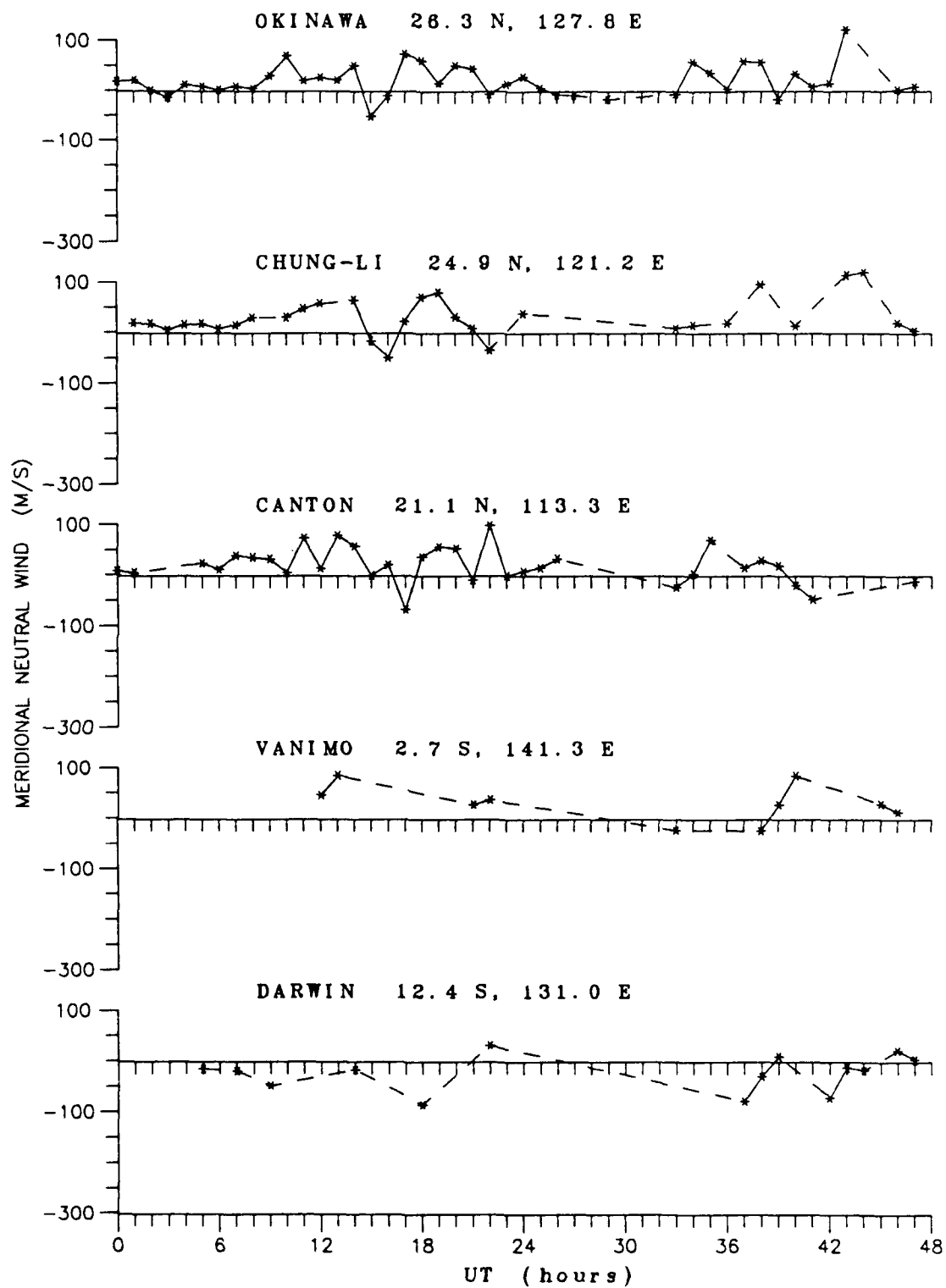


Fig. 11. (continued)

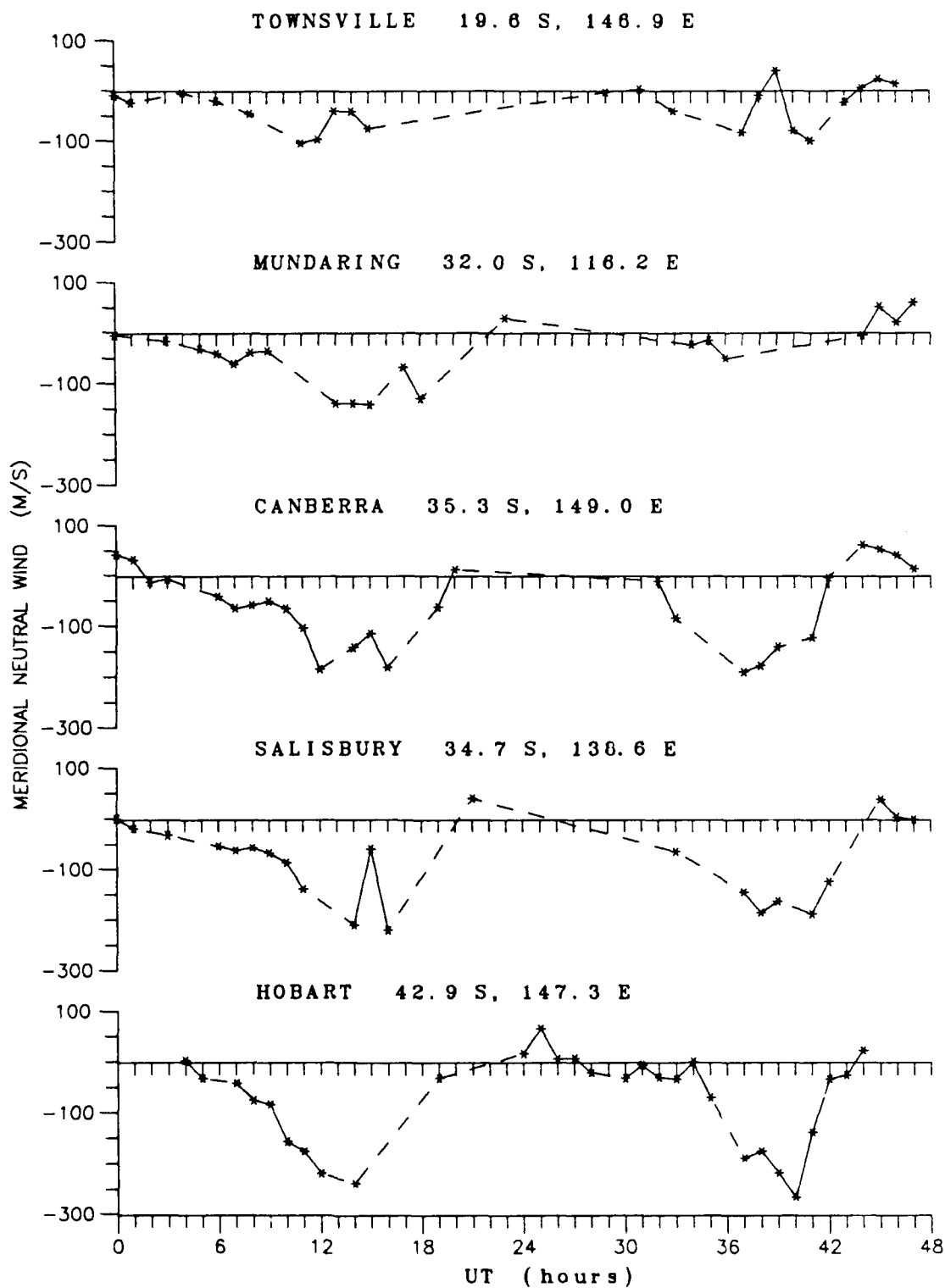


Fig. 11. (continued)

The most striking feature in Figure 11 is a change in the daytime neutral wind pattern on the 15th. At most locations, daytime winds are either close to zero or equatorward. Much of the data is missing on the night of the storm, between the 14th and 15th. However, there is still indications of minor equatorward surges, especially at higher latitudes. The magnitudes of the equatorward wind surges are not as strong as expected when compared with the two relatively quiet days of the 12th and 13th. This may be explained by considering dynamo electric fields.

A strong equatorward wind surge during the storm would cause a westward electric field during the build-up of the surge. This electric field drives the plasma downward, perpendicular to the field lines. Using hmF2 to calculate meridional neutral winds during a storm will therefore give a wind speed less than it really is. Blanc and Richmond [1980] and Foster and Aarons [1988] described this type of disturbance dynamo generated by equatorward neutral winds driven by enhanced auroral heating at high latitudes. In Section 4.3, comparisons of neutral wind techniques at Millstone Hill show that strong westward electric fields at the time of storm occurrence are responsible for most of the neutral wind correction when using the hmF2 method in calculating neutral winds.

Figure 12 shows the post-storm wind patterns. For the most part, neutral winds have returned to normal diurnal patterns. Overall poleward winds on the 16th are a little

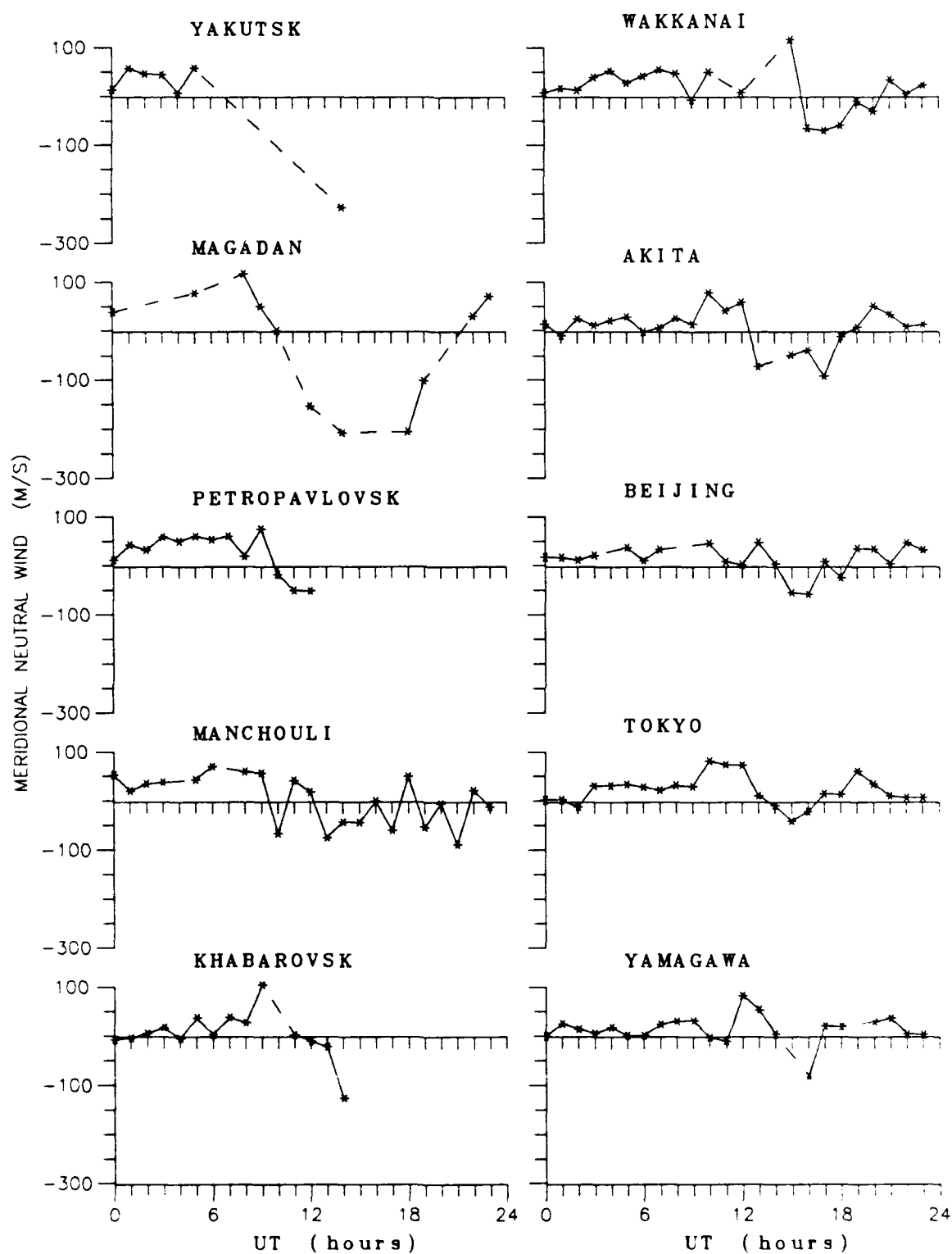


Fig. 12. Post-storm neutral winds for a meridional string of 20 ionosonde stations on 16 January, 1988 (GISMOS-88). Winds are calculated by USU servo model.

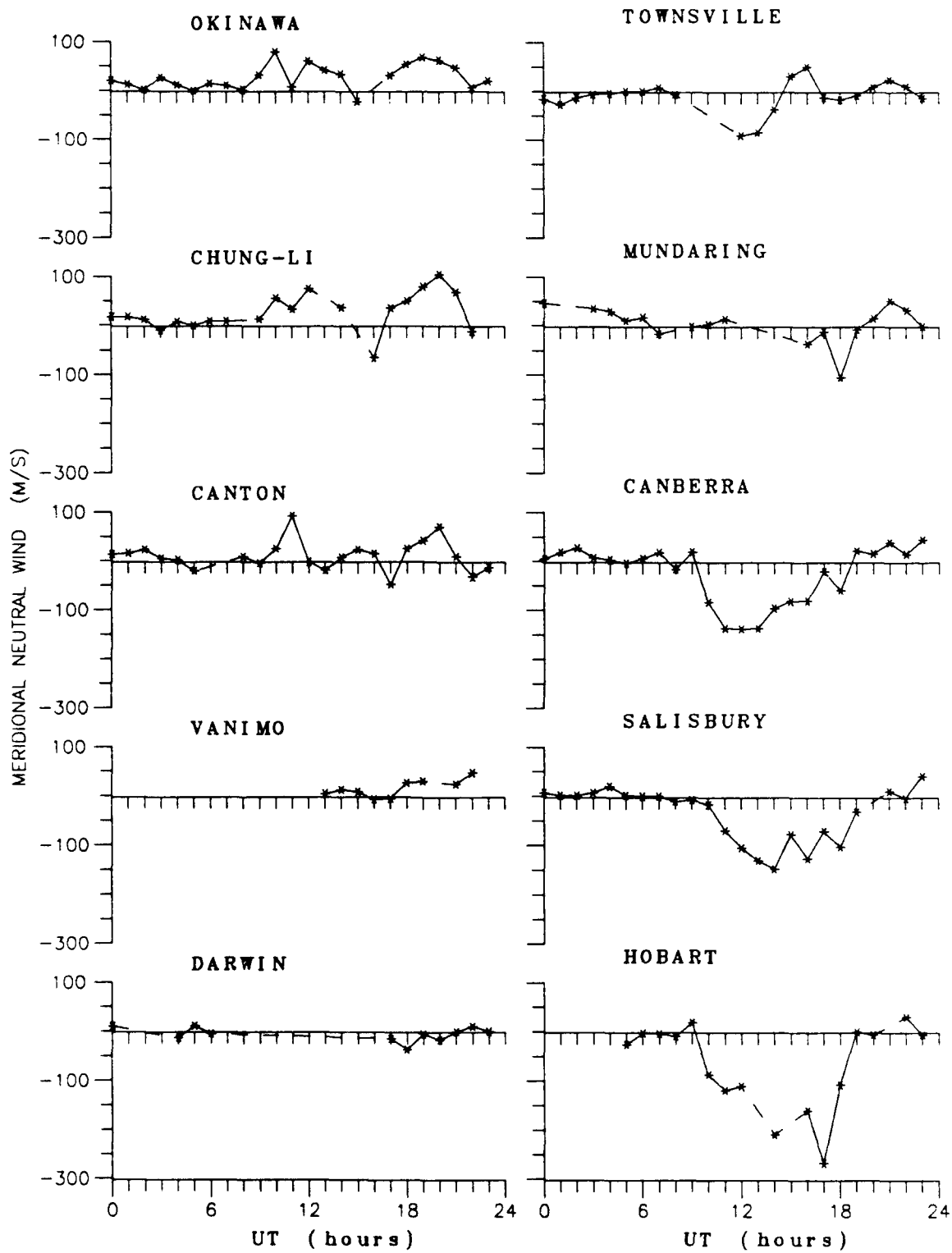


Fig. 12. (continued)

more enhanced than the prestorm period. An increase in the uncertainties in MSIS-86 neutral densities and temperatures after the storm event may account for the differences in pre and post-storm wind patterns, rather than a post-storm dynamic process.

The IRI neutral winds in Figure 9 presents a climatological background for comparison with Figures 10, 11 and 12. The general patterns in the IRI winds are reflected on the patterns of the ionosonde winds. Fluctuations departing from the climatological patterns may be caused by "ionospheric weather."

Figure 13 shows the ionosonde winds for the prestorm period (dashed line) at Petropavlovsk superimposed on the IRI wind pattern (solid line). Day 13 is the more quiet of the two days and the ionosonde pattern tends to follow the IRI pattern somewhat closer. Changes in neutral-wind or electric-field induced plasma motions may be responsible for the differences in the two patterns.

Figure 13 shows how IRI wind patterns approximate daily observed ionosonde wind patterns. Figure 13 also shows that IRI wind patterns may be used as a climatological basis in the study of transient neutral-wind and electric-field features.

4.3 Comparing Winds with Radar Data

The equinox transition study during September 17-24, 1984, provides a period of study in which to compare the

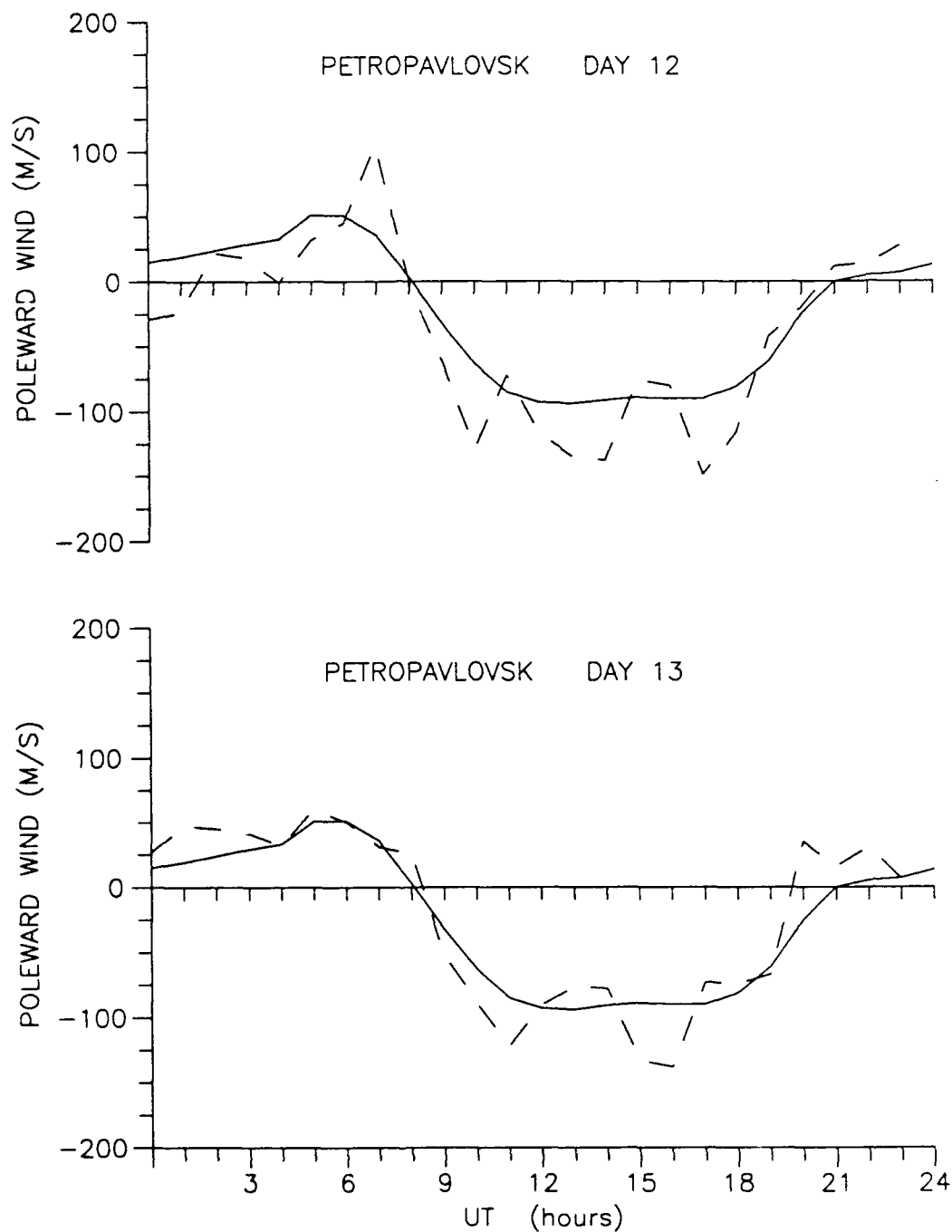


Fig. 13. Weather vs. Climatology: Neutral winds from the USU servo model for January 12 and 13, 1988 at Petropavlovsk, during GISMOS-88 prestorm period. Solid lines show IRI winds and dashed lines show ionosonde winds.

USU servo model with other wind calculation techniques, during a variety of geomagnetic conditions. The first part of the ETS period was geomagnetically quiet. A small storm ($A_p = 36$) occurred on 19 September, followed by a three day recovery period and then a major storm ($A_p = 112$) on 23 September.

Buonsanto et al. [1989] used this same period of study and made neutral wind comparisons between radar, the Miller et al. [1986] FLIP method and servo method adapted by Bounsanto et al. [1989]. To distinguish between the wind techniques, we will refer to the methods of calculation as FLIP winds, USU servo winds, servo winds and radar winds.

The FLIP and servo winds are similar during this ETS period of study, but the servo winds are consistently more negative (southward). The servo model is tuned for better agreement with the radar winds, which accounts for less than half this difference between FLIP and servo winds, since the FLIP winds are not radar tuned. Differences between the servo and FLIP winds are greatest during geomagnetically active times. This difference in winds between the two techniques partially prompted this investigation.

Figure 14 shows neutral winds above Millstone Hill during 18, 19 and 20 September calculated by the FLIP, USU servo and servo models. Local midnight at Millstone Hill corresponds to 0446 UT. Daily A_p history is input into MSIS-86 and 1.7 is used to increase the collision cross

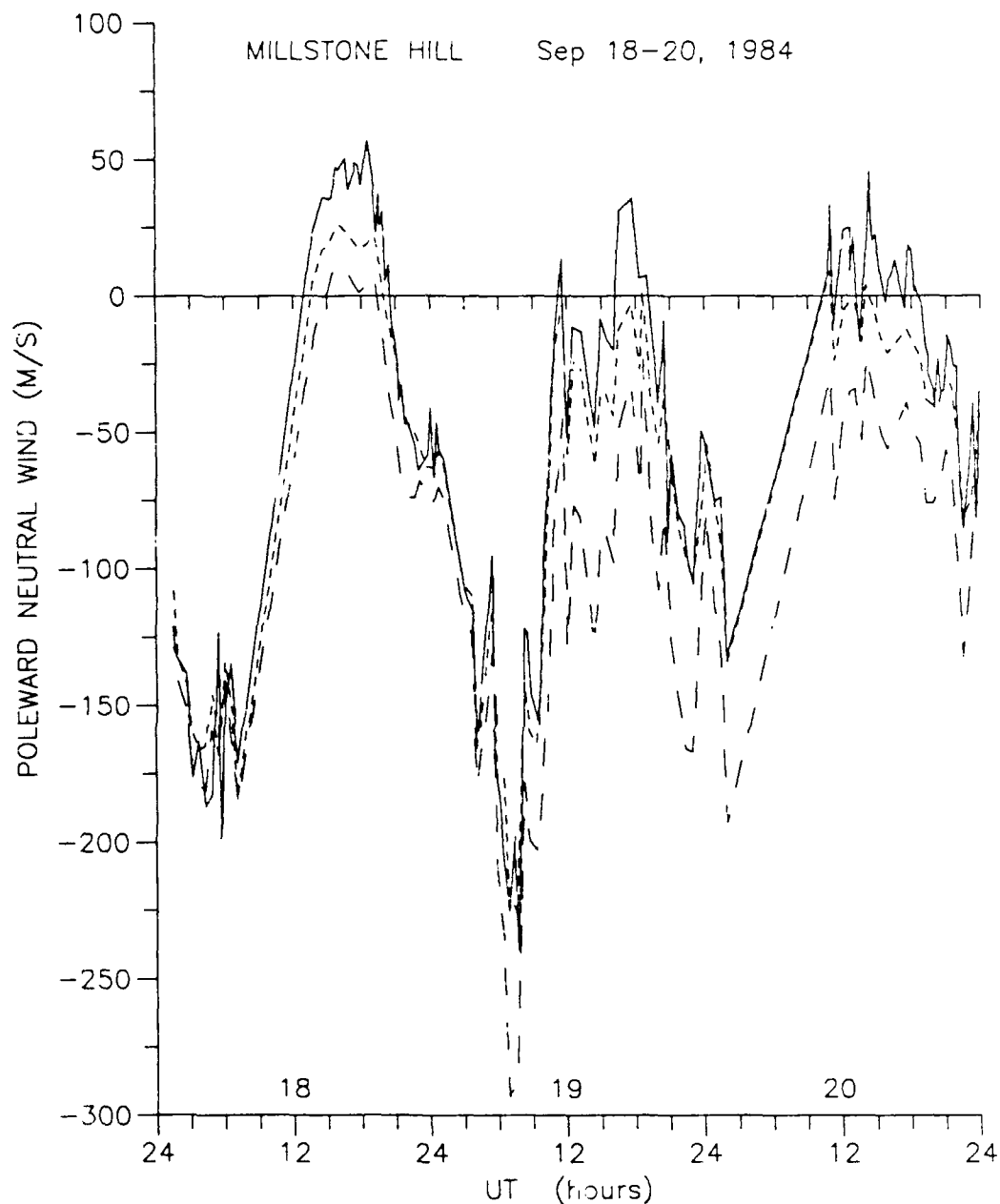


Fig. 14. Neutral wind comparison above Millstone Hill during ETS period. All calculations include daily A_p history and 1.7 increase to O^+-O collisions. Solid line is FLIP winds, short-dashed line is USU servo winds and long-dashed line is tuned servo model winds.

section of $O^+ \rightarrow O$ for neutral wind calculations. The solid line depicts FLIP winds, short dashes are for USU servo winds and long dashes are for servo winds. Measured T_i is used in USU servo, while measured T_i and T_e are used to calculate servo winds. The FLIP model internally calculates its own plasma temperatures. The USU servo and servo models assume daytime steady-state conditions, where c_d remains constant, as discussed in Section 3.1.7. The servo model is tuned with $c_d = 1$ and $c_n = 1.3$ as in Buonsanto et al. [1989]. The USU servo model requires no tuning because it uses a balance height adjustment technique described in Section 3.1.5. We can input the USU servo adjusted h_o values into Equation (21) or (22) and calculate equivalent tuning coefficients to compare with the Buonsanto et al. [1989] values. These USU servo equivalent tuning coefficients are $c_d = 1.05$ and $c_n = 1.41$.

Results from Figure 14 show that the USU servo winds are in closer agreement to the FLIP winds than are the servo winds. The USU servo winds are 5 to 20 $m s^{-1}$ more southward than the FLIP model winds, while the servo winds are between 20 to 50 $m s^{-1}$ more southward on the quiet day. On the active day of the 19th and continuing into the post-storm day of the 20th, the separation between FLIP and servo winds grow to about 50 to 70 $m s^{-1}$. The USU servo winds maintain about the same separation throughout the entire period.

There are two main reasons why the USU servo winds are

closer to the FLIP winds. The lesser reason is that the servo winds are empirically tuned to create greater southward wind speeds, which are in better agreement with the radar winds. The second and more physical reason, stems from the replacement of the peak vertical plasma velocity V_{zm} in Equation (11). In the USU servo derivation, Equation (7) is $V_{zm} = w - (g/v_m)\sin^2 I$. In the RGW servo model, which is used by Buonsanto et al. [1989], $V_{zm} = w - (D_{pm}/2H)\sin^2 I$.

Two improvements come about by the use of Equation (7). One is that v_m depends on T_i , while D_{pm} depends on both T_i and T_e , but the second and more important improvement is that Equation (7) does not assume diffusive equilibrium. At diffusive equilibrium, $T_n = T_i = T_e$ and H_p may be replaced by $2H$, as discussed in Section 2.4. The replacement of V_{zm} in Equation (11) affects both plasma drift w from Equation (18) or (19) and the balance height h_0 from Equation (20).

To explain the large differences between the FLIP and servo winds during geomagnetically active periods, consider Equation (19), rewritten here and followed by an RGW servo model equivalent

$$w = \frac{g \sin^2 I}{v_o} z_m(k + 1) \quad (30)$$

$$w = \frac{D_{po} \sin^2 I}{2H} z_m(k + 1) \quad (31)$$

At diffusive equilibrium, both Equations (30) and (31) are equal. During periods of increased T_e and T_i , diffusive equilibrium no longer applies and the two equations diverge. As plasma temperatures increase, w decreases in Equation (30) and increases in Equation (31). Physically, Equation (30) is more correct because collision frequency increases with increasing temperature. As collisions between the ions and neutrals increase, the neutral wind becomes more efficient in moving the plasma along the field lines and w decreases. Since the scale height H in the denominator of Equation (31) is of atomic oxygen, then the factor 2 may be replaced by $(T_i + T_e)/T_n$ to become the plasma scale height H_p . An increase in plasma temperature would then decrease w in Equation (31) and equal Equation (30).

Figure 15 shows the neutral and ion temperatures for 18, 19 and 20 September and Figure 16 shows T_e for the same period. T_i and T_e are measured with radar at 300 km, while T_n is from MSIS-86 at 300 km. Plasma temperature increases during and after the storm event on the 19th and servo winds in Figure 14 have grown consistently more southward.

How much does an increase in T_i affect the USU servo model winds? Figure 17 shows USU servo model winds calculated from assumed ratios of $T_i/T_n = 1, 1.5$ and 2.5 on 18 September, depicted by solid, short-dashed and long-dashed lines respectively. The hmF2 radar data used for the calculations shown in Figure 17 are from repetitive eleva-

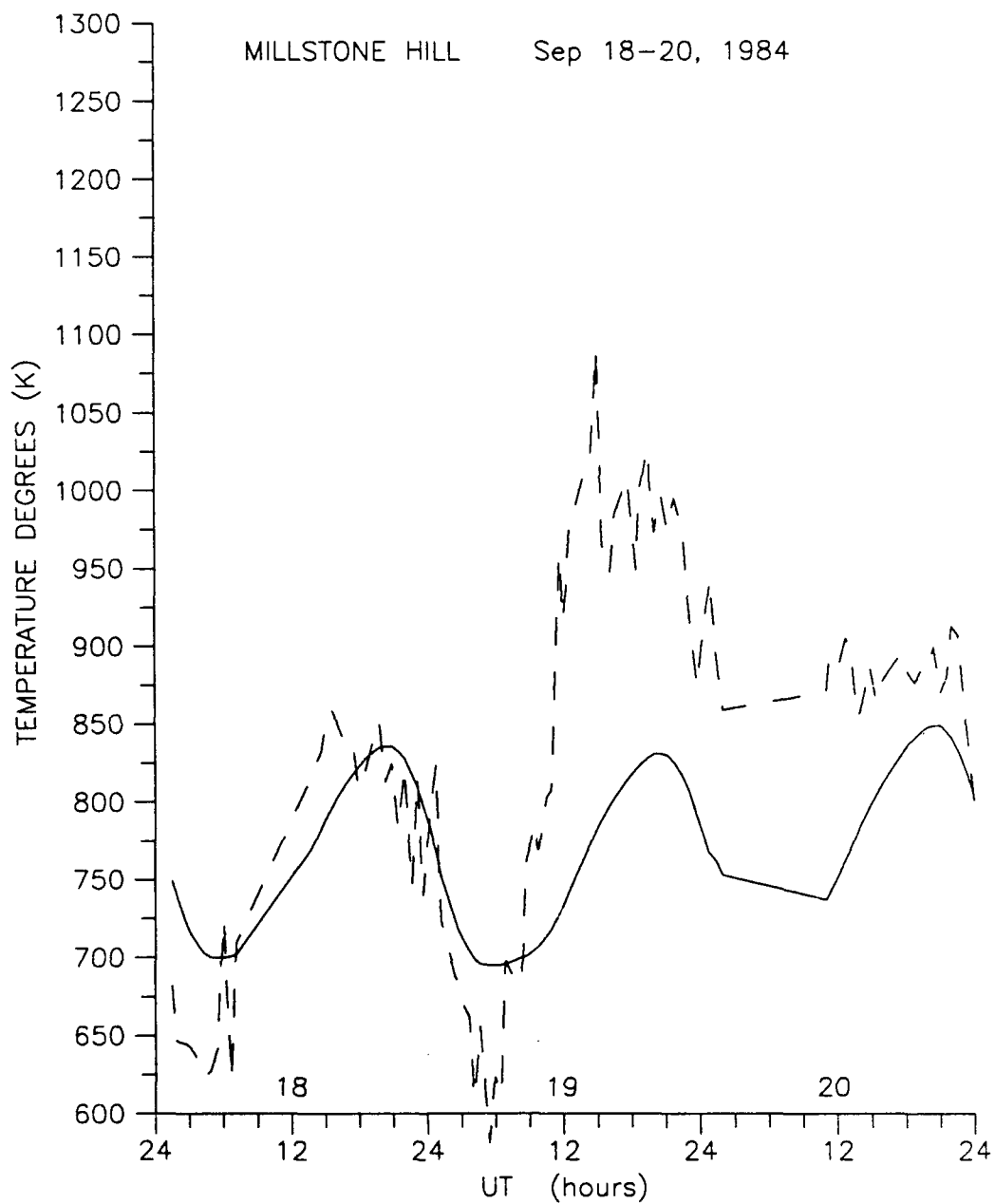


Fig. 15. Neutral and ion temperatures at 300 km above Millstone Hill, during ETS period. T_n is solid line from MSIS-86 and T_i is dashed line measured by IS radar.

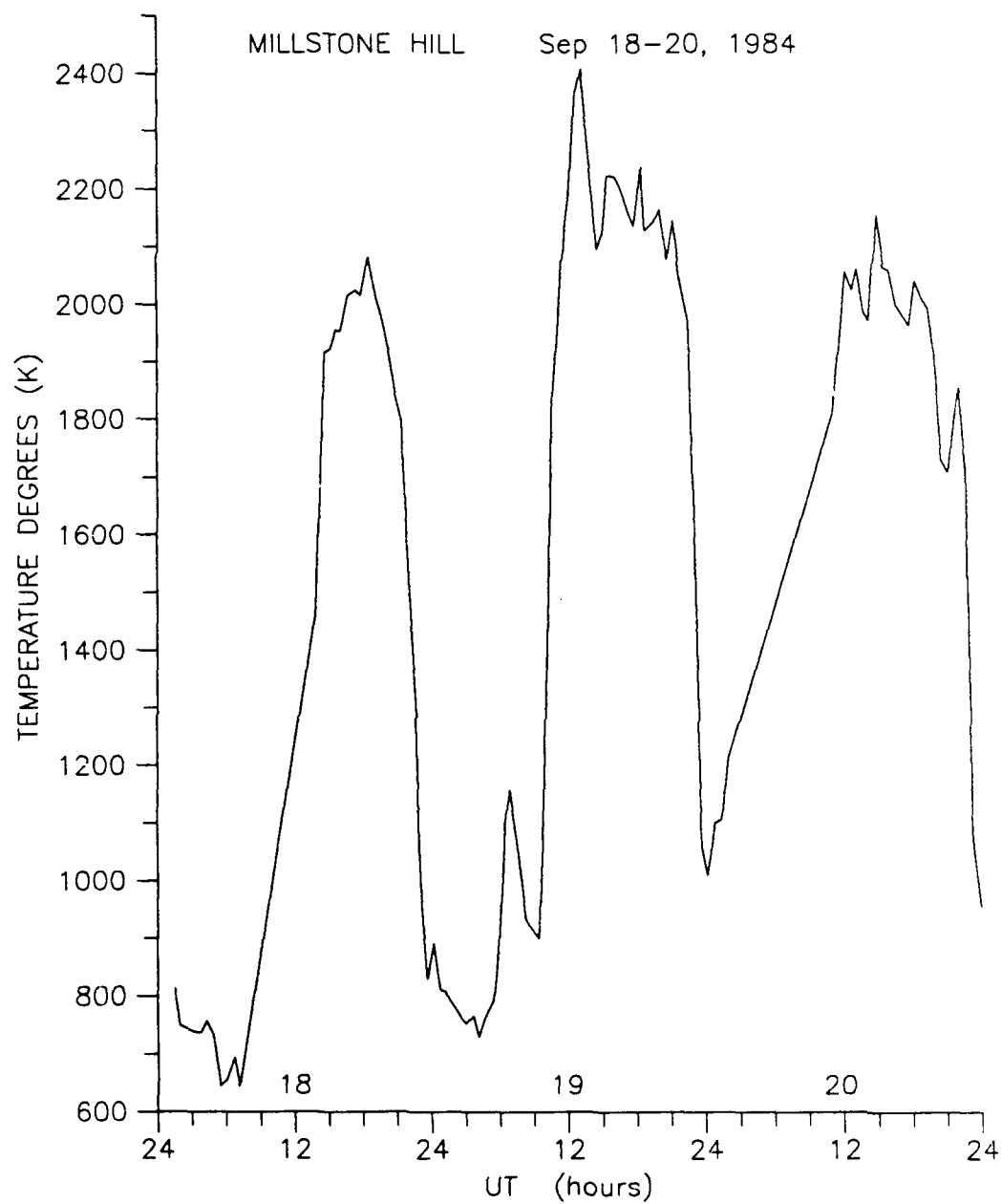


Fig. 16. Electron temperature measured by IS radar at 300 km above Millstone Hill during ETS period.

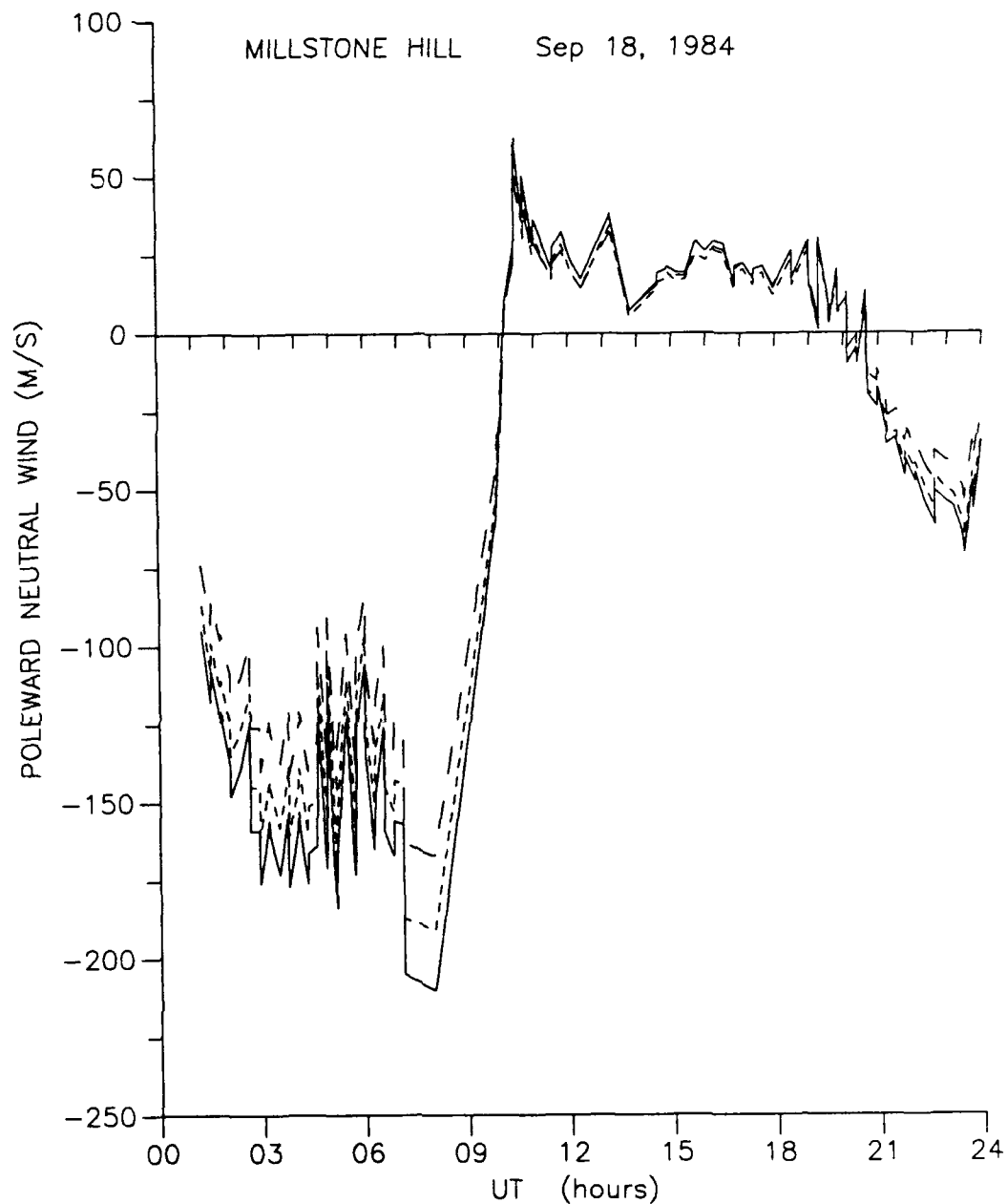


Fig. 17. USU servo neutral wind sensitivity to changes in ion temperature during Millstone Hill ETS period. Winds are calculated for different temperature ratios. Solid line is for $T_i/T_n = 1$, short-dashed line is for $T_i/T_n = 1.5$, and long-dashed line is for $T_i/T_n = 2.5$.

tion scans and have a higher resolution than the data used in Figures 14 or 18. Figure 17 shows that higher values of T_i tend to decrease the neutral wind, due to an increase in collision frequency.

Considering the large differences in T_i used in the neutral wind calculations of Figure 17, ion temperature is not a major contributor in the uncertainty of the USU servo model. We can therefore assume the uncertainty in the USU servo model from uncertainties in T_i is small compared with uncertainties from electric field effects during active geomagnetic periods. This is fortunate, since assumed ion temperatures are used in calculating neutral winds from ionosonde hmF2 data.

The effect of electric fields on plasma drift is significant during a geomagnetic storm. The perpendicular ion drift velocity term in Equation (29) must be included in calculations of neutral winds obtained by an hmF2 method [Buonsanto et al., 1989]. Figure 18 compares winds calculated by the USU servo model and incoherent scatter radar at Millstone Hill from 18-23 September. Radar winds are calculated at 300 km by the Salah and Holt [1974] method, with some modifications discussed by Buonsanto et al. [1989]. The 1.7 increase in $O^+ \rightarrow O$ collision cross section is used in both the USU servo and radar winds. The three hourly ap history is used in the radar calculation and daily Ap history is used for the USU servo calculation. The use of ap history generally gives stronger equatorward

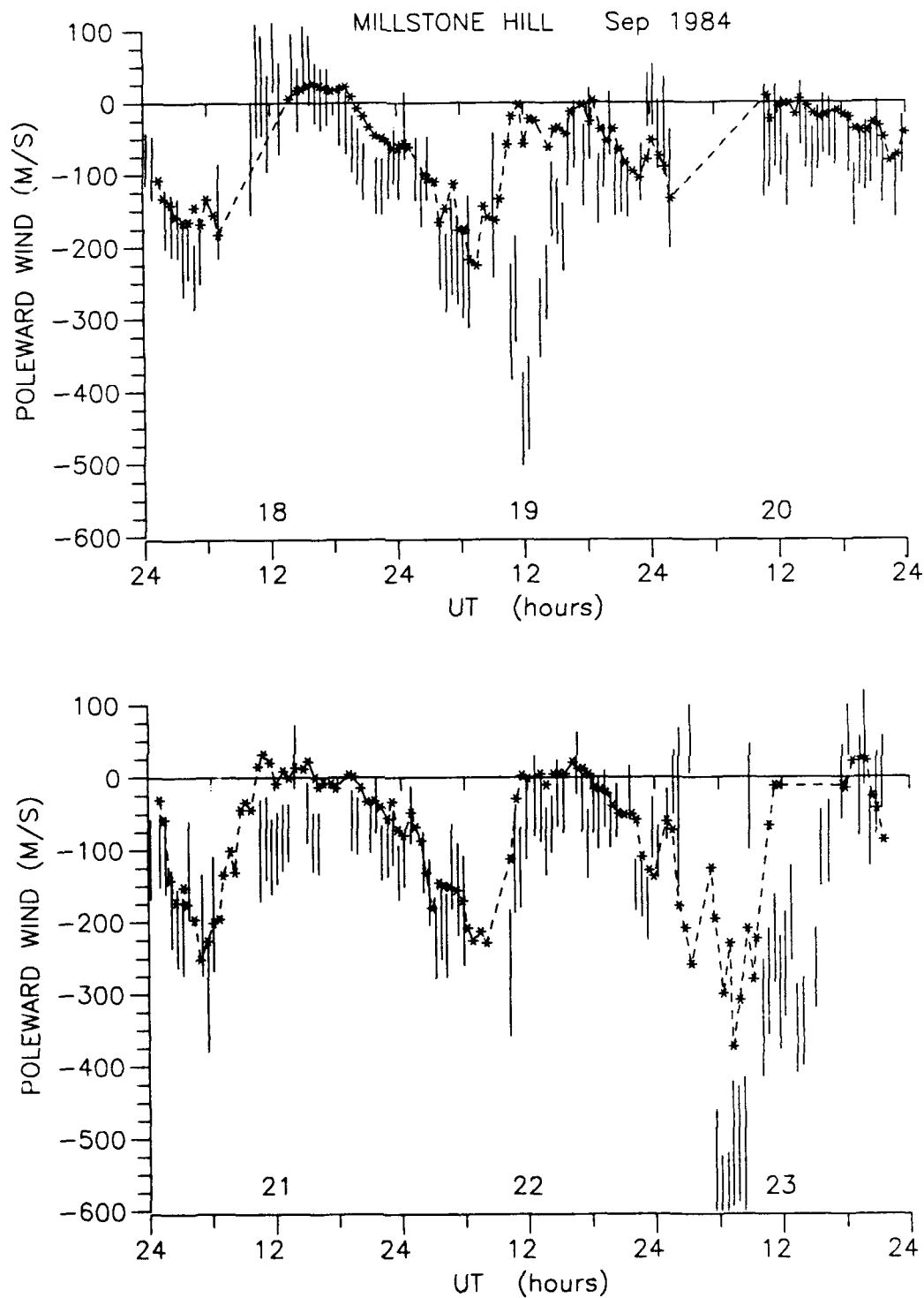


Fig. 18. Neutral wind comparison at Millstone Hill during ETS (18-23 Sep 84). Dashed line with stars is USU servo wind. Error bars show statistical uncertainties of radar wind at 300 km. Both calculations include the 1.7 increase in $O^+ \rightarrow O$ collisions. Daily A_p history for USU servo and three hour a_p history for radar was used in MSIS-86.

winds, especially at night and during the geomagnetic storm periods [Buonsanto et al., 1989]. Therefore, a slight equatorward bias in radar derived winds are evident when compared with the USU servo winds. Error bars indicate the statistical uncertainties in the radar wind and are used to gauge the USU servo wind approximation. Uncertainties in the USU servo model are not considered in this comparison, but as a minimum should approximate the same error as reflected by the radar.

Except for the storm times, USU servo winds generally fall within the radar wind error bars. This approximate agreement indicates that the balance height adjustment technique works and tuning the USU servo model is unnecessary.

Figure 18 shows large differences in the USU servo and radar winds during both storms. The mild storm on the 19th lasted for about 6 hours, while the strong storm on the 23rd lasted for about 15 hours. Ion drift velocity measurements calculated by Buonsanto et al. [1989] gives electric field corrections of nearly 200 m s^{-1} for the storms. This electric field correction, combined with increased uncertainties of about 100 m s^{-1} for both radar and USU servo model calculations during geomagnetic storm events [Buonsanto, et al., 1989, 1990], explains the observed large difference in the USU servo and radar winds.

CHAPTER V

CONCLUSIONS AND RECOMMENDATIONS

At mid-latitude thermospheric heights, solar UV and EUV radiation heating contributes most of the energy to drive the neutral winds. This level of solar radiation increases directly with solar activity. As solar activity increases, an increase in temperature variation will increase the horizontal pressure gradient, which is the main driver of the mid-latitude thermospheric winds.

An increase in solar radiation not only produces heat, but also increases the charged particle population. Collisions between ions and neutral particles become more frequent, so ion drag increases with increasing solar activity. The pressure gradient and ion drag are counterproductive in neutral-air motion and lead to a change in the balance of forces. The study of neutral wind force balance relationships from solar cycle variations leads to a better understanding of mid-latitude thermospheric circulation patterns. The use of IRI and ionosonde hmF2 data in the USU servo model provides a valuable means of calculating global scale variations in neutral wind patterns.

The USU servo model uses a balance height adjustment technique to compensate for changes in chemical and diffusive loss of ions at different mid-latitude locations and ionospheric conditions. This balance height adjustment technique physically replaces servo model empirical tuning by radar [Buonsanto et al., 1989; 1990] and greatly in-

creases the flexibility in the servo calculation method.

The USU servo model is physically more realistic than previous servo models. In the USU servo model, the vertical ion velocity V_{zm} is calculated by $w - (g/v_m)\sin^2 I$ instead of $w - (D_{pm}/2H)\sin^2 I$, as in the theoretical RGW servo model. The $2H$ in the RGW servo model assumes diffusive equilibrium and is not physically realistic. Electron and ion temperatures are used to calculate D_{pm} , but only ion temperature is required to calculate v_m , making this V_{zm} replacement a more practical one.

The IRI empirically models monthly averages of hmF2 for magnetically quiet conditions in the non-auroral ionosphere. Since the IRI gives average values of hmF2 for quiet conditions, its use is ideal in the calculation of neutral winds from hmF2 methods. Random errors and electric field variability, as compared to solar driven diurnal forces, are averaged out of the IRI hmF2 values. This allows calculation of global climatological, mid-latitude neutral winds for different solar conditions.

The USU servo model provides a fast and comparatively accurate means of calculating hmF2 neutral winds for any mid-latitude location, without regard to tuning. I recommend that a servo subprogram using the equations and procedures as described in this study, be implemented as part of the IRI program.

The generation of neutral winds from hmF2 proves to be a valuable technique. The major uncertainty is the result

of induced plasma motions from electric fields. Under quiet to moderate geomagnetic conditions, uncertainties from electric fields are usually less than the statistical uncertainties in wind calculations. For active geomagnetic periods, one should consider larger uncertainties produced by increased electric fields.

Figure 18 gives an indication of uncertainty magnitudes and duration in USU servo and radar-derived winds during mild and strong storm events at Millstone Hill. The duration of large uncertainties from electric field effects for the two ETS storms is about 6 hours for the mild storm and about 15 hours for the strong storm. Buonsanto et al. [1989] calculated electric field wind corrections, which compensate for most of the uncertainty between the radar and USU servo model winds in Figure 18. If electric field effects are not included in hmF2 neutral wind calculations during geomagnetically active periods, then neutral winds will include errors exceeding model uncertainties.

A recent paper by Sica and Schunk [1990] showed that the ionosphere/plasmasphere vertical exchange flux Φ_{∞} is important in modeling nighttime hmF2 values if only the peak ion density is known. The topside shape factor α , as defined by Equation (10) and discussed in Section 3.1.6, also affects F2-layer height and may be related to Φ_{∞} . The topside electron density profile can be measured by incoherent scatter radar and used to compute α and perhaps approximate Φ_{∞} . Changes in Φ_{∞} will affect the nighttime

decay rate and α should change as a result. To determine a relationship between the two parameters, Equation (21) or (22) may be used to calculate nighttime c_x values from the FLIP model for varying Φ_∞ values. The nighttime value of c_x is more sensitive to changes in decay rates than hmF2, making c_x a more desirable quantity in the study of vertical plasma flux effects.

The FLIP model indicates that the daytime ion production should be approximated by a steady-rate, rather than a steady-state assumption, especially during periods of low solar ionization (see Section 3.1.7). This allows for a daytime continuity equation of the form $q_m = c_d(t)\beta_m N_m$, where $c_d(t)$ changes at a steady daytime rate. How fast this change occurs is a function of solar ion production, which depends on geographic latitude (or solar zenith angle) and solar radiation flux. The FLIP model indicates that $c_d(t)$ approaches a constant value as daytime ion production increases, implying steady-state conditions. The USU servo model gives the option of inputting a steady-rate in $c_d(t)$ per hour. I recommend the development of a $c_d(t)$ linear change function based on solar zenith angle and solar flux intensity (perhaps a Chapman type function). The daytime slope function may then be included in the USU servo model for a physically better daytime output.

REFERENCES

- Babcock, R. R. Jr., and J. V. Evans, Seasonal and Solar Cycle Variations in the Thermosphere Circulation Observed Over Millstone Hill, J. Geophys. Res., 84, 7348-7352, 1979.
- Banks, P. M., and G. Kockarts, Aeronomy: Part A, Academic Press, New York, 1973.
- Blackadar, A., Using Your Computer: Solar Declination, Altitude and Azimuth, Weatherwise, 42, 109-113, 1989.
- Blanc, M., and A. D. Richmond, The Ionospheric Disturbance Dynamo, J. Geophys. Res., 85, 1669-1686, 1980.
- Berkey, F. T., G. H. Stonehocker, A Comparison of the Height of the Maximum Electron Density of the F2-layer from Real Height Analysis and Estimates Based on M(3000)F2, J. Atmos. Terr. Phys., 51, 873-877, 1989.
- Bilitza, D., N. M. Sheikh and R. Eyfrig, A Global Model for the Height of the F2-peak using M3000 values from the CCIR, Telecomm. J., 46, 549-553, 1979.
- Bilitza, D., K. Rawer, S. Pallaschke, C. M. Rush, N. Matuura, and W. R. Hoegy, Progress in Modeling the Ionospheric Peak and Topside Electron Density, Adv. Space Res., 7(6), 5-12, 1987.
- Bradley, P. A., and J. R. Dudeney, A Simple Model of the Vertical Distribution of Electron Concentration in the Ionosphere, J. Atmos. Terr. Phys., 35, 2131-2146, 1973.
- Burnside, R. G., C. A. Tepley, V. B. Wickwar, The O^+-O Collision Cross-Section: Can it be Inferred from Aeronomical Measurements?, Annales Geophysicae, 5A, 343-350, 1987.
- Burnside, R. G., C. A. Tepley, M. P. Sulzer, T. J. Fuller-Rowell, D. G. Torr and R. G. Roble, The Neutral Thermosphere at Arecibo During Geomagnetic Storms, J. Geophys. Res., 96, 1289-1301, 1991.
- Buonsanto, M. J., Seasonal Variations of Day-Time Ionization Flows Inferred from a Comparison of Calculated and Observed NmF2, J. Atmos. Terr. Phys., 48, 365-373, 1986.
- Buonsanto, M. J., J. E. Salah, K. L. Miller, W. L. Oliver, R. G. Burnside and P. G. Richards, Observations of Neutral Circulation at Mid-Latitudes During the Equinox Transition Study, J. Geophys. Res., 94, 16,987-16,997, 1989.

- Buonsanto, M. J., Observed and Calculated F2-peak Heights and Derived Meridional Winds at Mid-latitudes Over a Full Solar Cycle, J. Atmos. Terr. Phys., 52, 223-240, 1990.
- Buonsanto, M. J., J. C. Foster, A. D. Galasso, D. P. Sipler and J. M. Holt, Neutral Winds and Thermosphere/Ionosphere Coupling and Energetics During the Geomagnetic Disturbances of March 6-10, 1989, J. Geophys. Res., 95, 21,033-21,050, 1990.
- Chen, F. F., Introduction to Plasma Physics and Controlled Fusion, 1, 2nd Edition, Plenum Press, New York, 1984.
- Conkright, R. O., and H. I. Brophy, Catalog of Ionosonde Vertical Soundings Data, NOAA Report, UAG-85, 1982.
- Dudeney, J. R., The Accuracy of Simple Methods for Determining the Height of the Maximum Electron Concentration of the F2-layer from Scaled Ionospheric Characteristics, J. Atmos. Terr. Phys., 45, 629-640, 1983.
- Foster, J. C. and J. Aarons, Enhanced Antisunward Convection and F Region Scintillations at Mid-Latitudes During Storm Onset, J. Geophys. Res., 93, 11,537-11,542, 1988.
- Ganguly, S., J. C. G. Walker and H. Rishbeth, The Dynamic F2-layer Over Arecibo, J. Atmos. Terr. Phys., 42, 553-562, 1980.
- Hargreaves, J. K., The Upper Atmosphere and Solar-Terrestrial Relations, Van Nostrand-Reinhold, New York, 1979.
- Hedin, A. E., MSIS-86 Thermospheric Model, J. Geophys. Res., 92, 4649-4662, 1987.
- Hernandez, G., and R. G. Roble, Direct Measurement of Nighttime Thermospheric Winds and Temperatures 1. Seasonal Variations During Geomagnetic Quiet Periods, J. Geophys. Res., 81, 2065-2074, 1976.
- Herraro, F. A., H. G. Mayr, and N. W. Spencer, Low Latitude Thermospheric Meridional Winds between 250 and 450 km Altitude: AE-E Satellite Data, J. Atmos. Terr. Phys., 50, 1001-1006, 1988.
- Hess, S. L., An Introduction to Theoretical Meteorology, Robert E. Krieger Publishing Co., New York, 1979.
- Holten James R., An Introduction to Dynamic Meteorology, 23, 2nd Edition, Academic Press, New York, 1979.
- Kelley, M. C., The Earth's Ionosphere, Academic Press, New York, 1989.

- Killeen, T. L., R. G. Roble, An Analysis of the High-Latitude Thermospheric Wind Pattern Calculated by a Thermospheric General Circulation Model--Momentum Forcing, J. Geophys. Res., 89, 7509-7522, 1984.
- Melendez-Alvira, D. J., Theory and Measurements of Night-time Horizontal Gradients in the Mid-latitude F Region, Ph.D. dissertation, The University of Michigan, 1990.
- Miller, K. L., D. G. Torr, and P. G. Richards, Meridional Winds in the Thermosphere Derived from Measurement of the F2 Layer Height, J. Geophys. Res., 91, 4531-4535, 1986.
- Miller, K. L., J. E. Salah, D. G. Torr, The Effect of Electric Fields on Measurements of Meridional Neutral Winds in the Thermosphere, Annales Geophysicae, 5, 337-342, 1987.
- Miller, K. L., P. G. Richards, and D. G. Torr, The Derivation of Meridional Neutral Winds in the Thermosphere from F2-Layer Height, World Ionosphere/Thermosphere Study Wits Handbook Vol. 2, edited by C. H. Liu, pp. 439-471, SCOSTEP, University of Illinois, Illinois, 1989.
- Moyer, V., Notes on Physical Meteorology, Texas A&M University, College Station, Texas 1976.
- Ratcliffe, J. A., An Introduction to the Ionosphere and Magnetosphere, Cambridge University Press, Cambridge, 1972.
- Rees, M. H., Physics and Chemistry of the Upper Atmosphere, Cambridge University Press, Cambridge, 1989.
- Richards, P. G., and D. G. Torr, Seasonal, Diurnal and Solar Cycle Variations of the Limiting H^+ Flux in the Earth's Topside Ionosphere, J. Geophys. Res., 90, 5261-5268, 1985.
- Richards, P. G., and D. G. Torr, A Factor of 2 Reduction in the Theoretical F2-peak Electron Density Due to Enhanced Vibrational Excitation of N_2 in Summer at Solar Maximum, J. Geophys. Res., 91, 11,331-11,336, 1986.
- Richards, P. G., and D. G. Torr, Ratio of Photoelectron to EUV Ionization Rates for Aeronomic Studies, J. Geophys. Res., 93, 4060-4066, 1988.
- Richmond, A. D., Thermospheric Dynamics and Electrodynamics, Solar Terrestrial Physics, edited by R. L. Corovillano and J. M. Forbes, pp. 523-607, D. Reidel, Dordrecht, 1983.

- Rishbeth, H., The Effect of Winds on the Ionospheric F2-peak, J. Atmos. Terr. Phys., 29, 225-238, 1967.
- Rishbeth, H., and O. K. Garriott, Introduction to Ionospheric Physics, Academic Press, New York, 1969.
- Rishbeth, H., Thermospheric Winds and the F-region: A Review, J. Atmos. Terr. Phys., 34, 1-47, 1972.
- Rishbeth, H., S. Ganguly and J. C. G. Walker, Field-Aligned and Field-Perpendicular Velocities in the Ionospheric F2-layer, J. Atmos. Terr. Phys., 40, 767-784, 1978.
- Rishbeth, H., Ion-drag Effects in the Thermosphere, J. Atmos. Terr. Phys., 41, 885-894, 1979.
- Rishbeth, H., On the F2-layer Continuity Equation, J. Atmos. Terr. Phys., 48, 511-519, 1986.
- Rishbeth, H., Basic Physics of the Ionosphere: a tutorial review, J. IERE, 58, 207-223, 1988.
- Rishbeth, H., R. Edwards, The Isobaric F2-layer, J. Atmos. Terr. Phys., 51, 321-338, 1989.
- Roble, R. G., Dynamics of the Earth's Thermosphere, Rev. Geophys. Space Phys., 21, 217-233, 1983.
- Salah, J. E., and J. M. Holt, Mid-latitude Thermospheric Winds from Incoherent Scatter Radar and Theory, Radio Sci., 9, 303-313, 1974.
- Schunk, R. W., The Terrestrial Ionosphere, Solar Terrestrial Physics, edited by R. L. Corovillano and J. M. Forbes, pp. 609-675, D. Reidel, Dordrecht, 1983.
- Sica, R. J., R. W. Schunk, P. J. Wilkinson, A Study of the Undisturbed Mid-latitude Ionosphere Using Simultaneous Multiple Site Ionosonde Measurements During the Sundial-86 Campaign, J. Geophys. Res., 95, 8271-8279, 1990.
- Sica, R. J., R. W. Schunk, Interpreting Vertical Plasma Drift in the Mid-latitude Ionosphere Using Ionosonde Measurements, Planet Space Sci., 38, 1567-1571, 1990.
- Wickwar, V. B., J. W. Meriwether, P. B. Hays and A. F. Nagy, The Meridional Thermospheric Neutral Wind Measured by Radar and Optical Techniques in the Auroral Region, J. Geophys. Res., 89, 10987-10998, 1984.

APPENDICES

Appendix A. General Information on Station Locations

TABLE 4. Ionosonde/Radar Station Parameters

<u>Name</u>	<u>Geographic Location</u>		<u>Dip Angle</u> *
YAKUTSK	62.00° N	129.60° E	76.1°
MAGADAN	60.00° N	151.00° E	71.1°
PETROPAVLOVSK	53.00° N	158.60° E	64.3°
MANCHOULI	49.60° N	117.40° E	67.8°
KHABAROVSK	48.50° N	135.10° E	63.6°
WAKKANAI	45.40° N	141.70° E	59.3°
AKITA	39.70° N	140.10° E	53.4°
BEIJING	39.90° N	116.40° E	57.7°
TOKYO	35.70° N	139.50° E	48.7°
YAMAGAWA	31.20° N	130.60° E	44.1°
OKINAWA	26.30° N	127.80° E	36.8°
CHUNG-LI	24.91° N	121.24° E	35.1°
CANTON	23.10° N	113.30° E	32.3°
VANIMO	2.70° S	141.30° E	-22.5°
DARWIN	12.45° S	130.95° E	-40.7°
TOWNSVILLE	19.63° S	146.85° E	-49.3°
MUNDARING	31.98° S	116.22° E	-67.1°
CANBERRA	35.32° S	149.00° E	-66.4°
SALISBURY (AUST.)	34.70° S	138.60° E	-67.2°
HOBART	42.92° S	147.32° E	-72.9°
Millstone Hill	42.50° N	288.50° E	71.5°

* Magnetic Dip Angles from International Geomagnetic Reference Field (IGRF)

Appendix B. Geomagnetic and Solar Data

TABLE 5. Geomagnetic and Solar Data

MONTH	DAY	YEAR	F10.7	F10.7A	Ap	R ₁₂
1	10	1988	100.9	104.6	4	32.8
1	11	1988	101.7	104.6	11	32.8
1	12	1988	107.5	104.6	21	32.8
1	13	1988	108.1	104.6	7	32.8
1	14	1988	113.7	104.6	48	32.8
1	15	1988	112.4	104.6	63	32.8
1	16	1988	121.8	104.6	5	32.8
1	*	1985	72.6	73.1	6.3	16
1	*	1981	161.6	205.1	4.8	114
9	16	1984	73.4	78.9	8	---
9	17	1984	74.6	78.9	6	---
9	18	1984	73.8	78.9	3	---
9	19	1984	74.6	78.9	36	---
9	20	1984	74.1	78.9	21	---
9	21	1984	75.1	78.9	10	---
9	22	1984	75.9	78.9	22	---
9	23	1984	76.1	78.9	112	---

* Average of 10 most quiet days.

Appendix C. Copyright Permission Letters

Theodore R. Ballard
1454 E. 800 N.
Logan, UT 84321
(801) 753-7382 or 750-2657

12 March 91

Pergamon Press, Inc.
Maxwell House
Fairview Park
Elmsford, New York 10523

OK
17/8/91

Dear Sir:

I am in the process of preparing my thesis in the Center for Atmospheric and Space Science Department at Utah State University. I will complete my degree in the Spring quarter of 1991.

I am requesting your permission to include the attached material, also listed in the endorsement section below. I will include acknowledgements and/or appropriate citations to your work as required by U.S. copyright laws. If further requirements are necessary for inclusion of these works in my thesis, please make appropriate annotations in the endorsement section.

Please indicate your approval of this request by signing in the space provided and attach any forms or instructions required to confirm permission. If a reprint fee is required for the use of your material, please indicate that as well. If you have any questions, please call me at the numbers given above. Written correspondence should be sent to the above address to ensure prompt response to your requests for use of the listed material.

Please send your response to this request as soon as possible as I am in the final stages of completing my thesis and additional degree requirements. If you are not the copyright holder, please forward my request to the appropriate person or institution.

Thank you for your cooperation.


Theodore R. Ballard

I hereby give permission to Theodore Ballard to reprint the following material in his thesis. A reprint fee of \$_____ is/is not required for use of this material.

Bradley, P. A., and J. R. Dudeney, A Simple Model of the Vertical Distribution of Electron Concentration in the Ionosphere, J. Atmos. Terr. Phys., 35, 1973.

✓ Figure 1 p. 2133

Center for Atmospheric and Space Sciences
Utah State University
Logan, UT 84322-4405

3/10



PERGAMON PRESS, INC.

March 19, 1991

Prof. Theodore R. Ballard
1454 E. 800 N.
Logan, UT 84321

Dear Prof. Ballard:

With reference to your attached request to reprint/reproduce material from a Pergamon journal, we herewith grant permission to do so, provided:

1. The material to be reproduced has appeared in our publication without credit or acknowledgement to another source.
2. Suitable acknowledgement to the source be given, preferably as follows:

Reprinted with permission from [Journal Title, Volume Number, Author(s), Title of Article], Copyright [Year], Pergamon Press plc.

3. The author's approval in writing be obtained (the address or affiliation that appears in the journal is the most current available).
4. A copy of your work is submitted upon publication to the Journal Permissions Department.

This permission is for one-time use and for use in editions for the handicapped.

We only grant non-exclusive world English rights. Foreign language rights must be applied for separately.

Sincerely,

Andrew Adler
Journals Permissions

MATERIAL TO BE REPRINTED/REPRODUCED AND TO BE USED IN:

As per your attached letter(s).

Enclosure: original request(s) for permission

Journal of ATMOSPHERIC AND TERRESTRIAL PHYSICS

Editor-in-Chief

SIR GRANVILLE BEYNON, F.R.S., *Department of Physics, University College of Wales, Aberystwyth SY23 3BZ, U.K.*

Editorial Advisory Board

B. H. BRIGGS, *Department of Physics, University of Adelaide, S. Australia.*

B. LANDMARK, *Norwegian Defence Research Establishment, Division for Electronics, P.O. Box 25, Kjeller, Norway.*

A. P. MITRA, *National Physical Laboratory, Radio Propagation Laboratory, Hillside Road, New Delhi 12, India.*

J. S. NISBET, *Department of Electrical Engineering, Pennsylvania State University, University Park, Pennsylvania 16802, U.S.A.*

Publishing, Subscription and Advertising Offices

Pergamon Journals Ltd., Headington Hill Hall, Oxford OX3 0BW, U.K.
Pergamon Journals Inc., Maxwell House, Fairview Park, Elmsford, NY 10523, U.S.A.
Published monthly.

Subscription Rates 1986

For libraries, university departments, government laboratories, industrial and other multiple-reader institutions: \$410.00 per annum including postage and insurance, \$779.00 for two years (1986/87).

Back issues of all previously published volumes are available in the regular editions and on microfilm and microfiche. Current subscriptions are available on microfiche simultaneously with the paper edition and on microfilm on completion of the annual index at the end of the subscription year.

Subscription enquiries from customers in North America should be sent to: Pergamon Journals Inc., Maxwell House, Fairview Park, Elmsford, NY 10523, U.S.A., and for the remainder of the world to: Pergamon Journals Ltd., Headington Hill Hall, Oxford OX3 0BW, U.K.

Microform Subscriptions and Back Issues

Back issues of all previously published volumes are available in the regular editions and on microfilm and microfiche. Current subscriptions are available on microfiche simultaneously with the paper edition and on microfilm on completion of the annual index at the end of the subscription year.

Copyright © 1986 Pergamon Journals Ltd.

It is a condition of publication that manuscripts submitted to this journal have not been published and will not be simultaneously submitted or published elsewhere. By submitting a manuscript, the authors agree that the copyright for their article is transferred to the publisher if and when the article is accepted for publication. However, assignment of copyright is not required from authors who work for organizations which do not permit such assignment. The copyright covers the exclusive rights to reproduce and distribute the article, including reprints, photographic reproductions, microform or any other reproductions of similar nature and translations. No part of this publication may be reproduced, stored in a retrieval system or transmitted in any form or by any means, electronic, electrostatic, magnetic tape, mechanical, photocopying, recording or otherwise, without permission in writing from the copyright holder.

U.S. Copyright Law Applicable to Users in the U.S.A.

Photocopying information for users in the U.S.A. The Item-Fee Code for this publication indicates that authorization to photocopy items for internal or personal use is granted by the copyright holder for libraries and other users registered with the Copyright Clearance Center (CCC) Transactional Reporting Service provided the stated fee for copying beyond that permitted by Section 107 or 108 of the United States Copyright Law is paid. The appropriate remittance of \$3.00 per copy per article is paid directly to the Copyright Clearance Center Inc., 27 Congress Street, Salem, MA 01970.

Permission for other use.

The copyright owner's consent does not extend to copying for general distribution, for promotion, for creating new works, or for resale. Specific written permission must be obtained from the publisher for such copying. In case of doubt please contact your nearest Pergamon office.

The Item-Fee Code for this publication is: 0021-9169/86 \$3.00 + .00